ANALYZING ROTOR TILT ANGLES ON THE EFFICIENCY OF MONOPOLE TOWER FLOATING OFFSHORE WIND TURBINES

WONGSAKORN WISATESAJJA

A DISSERTATION SUMITTED IN PARTIAL FULFILLMENT OF THE REQUIREMENTS FOR THE DEGREE OF DOCTOR OF ENGINEERING PROGRAM IN ENERGY AND MATERIALS ENGINEERING (INTERNATIONAL PROGRAM)

FACULTY OF ENGINEERING

RAJAMANGALA UNIVERSITY OF TECHNOLOGY THANYABURI

ACADEMIC YEAR 2020

ANALYZING ROTOR TILT ANGLES ON THE EFFICIENCY OF MONOPOLE TOWER FLOATING OFFSHORE WIND TURBINES

WONGSAKORN WISATESAJJA

A DISSERTATION SUMITTED IN PARTIAL FULFILLMENT OF THE REQUIREMENTS FOR THE DEGREE OF DOCTOR OF ENGINEERING PROGRAM IN ENERGY AND MATERIALS ENGINEERING

(INTERNATIONAL PROGRAM)

FACULTY OF ENGINEERING

RAJAMANGALA UNIVERSITY OF TECHNOLOGY THANYABURI

ACADEMIC YEAR 2020

Dissertation Title Analyzing Rotor Tilt Angles on the Efficiency of Monopole Tower Floating Offshore Wind Turbines

Name-Surname Mr. Wongsakorn Wisatesajja

Program Energy and Materials Engineering

Dissertation Advisor Assistant Professor Wirachai Roynarin, Ph.D.

Academic Year 2020

DISSERTATION COMMITTEE

.... Chairman
(Assistant Professor Kiattisak Sangpradit, Ph.D.)

R. Tanit
.... Committee
(Associate Professor Tanit Ruangrungchaikul, Ph.D.)

.... Committee
(Assistant Professor Sorapong Pavasupree, Ph.D.)

.... Committee
(Assistant Professor Jakkree Srinonchat, Ph.D.)

.... Committee
(Assistant Professor Wirachai Roynarin, Ph.D.)

Approved by the Faculty of Engineering, Rajamangala University of Technology Thanyaburi in Partial Fulfillment of the Requirement for the Degree of Doctor of Engineering

.... Dean of Faculty of Engineering
(Assistant Professor Sivakorn Angthong, Ph.D.)
March 30, 2021

หัวข้อดุษฎีนิพนธ์	การวิเคราะห์มุมเอียงบนเสากังหันลมชนิดเสาเดี่ยวต่อประสิทธิภาพของกังหันลมลอยน้ำนอกชายฝั่ง
ชื่อ - นามสกุล	นายวงศกร วิเศษสัจจา
สาขาวิชา	วิศวกรรมพลังงานและวัสดุ
อาจารย์ที่ปรึกษา	ผู้ช่วยศาสตราจารย์วิรชัย โรยนรินทร์, Ph.D.
ปีการศึกษา	2563

บทคัดย่อ

การพัฒนากังหันลมลอยน้ำนอกชายฝั่ง โดยทั่วไปแล้วพยายามที่จะให้ได้มาซึ่งประสิทธิภาพการแปลงพลังงานที่สูงและมีประสิทธิภาพที่ดีทางด้านเศรษฐศาสตร์ ในการประยุกต์ใช้เทคโนโลยีกังหันลมดังกล่าว ปัญหาทั่วไปอย่างหนึ่งของกังหันลมลอยน้ำนอกชายฝั่ง คือ ผลกระทบของกระแสลม ซึ่งจะทำให้บริบทของมุมเอียงและแท่นลอยที่มักจะไม่เสถียรและนำไปสู่การเยื้องหนีจากศูนย์แนวแกนตั้งของใบกังหัน ซึ่งจะทำให้ลดพื้นที่กวาดในการทำงานของกังหันลมซึ่งจะมีผลต่อประสิทธิภาพในการแปลงพลังงานสูงสุด เพื่อแก้ปัญหาดังกล่าว การศึกษานี้จึงมีวัตถุประสงค์เพื่อทำการวิเคราะห์ผลกระทบของมุมเอียงของใบกังหันที่มีต่อประสิทธิภาพของกังหันลมชนิดเสาเดี่ยวและเพื่อเปรียบเทียบระหว่างกังหันลม 2 ประเภทที่แตกต่างกัน คือ กังหันลมลอยน้ำนอกชายฝั่งและกังหันลมแบบเสายึดตรึงที่อยู่บนพื้นดิน

การศึกษานี้จะใช้วิธีการสร้างต้นแบบกังหันลมขนาดเล็กทดสอบในอุโมงค์ลมเปรียบเทียบกับแบบจำลองโดยใช้โปรแกรมวิเคราะห์ทางพลศาสตร์ของไหล (Computational Fluid Dynamics หรือ CFD) ซึ่งอุโมงค์ลมในการศึกษานี้มีความยาว 4.5 เมตร สูง 3 เมตร และกว้าง 4 เมตร มีช่องลมเข้าอุโมงค์ลมรูปร่างหน้าตัดสี่เหลี่ยมขนาดพื้นที่ 1 ตารางเมตร อยู่ตรงกลางอุโมงค์ ต้นแบบของกังหันลมทั้งสองประเภทที่ใช้ในการทดลองในอุโมงค์ลมและ CFD ใช้ใบกังหันรูปทรงแพนอากาศมีชื่อว่า R1235 ที่มีเส้นผ่านศูนย์กลางใบ 82 เซนติเมตร และทำการวัดค่าตัวแปรต่าง ๆ ในอุโมงค์ด้วยเครื่องวัดความเร็วลม เครื่องวัดความเร็วรอบของใบกังหัน และเครื่องวัดองศามุมเอียงของใบกังหัน โดยในการทดสอบใช้ความเร็วลมระหว่าง 2-5.5 เมตรต่อวินาที และในระหว่างขั้นตอนการทดลองจะมีการเปรียบเทียบระหว่าง ความเร็วในการหมุนของใบกังหัน (Rotational Speed) อัตราส่วนความเร็วปลายใบ (Tip Speed Ratio) และค่าสัมประสิทธิ์กำลัง (Power Coefficient) ของการทดสอบในอุโมงค์ลมที่ตัวแปรมุมเอียงที่เกิดขึ้นจริงจากนั้นจะนำไปใช้ในแบบจำลองทาง CFD เพื่อนำค่าตัวแปรมาเปรียบเทียบระหว่างความเร็วในการหมุนของใบกังหัน อัตราส่วนความเร็วปลายใบ และค่าสัมประสิทธิ์กำลัง ของทั้งต้นแบบทดลองกังหันลมลอยน้ำนอกชายฝั่งในอุโมงค์ลมและแบบจำลอง CFD จะใช้ความเร็วลมระหว่าง 2-5.5 เมตรต่อวินาที ซึ่งเป็นตัวแปรเดียวกัน

ผลการทดลองของต้นแบบแสดงให้เห็นว่ากังหันลมลอยน้ำนอกชายฝั่ง มีค่าความเร็วในการหมุนของใบที่ต่ำกว่ากังหันลมแบบเสายึดตรึง อันเป็นผลมาจากมุมเอียงที่เปลี่ยนแปลงซึ่งทำให้ความเร็วในการหมุนของใบแตกต่างกันเฉลี่ยประมาณ 36.8% และได้ค่ามุมเอียงแบบจำลองการทดลองของกังหันลมลอยน้ำนอกชายฝั่งมีค่าระหว่าง 3.5°- 6.1° ในความเร็วลมอยู่ที่ระหว่าง 2-5.5 เมตรต่อวินาที อีกทั้ง

ผลลัพธ์เปรียบเทียบของค่าความเร็วในการหมุนระหว่างกังหันลมเสายึดตรึงและกังหันลมลอยน้ำนอกชายฝั่งในแบบจำลอง CFD มีเปอร์เซ็นต์ความแตกต่างเฉลี่ยอยู่ที่ประมาณ 17.7% อย่างไรก็ตามผลการจำลองทาง CFD สำหรับกังหันลมลอยน้ำนอกชายฝั่งนั้นได้ค่าความเร็วในการหมุนของใบเร็วกว่าที่ทดสอบในการทดลองในอุโมงค์ลมโดยมีค่าเฉลี่ยความเร็วรอบที่แตกต่างกันประมาณ 16.4% อย่างไรก็ตามจากผลการศึกษา พบว่า กังหันลมลอยน้ำนอกชายฝั่ง ไม่ว่าจะมาจากการทดลองในอุโมงค์ลมหรือการจำลอง CFD นั้นได้ค่าความเร็วรอบไม่สูงเท่ากับค่าของกังหันลมแบบเสายึดตรึงอยู่ดี แต่ในกรณีของกังหันลมลอยน้ำนอกชายฝั่ง ค่าอัตราส่วนความเร็วปลายใบและค่าสัมประสิทธิ์กำลังจะสามารถรักษาในระดับค่าที่สูงสุดไว้ได้ในช่วงมุมเอียงที่เกิดขึ้น โดยในระหว่างการทดลองและการจำลอง CFD นั้นค่าสัมประสิทธิ์กำลังสูงสุดอยู่ในช่วง 0.35-0.36 และมีอัตราส่วนความเร็วปลายใบอยู่ในช่วง 7.7-9.6 ของความเร็วลม 3-5 เมตรต่อวินาที ที่มุมเอียงจาก 3.9°- 5.8° ในขณะเดียวกันผลที่ได้รับจากกังหันลมแบบเสายึดตรึงจะมีค่าสัมประสิทธิ์กำลังสูงสุดเกิดขึ้น ในช่วงความเร็วลม 2-2.5 เมตรต่อวินาทีเท่านั้นและมีค่าสัมประสิทธิ์กำลังอยู่ระหว่าง 0.33-0.36 หลังจากความเร็วลม 2.5 เมตรต่อวินาทีจะมีค่าสัมประสิทธิ์กำลังที่ลดลงไม่เหมือนกับกังหันลมลอยน้ำนอกชายฝั่งที่จะรักษาค่าสัมประสิทธิ์กำลังไว้ในช่วงความเร็วลม 3-5 เมตรต่อวินาที ดังนั้น จึงสามารถสรุปได้จากการวิเคราะห์กังหันลมทั้งสองประเภทจากการทดลองในอุโมงค์ลมและการจำลองโปรแกรม CFD ได้ว่าที่ช่วงความเร็วลม 3-5 เมตรต่อวินาที และมุมเอียงที่ 3.9°- 5.8° กังหันลมลอยน้ำนอกชายฝั่งจะสามารถรักษาค่าสัมประสิทธิ์กำลังของกังหันลมในค่าสูงสุดไว้ได้เมื่อมุมเอียงเปลี่ยนไปในช่วงมุมดังกล่าวแต่กังหันลมชนิดแบบเสายึดตรึงไม่สามารถทำได้ นอกจากนี้จากผลการวิจัยนี้ยังนำเสนอความเข้าใจในทฤษฎีใหม่ของการรักษาค่าสัมประสิทธิ์กำลังโดยการใช้มุมเอียงที่ปรับเองได้จากทุ่นลอยน้ำในการประยุกต์ใช้งานกังหันลมลอยน้ำนอกชายฝั่งที่มีขนาดเล็กถึงขนาดกลางแบบใบกังหันลมชนิดปรับมุมเอียงไม่ได้ (Fixed Pitch Blade) ซึ่งการค้นพบนี้สามารถนำมาใช้กับกังหันลมลอยน้ำนอกชายฝั่งชนิดทุ่นลอยนี้ได้และยังสามารถลดต้นทุนค่าใช้จ่ายในการสร้างระบบควบคุมการปรับใบกังหัน (Pitch Control) ลงได้อีกด้วย

คำสำคัญ: โปรแกรมพลศาสตร์ของไหล กังหันลมลอยน้ำนอกชายฝั่ง มุมเอียงใบกังหัน

Dissertation Title	Analyzing Rotor Tilt Angles on the Efficiency of Monopole Tower Floating Offshore Wind Turbines
Name – Surname	Mr. Wongsakorn Wisatesajja
Program	Energy and Material Engineering
Dissertation Advisor	Assistant Professor Wirachai Roynarin, Ph.D.
Academic Year	2020

ABSTRACT

The development of Floating Offshore Wind Turbines (FOWTs) has typically sought to achieve superior power efficiency as well as economic performance by enhancing the application of wind turbine technology. One common difficulty of floating offshore wind turbines is the effect of airflow which contextualises the angles and an unstable floating platform. The condition can cause the wind turbine axis to move out of its vertical alignment, which can reduce the area of the rotor blades exposed to the wind, preventing the blades from maximizing the extraction of energy from the available wind flow. In order to manage this particular challenge, this study aims to examine the effects of the rotor tilt angles upon the efficiency of wind turbine performance; and to compare two different types of wind turbines: the FOWTs, and the fixed tower wind turbines.

The study made use of wind turbine modeling in a wind tunnel along with Computational Fluid Dynamics (CFD) simulation models. The experimental wind tunnel measured 4.5 m in length, 3 m in height, and 4 m in width, with a square airflow duct measuring 1 m^2 located in the center of the tunnel. The models of both wind turbine types used in the wind tunnel experiments made use of 82 cm diameter R1235 airfoil blades, and the measurements in the tunnel were taken using an anemometer, a tachometer, and an angle meter. The wind speeds varied between 2-5.5 m/s during the testing procedure and comparisons were drawn between the rotational speeds, power coefficients and tip speed ratios for the two different models. The tilt angle values obtained in the wind tunnel experimental model were then applied in the CFD simulation model in order to draw comparisons between the rotational speed, tip speed ratio, and power coefficient for the

FOWTs experimental model and the CFD model with the wind speed set in the range of 2-5.5 m/s.

The wind tunnel experimental results revealed that the FOWTs offered lower rotational speeds than that of the fixed tower wind turbines, as a consequence of the altered tilt angles, which accounted for average percentage difference of rotational speed of 36.8%. The FOWTs experimental model presented tilt angles in the range of 3.5°- 6.1° while the wind speeds ranged from 2-5.5 m/s. The outcome was comparable with that of the fixed tower wind turbines in the wind tunnel and FOWTs in the CFD, with average percentage difference of 17.7%. However, the CFD simulation results for the FOWTs exceeded the findings from the wind tunnel experiments, with the average percentage difference of 16.4%. These results for the FOWTs, whether from the experiments or the CFD simulation, were not as high as those recorded for the fixed tower wind turbine. In the case of the FOWTs, the values for the tip speed ratio and power coefficient were successfully held at an optimal level, both during the experimental models and the CFD simulations, when the power coefficient was in the range of 0.35-0.36, the tip speed ratios in the range of 7.7-9.6, the wind speed varied from 3-5 m/s at tilt angles from 3.9°- 5.8°. Meanwhile, the results from the fixed tower wind turbine showed that the optimal values were held when the wind speed was in a much narrower range of 2-2.5 m/s, and the power coefficient ranged from 0.33-0.36. The analysis of the two wind turbine types via the wind tunnel experiments and the CFD simulations led to the conclusion that when the wind speeds reach 3-5 m/s and the tilt angles measure 3.9°- 5.8°, it is possible to maintain the wind turbine power efficiency at an optimal value. In addition, the findings offered further understanding of the new theory of maintaining the power coefficient by utilizing an adjustable tilt angle for small to medium fixed pitch FOWTs. Thus, the utilization of these floating offshore wind turbines could decrease the expense of the pitch control system.

Keywords: CFD, floating offshore wind turbines, tilt angle

Acknowledgements

For this thesis, first of all, I would like to express my sincere gratitude to my thesis advisor Assistant Professor Dr. Wirachai Roynarin for the valuable of guidance and encouragement which helped me in all the time of my research. I would also like to thank my colleague, Mr. Decha Intholo, for his support and consultation on this paper. I am grateful to the staff of the Energy Research and Service Centre.
ERSC) of the Engineering Faculty of RMUTT for allowing me to use the experiment resources. Finally, I would like to thank my family for their consistent support.

Secondly, I would like to thank to the thesis committees, Associate Prof. Dr. Tanit Ruangrungchakul from Thammasat University, Assistant Prof. Dr. Kiattisak Sangpradit, Assistant Prof. Dr. Jakkree Srinonchat and Assistant Prof. Dr. Sorapong Pavasupree for their valuable comments and helpful suggestions.

Finally, I would like to thank to my family for all their loves and encouragement.

Wongsakorn Wisatesajja

Table of Contents

Table of Contents (Continued)

Page

List of Tables

Page

List of Figures

List of Figures (Continued)

Page

List of Figures (Continued)

Page

List of Figures (Continued)

Page

List of Abbreviations

AC	Alternating Current
B	Focal Point of Buoyancy
BEM	Blade Element Momentum
CAPEX	Capital Expenditures
CFD	Computational Fluid Dynamics
CFM	Cubic Feet per Minute
C_P	Power Coefficient
$CP_{(env)}$	Middle of Pressure of Environment Forces
DC	Direct Current
DEDE	Department of Alternative Energy Development and Efficiency
DLRM	Direct Local Relative Velocity Method
EGAT	Electricity Generating Authority of Thailand
EqAM	Equivalent Averaged Method
F	Focal Point of Floatation
$F_{(env)}$	Environmental Force
FAST	Fatigue, Analysis, Structure and Turbulence
FOWTs	Floating Offshore Wind Turbines
FP	Fixed-Pitch
FS	Fixed-Speed
FVM	Free Vortex Method
G	Center of Gravity
GW	Gigawatt
HAWTs	Horizontal Axis Wind Turbines
IEC	International Electrotechnical Commission
kW	Kilowatt
LCOE	Levelized Cost of Energy
LES	Large Eddy Simulation
MLA	Middle of Mooring Line Action

List of Abbreviations (Continued)

MIT	Massachusetts Institute of Technology
MW	Megawatt
m/s	Meter per Second
NREL	National Renewable Energy Laboratory
NIA	National Innovation Agency
OPEX	Operating Expenditures
OWTs	Offshore Wind Turbines
PEA	Provincial Electricity Authority
PM	Permanent Magnet
Re	Reynold’s Number
RMUTT	Rajamangala University of Technology Thanyaburi
SES	Social Ecological System
SIMPLE	Semi-Implicit Method for Pressure-Linked Equations
SST	Shear Stress Transport
TLP	Tension Leg Platforms
TSR	Tip Speed Ratio
VAWTs	Vertical Axis Wind Turbines
VP	Variable-Pitch
VS	Variable-Speed
WAMIT	Wave Analysis at Massachusetts Institute of Technology

List of Nomenclatures

Roman Letters

A	Cross-sectional region of the rotor disc	(m^2)
A_0	Entrance cross-section region of the wind tunnel	(m^2)
A_1	Exit cross-section region of the wind tunnel	(m^2)
c	Scale parameter	(m/s)
c	Chord length of the airfoil	(m)
C_d	Drag coefficient	
C_l	Lift coefficient	
C_m	Pitching moment coefficient	
C_P	Power coefficient	
D	Drag force	(N)
dFD	Indicates the incremental drag force	(N)
dFL	Incremental lift force	(N)
dFN	Incremental force normal to the plane of rotation	(N)
dFT	Incremental force at a tangent to the circular path	(N)
F_B	Buoyant force	(N)
F_H	Hydrostatic force	(N)
F_{Mg}	Force acting by the object	(N)
$f(v)$	Prospect of wind speed	
F_W	Force applies on wind turbines	(N)
g	Force of gravity (9.81 N/kg)	(N/kg)
H	Draft height	(m)
k	Shape parameter	
L	Lift force	(N)
l	Span of the airfoil	(m)
m	Object mass	(kg)
M	Pitching moment	(Nm)
M_{Total}	Total mass	(kg)
N	Rotational speed	(rpm)

List of Nomenclatures (Continued)

P_0	Atmospheric pressure	(N/m^2)
P_2	Air pressure moving through the rotor disc	(N/m^2)
P_3	Air pressure prior to hitting the rotor disc	(N/m^2)
P_a	Power in the wind	(W)
P_w	Wind turbine power output	(W)
Q	Airflow rate utilized for the examination	(m^3/s)
r	Radius of the rotor	(m)
S'	Control volume	
T_a	Thrust at the rotor blade	(N)
u_1	Wind speed after moving through the rotor disc	(m/s)
u	Mean wind speed in the system	(m/s)
U	Speed of the rotor tip	(m/s)
U_a	Undisturbed air flow velocity	(m/s)
U_{rel}	Relative wind velocity	(m/s)
V_0	Wind speed at the inlet and outlet of control volume	(m/s)
V	Object volume	(m^3)
V	Wind speed	(m/s)
V_m	Mean speed	(m/s)
V_{ref}	Average wind speed at the orientation height z_{ref}	(m/s)
$V(z)$	Average wind speed at height z	(m/s)
z_0	Surface roughness length	(m)
z_{ref}	Orientation height	(m)

Greek Letters

α	Angle of attack	(degree)
β	Tilt angle	(degree)
θ_p	Section pitch angle	(degree)
$\theta_{p,0}$	Blade pitch angle	(degree)
θ_T	Section twist angle	(degree)
λ	Tip speed ratio	

ρ_{Object}	Object density	(kg/m^3)
ρ_{Air}	Air density (1.225 kg/m^3)	(kg/m^3)
ρ_{Water}	Water density (1000 kg/m^3)	(kg/m^3)
φ	Angle of relative wind	(degree)
ω	Angular velocity	(ra

CHAPTER 1
INTRODUCTION

1.1 General Overview

At least 80% of the world's energy supply is currently obtained from fossil fuels, leading to environmental damage and the dangers of climate change [1]. These clear disadvantages have provided the impetus for renewable energy sources to be explored. These are also known as natural or alternative energy sources, and they offer the advantages of being unlimited, inexpensive, and environmentally clean and safe [2]. One potential energy source is to use wind turbines in order to generate electricity by harnessing the power of the wind through the conversion of kinetic energy into electrical power [3]. Wind turbines create electricity with vary levels of efficiency, which will depend upon the prevailing conditions in the geographical regions in which the wind turbines operate. The BP Statistical Review of World Energy 2018, noted that wind energy accounts for at least 50% of the current growth in renewable energy, and is poised to become the leading alternative energy source [4]. By 2019, the total capacity of wind power was 622,704 MW, with offshore wind turbines accounting for 28,308 MW [5].

Offshore Wind Turbines (OWTs) are now broadly understood to have the potential to meet the growing demand for energy worldwide and are therefore likely to increase in number in support of the need to provide a secure supply of electrical power. In comparison to other ocean-based energy sources, including wave or tide power, the technology related to wind power is already considered mature, and in the case of OWTs, the technology for shallow water and bottom-fixed wind turbines is well-established [6]. The OWTs industry has shown substantial growth in recent years, and its expansion is ongoing around the world [7]. One important benefit for OWTs when compared to those onshore is that the wind speeds tend to be higher at sea as a consequence of the flat sea surface, and therefore the greater wind speed leads to greater power generation. Furthermore, there are no issues with visual and noise pollution at sea, adding to the advantages of OWTs [8].

For those countries which have already started to generate offshore wind power, there are relatively few shallow-water offshore sites still available. Instead, much of the wind available worldwide is to be found in locations where the water has a much greater depth than is currently the case for the OWTs which operate at present. These deep-water sites which offer so much potentials are also beyond the reach of fixed-bottom structures, and can be found along the coasts of Japan, Norway, Spain, and the USA. There were feasible to mount wind turbines on support platforms which float, that would present an effective means of gaining access to these deep-water offshore wind resources. It would also be the case that Floating Offshore Wind Turbines (FOWTs) would offer greater economy that their fixed-bottom counterparts in deeper waters due to savings on structural costs and installation of the wind turbines [9].

One important problem facing wind turbines is the potential for vertical misalignment of the wind turbine axis which is the result of the tilt angle. If the rotor axis of the wind turbine is turned away from the direction of the wind, this alters the area of the rotor blade available to the wind, and as a result leads to a decline in the level of energy obtained. If the effectiveness of wind energy is to be maximized, a positioning mechanism is necessary in order to ensure that the rotor axis maintains the optimal direction in terms of the wind flow. The tilt angle must also be considered carefully to ensure that the rotor blades do not tilt and come into contact with the tower itself [10].

In this research, the influence of the angle of rotor tilt upon the performance of the wind turbine is examined, and two different wind turbine types are compared: the FOWTs, and the onshore fixed tower wind turbine. Wind turbine modeling is carried out using a wind tunnel, and Computational Fluid Dynamics (CFD) simulation models are also created for evaluation. The wind tunnel used for the experiments had a length of 4.5 m, a width of 4 m, and a height of 3 m, with a square airflow duct measuring 1 m^2 located in the center of the tunnel. For both wind turbine types tested in the wind tunnel, the blades used were R1235 airfoil blades with a diameter of 82 cm, while the measuring tools employed included a tachometer, an anemometer, and an angle meter. The tests required wind speeds from 2-5.5 m/s, whereupon the rotational speed, tip speed ratio, and power coefficient could be compared for the two different types of model used. In the CFD simulation, the tilt angle values recorded from the experiments in the wind tunnel were used in order to compare the CFD model with the experimental FOWTs model in terms of rotational speed, tip speed ratio, and power coefficient when the wind speeds were varied from 2-5.5 m/s.

1.2 Historical Wind Energy Background

In the past, wind energy has been used in numerous ways, including transport, water pumps, or the milling of grain. Before the steam engine, water mills and windmills were the most important sources of energy. Among the earliest records of wind power came from the Egyptians, who used it as a means of powering their boats on the Nile 5000 years ago [11]. Later, one of the earliest windmills was created by Heron of Alexandria in Egypt under the Romans around 2000 years ago. This was understood to be the first instance of wind power being used as a fixed source of power [12]. The Persians were known to be using vertical axis windmills fast a means of grinding grain in the tenth century, and this technology had been adopted by the Chinese by the thirteenth century [13]. The Dutch were known to be using windmills as long ago as AD 1350 in order to pump water from low-lying areas to reclaim land for agricultural use. By the nineteenth century, the Americans were constructing windmills in the form of vertical steel structures which had a rotating multibladed drag or impulse propeller which could be turned by the flow of the wind. The rotation would then be converted into a form of linear motion in order to pump water from the ground which could then be stored for irrigation, for cattle, or for steam engines [14].

Although windmills had already been used for milling grain or pumping water, the first time one was used to generate power from wind energy was constructed in 1887 in Scotland by James Blyth of Strathclyde University in Glasgow. He built a small-scale windmill capable of generating electricity which could then be diverted to storage cells in his garden and used to power electric lights. Although generating power on a small scale, his windmill was large, comprising a vertical axis and a set of cup-shaped blades exposed to the wind. The wooden tower was of a tripod design which had the windshaft positioned about ten meters high, with four canvas sails of four meters in length set perpendicular to each other. A Burgin dynamo was then connected to the flywheel using a rope, allowing the windmill to operate even when the wind speeds were relatively low. Blyth’s house thus became the first in the world to have wind-powered electric light, and was able to operate in this manner for 25 years [15]. At around the same time, in 1888, an American, Charles Brush, constructed a windmill in Ohio to generate electricity for his mansion. It was large, with a tower 18 m high and 6 m wide. The diameter of the rotor was 17 m, with 144 cedar rotor blades. Although the wind turbine was huge, it only provided power for a 12 kW electric generator, because American wind turbine designs were rather inefficient due to the slow drag force on the wind turbine. This particular windmill was also the first to make use of a step-up gearbox, in this case setting a gear ratio of 50:1 so that the DC generator could turn at the necessary operating speed of 500 rpm. This wind turbine ran successfully for 20 years, charging batteries which were installed in the mansion [16].

The breakthrough from traditional windmills to the modern power-generating wind turbines was made by Poul La Cour in Askov, Denmark. He developed the first modern wind turbines which were specifically created for the purpose of generating electrical power in order to supply the Danish government in support of a rural electrification program in 1891. In this case, the experimental wind turbine was designed to drive a dynamo, although in many ways the design followed traditional models. While La Cour understood the benefits of aerodynamic windmill sails, he instead chose to employ a rotor which had four shutter sails. This did not work to the detriment of the design, however, and the Lykkegard company soon began to produce the design for industrial purposes. La-Cour-Lykkegard wind turbines were soon produced in a range of sizes, while the power output ranged from 10 kW to 35 kW. Since the largest rotors had a diameter of 20 m and four shutter sails, it was feasible to operate below a set limit for rotational speed. Yawing was managed by a pair of fantail side wheels, while the generator was located at the bottom of the tower where it could be driven by a long rotor shaft controlled through a gearbox. The electrical power it generated could then be sent to small consumer grids through a buffer battery. One advantage of this wind turbine design was the high degree of reliability they exhibited. Some were reported to have operated from 1924 until 1943 without having to replace the gear or bearings until at least 20 years had passed [17]. In 1941, the first wind turbine capable of generating a megawatt of electricity was constructed near Rutland, Vermont, USA. Its designer, Palmer C. Putnam, was interested in building a wind powered generator to lower the cost of electricity for his house at Cape Cod, and so created this 1250 kW wind turbine. Initially, the idea was presented to the S. Morgan Smith Company of York, Pennsylvania, who examined the preliminary results and approved the funding of the project, which came to be known as the Smith-Putnam wind turbine experiment. The aim was to link the wind turbine to the Central Vermont Public Service Corporation network. This particular facility also incorporated some hydro-electric generating capacity, which allows for operational convenience whereby water can be stopped when the wind blows, and then allowed to flow if the wind drops, so it is always possible to be generating power. The tower of the Smith-Putnam structure had a height of 34 m while the rotor had a diameter of 53 m. The distance from the leading edge to the rear edge of the rotor, also known as the chord length was 3.45 m. The two blades had a weight of 7300 kg and had ribs made of stainless steel which supported a stainless-steel skin. The adjustable blade pitch allowed the rotor to hold a steady speed of 28.7 rpm, which could be maintained even when the wind speed was as fast as 32 m/s. If the wind exceeded that speed, the blades could then be feathered, and the machine halted. The rotor served to power an AC synchronous generator capable of generating 1250 kW of electricity when wind speeds exceeded 13 m/s [18]. In 1980, New Hampshire, USA, became the site of a new wind farm comprising twenty 30 kW wind turbines offering a total capacity of 600 kW. This wind farm did not succeed, however, for two reasons, Firstly, the wind turbines were unreliable and prone to malfunction, and secondly, the wind conditions did not meet the requirements for efficient operation [19]. More recently, the Vestas company began to operate its largest new wind turbine with a capacity of 9.5 MW, known as the MHI Vestas V164-9.5 MW. While these wind turbines have now been installed at various sites worldwide, the latest project has involved 77 of these wind turbines being installed at the Borssele III/IV site in the North Sea off the coast of the Netherlands [20]. More recently, GE Renewable Energy created a 14-MW capacity wind turbine known as Haliade-X which had an enormous rotor diameter of 220 meters, making it the world’s largest to date in 2020. It was intended for installation at the Dogger Bank wind farm located in the North Sea off the British coast [21]. The largest onshore wind farm in the world today is the Gansu wind farm project located in Gansu province, China. The planned capacity stands at 20 GW, but at present only 8 GW has been achieved. Construction work commenced in 2009 as part of a series of major wind power projects promoted by the Chinese authorities. It was expected to reach completion during 2020 [22].

Vindeby, Denmark, was the location of the first wind farm to be constructed offshore in 1991. The farm comprised 11 wind turbines, each of 400 kW capacity, amounting to 5 MW in total. The project employed a simple design, using onshore wind turbines which had been mounted on concrete foundations positioned in relatively shallow water. This was a government project, designed to supply 100 MW demanded by the state [23]. Currently, the largest offshore wind farm is located in the North Sea around 120 km off the coast of Humberside in the UK. The project is known as Hornsea 1 and was first installed in 2019 with 174 Siemens Gamesa 7 MW wind turbines capable of generating a total capacity of 1.218 GW. This was the first offshore wind farm capable of exceeding 1 GW in total output, and it is expected to be able to meet the electrical demands of around one million households in the UK [24]. The first FOWTs was developed for use by the Dutch company, Blue H Technologies in 2008. The prototype was a deep-water platform fitted with an 80 kW wind turbine. It was operated 21 km off the Italian coast near Puglia in water which had a depth of 113 m. The aim was to use the small prototype to obtain data concerning sea and wind conditions, and this task was completed by the end of the year. This Blue H Technologies design involved a tension-leg structure and the wind turbine had two blades. This kind of blade design allows a greater chord length than the three-bladed designs, and thus leads to greater tip speeds. In 2009, Blue H constructed a commercial 2.4 MW wind turbine in Brindisi, Italy, ready for installation in the Adriatic Sea by 2010 [25]. The world’s first floating offshore wind farm is the Hywind project which is in the North Sea off the coast of Scotland. This farm has five wind turbines, each capable of producing 6 MW, so the total capacity stands at 30 MW. These FOWTs have rotor blades of 154 m and have anchors fixing them to the seabed, which is at depths of 120 m. The Hywind project commenced operation in 2017 and generates enough electricity for 22,000 households. In terms of offsetting carbon emissions, this is the equivalent of 63,000 tonnes annually [26].

1.3 Historical Wind Energy Background in Thailand

Wind energy has a long history in Thailand, and traditional wooden windmills can still be seen in rural areas, usually for the purpose of pumping water used to irrigate rice fields or in the farming of prawns. American-style windmills with multiple steel blades are also used in the agriculture sector, predominantly for pumping water [27].

Over a nine-year period from 1983 to 1992, the Electricity Generating Authority of Thailand (EGAT) conducted a study of wind turbine efficiency focusing on a location at Promthep Cape, Phuket, in the south of Thailand. Small wind turbines offering a total capacity of 42 kW were used to test the feasibility of electricity generation. The results were deemed to be satisfactory, and in 1990, EGAT decided to link their wind turbines to the distribution network of the Provincial Electricity Authority (PEA) to supply electricity, and to test the application of grid connected distribution systems, since this was the first instance of wind power being used to generate electricity for distribution. The distribution trial was also a success, and therefore EGAT extended the project via the installation of two further 10 kW wind turbines connected to the grid. Then in 1996, a 150 kW wind turbine was added, which was the largest ever to have operated in Thailand. The wind power technology was shown to be reliable in generating electricity and was also commercially viable. Although some of the smaller wind turbines fell into disrepair and were abandoned, the final capacity of the project stood at 170 kW [28]. In 2009, EGAT embarked upon a second project located at Lam Takhong Dam in Nakhon Ratchasima province. The aim was to create a learning center focusing on renewable energy, which would also serve as a destination to attract eco-tourists. This would operate in line with the government's policies on renewable energy and would also serve to support the extension of electricity supplies into rural areas. The initial phase opened with a pair of 1.25 MW wind turbines, before the second phase in 2017 which added a further twelve 2 MW wind turbines. Each had rotor blades of 116 m in diameter mounted on towers of 94 m in height, amounting to a total electrical power capacity of 26.5 MW [29]. In another project starting in 2008, the Department of Alternative Energy Development and Efficiency (DEDE) began to operate a pair of wind turbines at Hua Sai, in Nakhon Si Thammarat, Thailand. The first had a capacity of 250 kW and the second was larger at 1.5 MW. This project sought to show off the future potential for electricity generation from wind power, and to encourage private sector participation and investment in wind energy [30]. The DEDE then enlisted the support of King Mongkut's University of Technology Thonburi, and Prince of Songkla University to develop low wind speed experimental wind turbines located at Sirindhorn International Environmental Park, Phetchaburi, Thailand. This project had three 1 kW wind turbines capable of low speed operation which could serve as prototypes for study, since much of Thailand experiences wind speeds which typically do not exceed 4 m/s [31]. Thailand's first wind farm was constructed in 2007 on the island of Koh Lan, Chonburi, with the goal of supplying electricity to the island. In total there were 45 wind turbines of 4.5 kW capacity each, allowing the farm to generate around 200 kW. This project was developed and managed by Rajamangala University of Technology Thanyaburi (RMUTT) [32]. There were numerous other wind farms around Thailand which used imported megawatt size wind turbines. These included major wind farms in the provinces of Chaiyaphum, Nakhon Ratchasima, Phetchabun, and Songkhla [33]. The effect of these projects was to raise the total capacity for wind energy in Thailand to 1,507 MW [5].

1.4 History of the R1235 Airfoil Blade in Thailand

In 2009, the King Rama 9 Chang Hua Man Royal Project in Phetchaburi province sought to develop a wind farm to provide electricity. The project had twenty wind turbines, each of 5 kW capacity, generating 100 kW in total. The R1235 airfoil blade was specifically created for use in areas with low wind speeds by Prof. Dr. Wirachai Roynarin from RMUTT. This was the first wind turbine to be designed in Thailand. Its components were manufactured in Thailand, with the exception of the generator [34]. Following the success of this project, the R1235 airfoil blade was used in numerous other projects around the country. For example, ten 5 kW wind turbines came into operation at the Agricultural Development Station at Doi Mon Lan, Chiang Mai, in 2010, mixing different alternative energy sources using wind power, solar power, and diesel generators [35]. In 2011, the R1235 airfoil blade was used for wind turbines installed at Laem Chabang port in Chonburi, as part of a drive towards environmental protection. A total of 84 wind turbines were installed, each of which offered a capacity of 10 kW for a total of 840 kW. The electricity generated was used in the port to provide lighting for streets and storage facilities [36]. More projects around the country also adopted the R1235 airfoil blade including the Coastal Fisheries Research and Development Center in Klongwan, Prachuap Khiri Khan, which had a capacity of 10 kW, the Nong Pla Thao Public Park in Chaiyaphum in 2018 which had four wind turbines offering a total of 40 kW used to pump water through a treatment plant, and the Sarae Aditaya Agricultural Project which had five 10 kW wind turbines producing electricity for local consumption by 2020 [37]. Meanwhile, the largest R1235 airfoil blade to be designed which had a capacity of 100 kW became operational at the MRP Engineering Company in Chonburi to supply the business with electrical power. In 2018, the province to supply electricity for industrial purposes [38]. Then, in 2018, the Department of Industrial Works, the National Innovation Agency (NIA), and RMUTT modified the R1235 airfoil blade to serve in air compressors for industry, building a 5 kW compressed air wind turbine to use for pumping water at reduced cost, increasing the air flow in the system, lowering the loss of air, and improving the air stability in the system. The standard compressed air system requires compressors and storage tanks, but the wind turbine can be used simultaneously alongside the original system [39].

1.5 Purpose of This Study

This study was conducted to achieve the following aims:

1.5.1 To study the influence of tilt angle upon FOWTs performance using a small model.

1.5.2 To analyze results and draw comparison between an experimental model and a CFD simulation model.

1.6 Scope of This Study

This study comprises experimental testing using a wind tunnel, and simulations using Computational Fluid Dynamics (CFD) software. The scope includes:

1.6.1 The use of R1235 blades for the study models

1.6.2 The experimental wind turbine in both fixed tower and FOWTs scenarios has a diameter of 820 mm

1.6.3 Testing using wind speeds from 2 m/s to 5.5 m/s in the wind tunnel and CFD simulation

1.6.4 Evaluation of the tilt angle effects on the wind turbine blade performance of the FOWTs

1.6.5 The use of a CFD k-ε turbulence model to draw comparisons with the wind tunnel experimental results

1.7 Benefits of This Study

1.7.1 The first study of FOWTs technology conducted in Thailand

1.7.2 Test results obtained for both fixed tower wind turbines and FOWTs

1.7.3 Results providing useful insights into the optimization of power coefficients by applying variable tilt angles for small-to-medium fixed pitch FOWTs in order to lower the cost of using pitch control mechanisms

1.8 Thesis Outline

CHAPTER 1 INTRODUCTION

Chapter 1 describes the background of the study and provides an explanation of the purpose and scope along with a broad overview.

CHAPTER 2 LITERATURE REVIEW

In Chapter 2, a summary of the literature review pertaining to FOWTs is outlined.

CHAPTER 3 THEORY

Chapter 3 presents the theoretical background which explains the parameters to be evaluated in developing a better understanding of FOWTs.

CHAPTER 4 METHODOLOGY

Chapter 4 presents a description of the methods used, the material required, and the techniques applied in analyzing the FOWTs experimental models in the wind tunnel and performing the CFD simulations.

CHAPTER 5 RESULTS AND DISCUSSION

In Chapter 5, the results are discussed concerning the fixed tower wind turbines and the FOWTs for both the experimental models in the wind tunnel and the CFD simulations. The effects of the tilt angles are discussed and compared along with the performance parameters including rotational speed, tip speed ratio, and power coefficient. The wind speeds in the experiments were in the range of 2 m/s to 5.5 m/s, and the tilt angles ranged from 3.5° to 6.1°.

CHAPTER 6 CONCLUSIONS

The final chapter presents the conclusions of the study and provides recommendations for managing the tilt angle to improve the FOWTs performance.

CHAPTER 2
REVIEW OF THE LITERATURE

The following chapter presents a review of the literature pertaining to the current study topic of onshore and offshore wind turbines.

2.1 The Impacts of Onshore Wind Turbines

Floating Offshore Wind Turbines (FOWTs) represent the next generation of wind energy conversion technology. It could improve the wind turbine potential to harness wind energy at greater ocean depths where higher wind speeds are often to be found. Also, they could compensate for the disadvantages of onshore wind turbines that affect both the environment and human health. The Global Warming Policy Foundation states that the primary drawbacks of onshore wind turbines include the noise impacts, visual impacts, wildlife impacts, and issues related to land use [40]. There are several studies which have been conducted on the disadvantages of onshore wind turbines. For example, Kondili and Kaldellis (2012) observe that the principal environmental issues related to wind farms are the noise, the poor aesthetic aspect, and the adverse consequences for local wildlife [41]. Saidur et al. (2011) also pointed out that wind energy, while relatively clean, is not wholly a positive strategy. Problems include the deaths of wildlife species which come into contact with the wind turbines and are killed by the blades. Furthermore, the noise created by the wind turbines when the wind blows can be disturbing for those who live nearby. The visual aspect is also very important, as many windfarms are visually unattractive, and have a negative impact upon otherwise scenic areas [42]. In addition, Wang and Wang (2015) examined the evidence concerning the environmental effects of wind energy production including the consequences of noise pollution, greenhouse gas emissions, fatal accidents involving birds and bats, and also the impact upon the land area of the wind turbine site. Those authors note that the wind will be an important source of energy in the future, but prior to investing heavily in wind farms, consideration should be given to the environmental concerns give that the generation of wind power does cause environmental harm, especially through noise pollution. To date, however, no comprehensive evaluation has been carried out which compares wind power with alternative technologies, and which would therefore allow informed discussions and decisions to be made when considering the implementation of wind power and the costs and benefits of doing so [43]. The work of Nazir et al. (2020) touches upon harmful environmental consequences of wind energy, noting that these include noise, land erosion and deforestation, and also the visual impact of the wind farms. It is reported that the environmental impact is complex, and also that it is not consistent over time, with its severity changing with the seasons, the location, the prevailing climate, and the type of local ecosystem. The impacts can often be cumulative, and in some cases the adverse consequences can be exacerbated by each other through complex interactions leading to potential problems for human health around wind power sites [44].

2.2 Offshore Wind Turbines

There are several methods that could minimize the wind turbine impacts, including working closely to standardize the wind turbine policies, and carefully designing and planning for wind farms. However, another solution that would reduce the wind turbine impacts and improve the wind turbine performance at the same time could be offshore wind turbines.

There are several studies which have suggested that OWTs offer benefits as an alternative solution for wind turbine technology.

Leung and Yang (2011) describe the attraction of offshore wind power, noting that as a novel energy source it offers a number of advantages over the onshore variant. At present, the countries of Europe are taking a leading role in developing the technology for offshore wind farms, while in other parts of the world, the USA and China are also moving forward in this field [45].

The work of Dinh and McKeogh explains that there are a number of advantages offered by offshore wind energy, one of which is the potential for a substantially lower cost. Wind speeds offshore tend to be relatively stable, thus minimizing the wear upon the mechanical components of the wind turbines, reducing maintenance costs and increasing the equipment lifespan. Moreover, the greater speed of offshore winds, along with a reduction in wake effects, can lead to an increase in overall power generation in the range of 45-60%. There is less variability in the ocean weather, and this allows more hours where the equipment can operate at a full load level throughout the year. The fact that offshore winds are usually stronger during the daytime, when power consumption is also at its highest, means the energy production takes place in a much more timely manner, adding to the overall efficiency of the system [46].

The latest trends in large-scale offshore wind farms are investigated by Ramos et al. (2019) who focused on those farms in Europe offering an installed capacity exceeding 150 MW. The findings concerning trends indicate that the expected power capacity by 2025 will be 47.4 GW while by 2030 it will reach 76 GW. Offshore wind farms are expected to number 139 projects by 2025, rising to 172 by 2030. Europe is currently the major developer of offshore wind farms with a capacity above 150 MW, with Germany and the UK the most prominent, accounting for around 8% of the total capacity. China is becoming increasingly important, however. In comparison to other sources of energy, the costs of power generated by offshore wind farms are highly competitive. As this source has grown, the global weighted average levelized cost of energy (LCOE) saw a drop of at least 13% from 2010 to 2017. It is anticipated that projects starting after 2020 will see capital expenditure (CAPEX) fall by around 22% in comparison to the years from 2013 to 2017. It is also expected that operating expenses (OPEX) will drop by 2025, with the decrease falling in the range of 27-43% [47].

Bilgili et al. (2010) note that the offshore wind energy tends to be faster than those onshore, increasing the potential electricity production. It is anticipated that the development of offshore wind energy will expand substantially during the next two decades; by 2008, the total capacity for OWTs in Europe were already 1471 MW, amounting to 2.23% of the overall European wind power capacity. Furthermore, it is expected that by 2030, the projected installed capacity of 150 GW will generate 563 TWh of electricity, amounting to as much as 16.7% of the total electricity consumption in the EU, assuming demand for power matches forecasts. By this point, half of Europe's wind energy would be generated from OWTs [48].

Haraldsson et al. (2020) made use of social-ecological system (SES) modeling as a means of understanding the relationships between humans and the environment when developing offshore wind farms, and understanding how the structures affect ecosystems and the quality of human life. A qualitative mathematical modeling approach makes it possible to rapidly assess the properties of a system without the need for quantitative data, these allowing comparisons to be drawn between alternative systems by considering the way each system works. The inclusion of similar numbers of variables from the systems when creating the subsystems allows a balance of complexity to be achieved. The findings indicate that the participation of stakeholders in local socio-ecological systems provides greater benefits for that society overall. Heightened levels of involvement through project participation or a rise in job opportunities based on the offshore wind farm can help to counterbalance any negative impacts from the offshore wind farm upon the local community. Further enhancement of such benefits occurs when the windfarm is fully accepted by local communities [49].

Smythe et al. (2020) conducted some interesting research into the idea of wind farms and tourism, examining how the changes to the seascape will be perceived by visitors to a particular area. The study focused on the Block Island Wind Farm, a 30 MW facility which was the first offshore wind farm to be developed in the USA, and which stands in a location popular with tourists. This site is therefore an ideal candidate for further examination to learn how offshore wind farms can affect tourism and recreational activity. A number of focus groups were staged involving tourism professionals who discussed their own observations and experiences concerning this particular offshore wind farm project. While opinions differed strongly, they were broadly positive, although in any kind of cost benefit analysis there will be negative aspects identified, as was the case in this study. Opinions were heavily influenced by the way participants perceived the planning process. The visual impact of the offshore wind farm was considered highly important, although a majority of the respondents had neutral or even positive feelings towards the appearance of the offshore wind farm. In general, the offshore wind farm was perceived to be likely to attract visitors through its novelty, or its ability to serve as a site for recreational fishing. The participants argued that the site had some potential for promotion as a tourist attraction, but noted that the interest may only be present in the short term, and that this interest might not extend to other, larger, offshore wind farm projects [50].

2.3 Previous Research Studies

William Heronemus of the University of Massachusetts achieved fame around the start of the 1970s as he devised the first floating wind power generator, which comprised a number of rotors which would either produce electricity or hydrogen, as can be observed in Figure 2.27 [51][52].

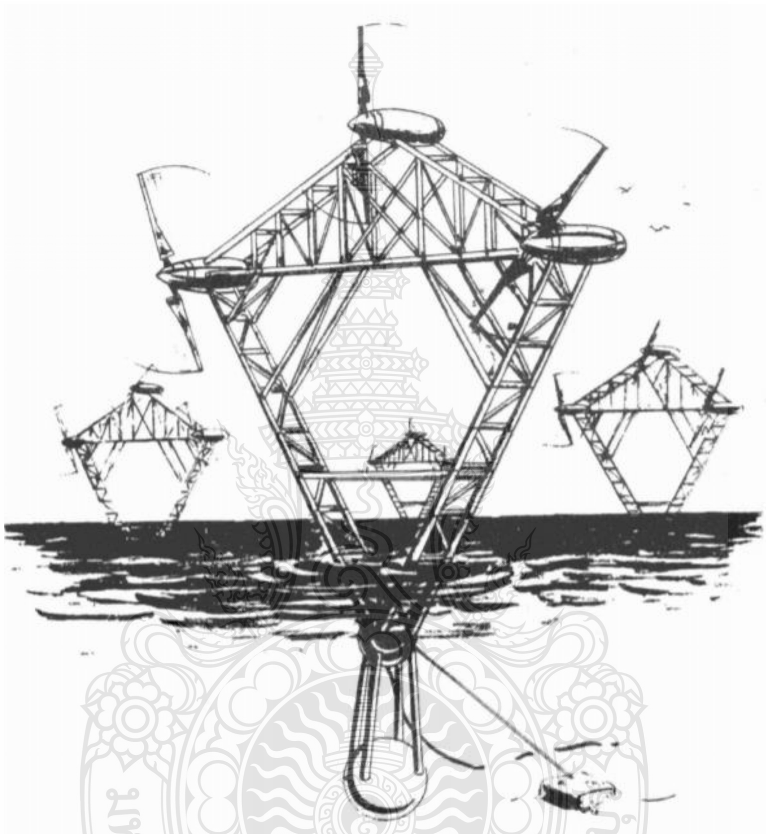

Figure 2.1 Design for a multiple-array wind turbine structure [52].

A dynamic response analysis was performed by Robertson and Jonkman (2011) to assess six FOWTs concepts. The six models each involved identical NREL 5 MW wind turbines and aimed to address the question of balancing the various aspects of FOWTs design to optimize the floating system concepts. The six models comprised the following platforms: MIT/NREL tension leg platform (TLP), the OC3-Hywind spar-buoy, the UMaine TLP, the UMaine-Hywind spar-buoy, the UMaine semi-submersible, and the ITI Energy barge system. All platforms were tested at two differing depths. For each model, the overall performance underwent comparisons with the performance of a base model involving a wind turbine supported by an onshore fixed tower based. Assessment of the performance was based on stability analysis and comprehensive loads, in line with the standards set by the International Electrotechnical Commission (IEC) 61400-3 design standard for OWTs. Under testing conditions, all the models were subjected to greater loads upon the components of the wind turbines than was the case for land-based systems, and therefore require to be made stronger. The ITI Energy barge saw the highest motion-induced ultimate and fatigue loads exerted upon the wind turbine components when comparisons were drawn among the six model types. The TLP systems had rather different designs, but the responses generated by each were found to be quite similar to each other, indicating that the chosen approach for floating system stabilization has a greater effect upon the system dynamics than is the case for the actual design details. While the ultimate and fatigue loads do show small differences between TLP systems and the spar-buoy and semi-submersible systems, these are not statistically significant with the exception of the tower loads, which were smaller in TLP systems. The OC3-Hywind spar-buoy system model is more stable than the ITI Energy barge system in terms of pitching and rolling motion, but its performance is far less stable than the TLP systems which display minimal rolling and pitching. Meanwhile, the UMaine semi-submersible system shows the greatest similarity to the spar-buoy system motion, although the heaving motion is greater, and the pitching less [53].

Bagbanci (2011) performed research into fixed monopile foundations as well as examining other concepts related to FOWTs such as spar-buoy, barge platform, and semi-submersible designs capable of supporting NREL 5MW wind turbines through the use of WAMIT software and the FAST code created via NREL. For fixed wind turbines, the effects of the local conditions on the design loads for a wind turbine in the case of monopole foundations can be assessed by measuring the bending moment which arises at the base of the tower and at the tower root when taking into consideration the height of the tower and the depth of the water along with the diameter of the piling and the turbulence model. To study FOWTs, fully-couple dynamic analysis requires the use of a numerical time-domain model, while the floating platforms' hydrodynamic properties can be assessed using the panel method. The forces for hydrodynamic added mass, damping, and exiting can be obtained for the frequency domain, whereupon the results can be used for validation. By combining the hydrodynamic study of the floating platform with analysis of an aerodynamic model, it is possible to develop an aero-servo-hydro-elastic model. The moorings for such systems are typically fixed to the floaters. For the FOWTs of the spar-buoy type, three mooring lines are used, while for the barge platform type, the floaters are attached by eight mooring lines with a pair of lines at the corner of each floater. Meanwhile, semi-submersible designs have four connecting mooring lines. Mooring lines can increase the floater stability, and it is apparent that when the number of lines is increased, the pitching motion of the floater is reduced. When exposed to surge motion, the semi-submersible type offers greater stability than the wind turbines of the barge platform and spar-buoy types. When faced with pitching and heaving, however, the spar-buoy type wind turbine offers better stability than the other types. For pitching, the semi-submersible design performs worse than the barge platform type, but if the motion involves swaying, rolling, yawing, and surging, the barge platform type performs better. Simulation results were also obtained for the motion of the platform and tower base using different wind speeds while the wave heights and headings are held constant, with the wave heading angle set to 30º. As wind speed increases, there is an increase in surge and pitch motion until the wind reaches 12 m/s. At 24 m/s, however, the motion declines, as would be expected as a result of using the blade pitch controller of the wind turbine. The rolling and yawing motion tends to rise with wind speeds under the simulation conditions [54].

A summary of WindFloat technology is offered by Roddier (2010), who summarizes that the WindFloat is a semi-submersible floating foundation with three legs which is suitable for multimegawatt FOWTs. The design is created to hold a 5 MW wind turbine, or larger, on one column of the hull, while it is not necessary to make any notable changes to the rotor and nacelle. The technology applied in floating foundation design for FOWTs continues to evolve, so this study initially emphasizes the design of the floating foundation and then considers the concepts which must be taken into account by designers working in this developing field. This will include analysis of the hydrodynamic properties of the hull, as well as the need to integrate hull hydrodynamics with consideration of the aerodynamic forces affecting the wind turbines. There are three principal approaches which can be taken: development of a numerical hydrodynamic model for the platform and mooring system; scale model tests in a wave tank with basic aerodynamic simulation for the wind turbine; use of FAST code, which is an aero-servo-elastic software package allowing analysis of wind turbines and capable of linking to the hydrodynamic model. The analysis finally examines factors of structural engineering including strength and fatigue analysis with a focus on the joints between the hull and the wind turbine, as well as the interface of hydrodynamic loading and the structural response [55]. Roddier et al. (2011) add that semi-submersible technology has a number of benefits, including the fact that the construction and assembly can all be performed on land before towing the completed structure out to sea for installation. The fitting of the wind turbine is done before the deployment at sea, which reduces the costs which would be incurred if heavy barges or other vessels necessary for installation had to be used to convey wind turbines separately. The current authors have altered their original WindFloat concept in order to fit a 5 MW wind turbine. Inertial resistance to unwanted movement is achieved by fixing octagonal heave plates at the column base. The platform displaces 4640 tonnes, representing a 60% weight saving over an alternative spar-buoy design which could carry a wind turbine of this size. Furthermore, the draft is only 17 m, which is substantially less than the 120 m draft of a spar-buoy design. However, as a result, the performance of the spar-buoy in terms of hydrodynamic motion in stormy sea conditions will offer greater stability than the semi-submersible design [56].

Research into semi-submersible FOWTs was conducted by Chen (2018), who tested two different models: a model with geometrically matched blades, and a model with performance-matched blades. A wind/wave basin was employed to carry out the test procedure. The dynamic properties of the two different models were then compared in order to assess the model validity and to set references for the future optimization of FOWTs models. The study reported that the two models were both able to exhibit the required dynamic characteristics but some differences were observed in terms of the system eigenfrequencies and the response amplitudes. In comparison to the geometrically matched blade model, the aerodynamic qualities and effectiveness of the performance-matched blade model were clearly superior. However, the performance-matched blade model had overweight blades, resulting in differences in comparison to the yields obtained by the original design. [57]

Platform pitching motion was examined by Tran (2015) in the context of FOWTs along with a preliminary aerodynamic analysis. The study investigated the periodic pitching of the wind turbine blades as they rotated as a consequence of the platform motion in evaluating the vortex–wake–blade interactions which influence the overall aerodynamic performance of the FOWTs. CFD simulations using the dynamic mesh technique were implemented to assess the wind turbine pitching resulting from the motion of the platform. The in-house unsteady blade element momentum code using a direct local relative method (DLRM) was used for the simulations of unsteady aerodynamic performance. Meanwhile, the equivalent average method (EqAM) was also applied as a means of simplifying the relative velocity contribution which results from the movement of the platform This factor was then added to the in-house code. The findings revealed that unsteady aerodynamic loads for the FOWTs can undergo changes as a consequence of variation in the amplitude and frequency of the movement of the platform. Furthermore, powerful flow interaction phenomena exist between oscillating rotating blades and the blade-tip vortices which are generated [58].

Wen et al. (2018) observed that in FOWTs, the pitching motion of the platform will have an effect upon the wind profile of the rotor and can therefore have an impact upon the efficiency of the wind turbine in generating electrical power. The Free Vortex Method (FVM) offers a means of examining the power performance of a pitching FOWTs platform. In the opening step, comparisons are drawn between the pitching and non-pitching scenarios, and then the power output for the FOWTs are various pitching amplitudes and frequencies is evaluated for the design point (using a tip speed ratio of $\lambda = 7$). Measured at the design point, there is a rise in the mean power output in pitching conditions when compared to the alternative with the fixed foundation. As the pitch amplitude and frequency of the platform increases further, the power output also rises, with the caveat that the mean power coefficient is lowered while there is a rise in power fluctuation. A lowered frequency k is suggested in order to better to integrate the effects of pitching amplitude and frequency on the platform. The pitching of the FOWTs leads to power performance curves which can be derived as functions of λ and k over the entire operating region. The findings reveal that as k rises, the mean power output falls at low values of λ but rises at high values of λ. Meanwhile, the mean power coefficient falls as k increases, while power variation is increased as λ and k increase [59]. Further work was carried out by Wen et al. (2018) who examined FOWTs power performance in surge oscillations, revealing that it is possible for the instantaneous power coefficient to exceed the Betz limit in circumstances where the tip speed ratio is close to optimal and there is sufficient severity of the surging motion of the platform. This situation is known as a power coefficient overshoot. The numerical simulations involving FVM confirm that power coefficient overshoots are the result of a time lag which occurs between the power output and the power of the wind farm. If the surge frequency increases, this time lag and power coefficient overshoot become more prominent. According to the results from equivalent dynamic modeling, this time lag is primarily a consequence of the effects of added mass, which can be further amplified by the surge frequency. As a result, the time lag and power coefficient overshoot can be explained in part by the unsteady profile dynamics and also by the blade- wake interactions [60].

The work of Wang (2020) examined the practical significance of tilt angles upon fixed wind turbines by assessing the aerodynamic performance via the CFD STAR-CCM+ method. The investigation set tilt angles of 0°, 4°, 8°, and 12° on the basis of a uniform wind speed and wind shear. It was found that when the tilt angle changed, the airfoil section of the wind turbine blade has an altered angle of attack, thus changing the power levels delivered by the wind turbine. The best aerodynamic performance for the wind turbine occurred when the tilt angle was set to around 4°. However, wind shear can lower the power of the wind turbine, while the influence of wind shear exponents upon the aerodynamic performance becomes much greater than the anticipated influence of turbulence intensity [61].

Gumula (2016) investigated the effects of controlling the wind turbine rotor axis by taking into account the wind direction to see if this would affect the total energy volume generated by the wind turbine. The importance of optimal blade settings for the wind turbine rotor was also a focus of that study. The measurements suggest that if the axis tilt angle is changed in the context of the air flow direction, this will result in changes in the efficiency of wind energy usage. The influence of the operating conditions for wind turbines upon the effective potential of wind energy is also considered, noting that a number of factors will have an effect upon the way the wind turbine is operated and therefore upon the total energy generated. These factors can include the wind power plant design parameters as well as factors pertaining to location or climate. It has been shown to be very important to set the rotor axis direction in alignment with the air flow, and accordingly it is necessary to be able to identify the optimal angle for the rotor axis since this will have a powerful effect upon the operational characteristics of the wind turbine [62].

Abdelsalam (2013) carried out horizontal axis wind turbine simulations by directly modeling the rotor blades in order to understand how the wake development takes place and to predict the extent to which power is available in the wake to serve downstream wind turbines. To test the levels of power extracted from the wind turbine and available in the wake, the study used varied tilt angles for the blades from 0° to 15°. The findings indicate that the loss in rotor power can be as high as 14% when the tilt angle is set to 15°. However, when the rotor blades are tilted, the effects upon the wake are significant, with power recovery gains in the downstream region growing as the tilt angle increases, especially in the region close to the wake. When taking into account the separation distance between wind turbines and the upstream wind speeds, it may be possible to operate the upstream wind turbines at sub-optimal levels in terms of the tilt angle selection, yet still increase the overall power output due to beneficial effects upon the downstream wind turbines [63].

CHAPTER 3
THEORETICAL BACKGROUND

3.1 Wind Energy Characteristics

The flow of air around the globe results from areas of different of pressure, the absorption of solar radiation, and the extent of relative humidity. In each particular location it is necessary to assess wind speeds because the design of wind turbines and the configuration of the blades must be appropriate. The wind speed factors which must be taken into account from a design perspective are the mean wind speed, the distributions of speed over time, and the speed of the wind at different heights, which is important when choosing the location [64].

3.1.1 Global Winds

At the global level, winds arise as a consequence of differences in the absorption of solar radiation at different areas on the surface of the planet, which then leads to pressure differences. The wind is created as air flows from high pressure zones to low pressure zones, in the same manner as air from hot areas flowing to areas with low temperatures as can be seen in Figure 3.1. The equator is the zone which has greater solar radiation than is the case at the poles, and the differences in this absorbed radiation serves to form areas of convective activity located in the troposphere as can be observed in Figure 3.2. As a result, circulating winds are generated around the equator which sink towards the poles. This atmospheric circulation is further affected by the Earth's rotation, as well as the variation in solar distribution throughout the year as the seasons change [65].

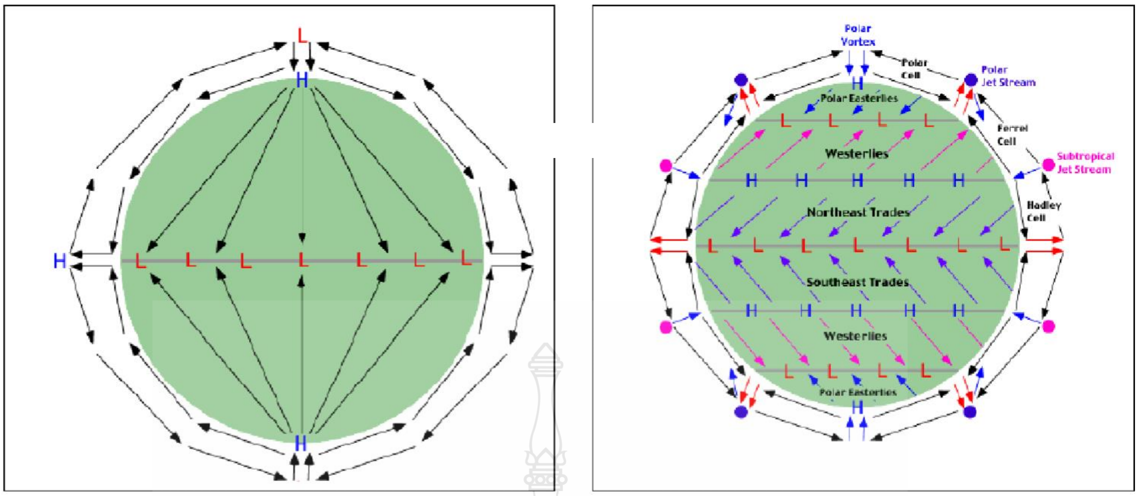

Figure 3.1 Global winds [64].

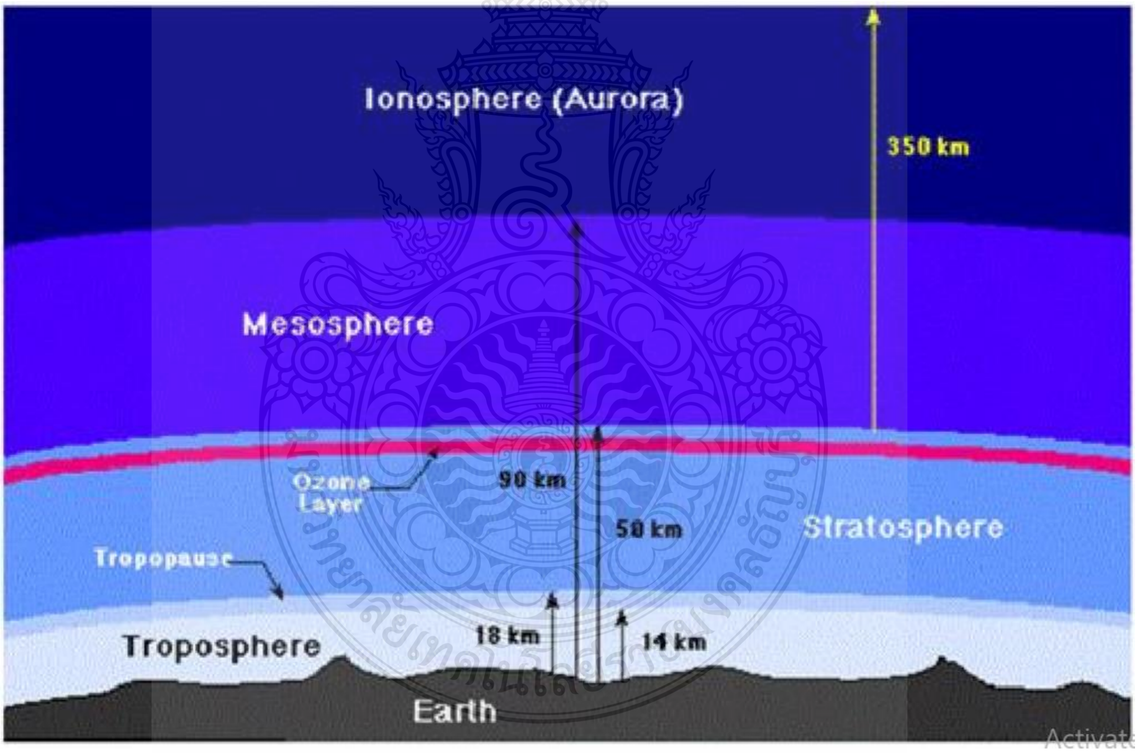

Figure 3.2 Surface winds [65].

3.1.2 Local Winds

The attributes of local winds are determined by the combined influence of both global effects and local factors such as mountains, bodies of water, buildings, forests, etc.

3.1.2.1 Land and Sea Breezes

During the mornings, land temperatures tend to increase more quickly than those at seas, and therefore the warm air over the land will rise and flow out to sea while cool air flows inland creating the sea breeze, as indicated in Figure 3.3. The land and sea temperatures tend to be equal by the evening, but the land loses heat faster causing the wind to flow in the opposite direction, creating a land breeze which can be seen in Figure 3.3. However, the temperature differences will be small, so these winds are not strong [65].

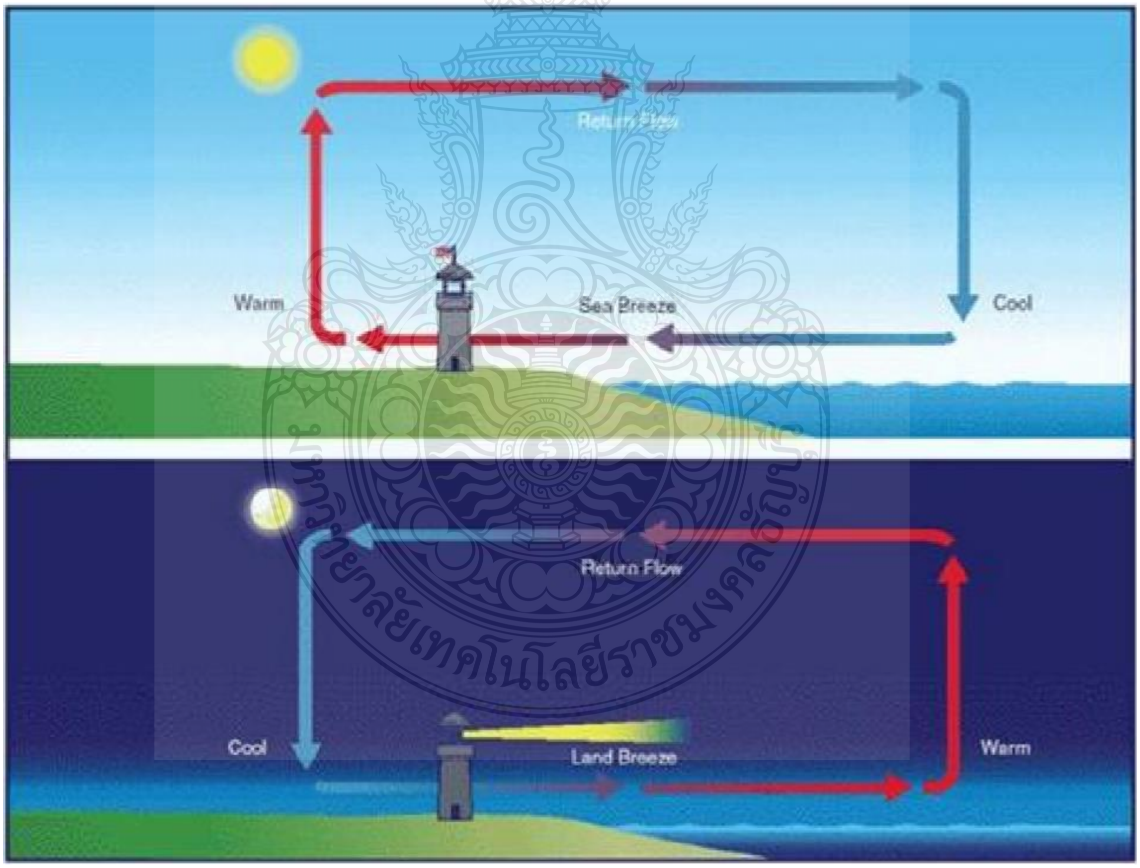

Figure 3.3 Land and sea land breezes [65].

3.1.2.2 Valley and Mountain Breezes

Figure 3.4 illustrates the warm air rising towards the top by following the surface of the valley sides during the morning, whereas this is reversed during the evenings [65].

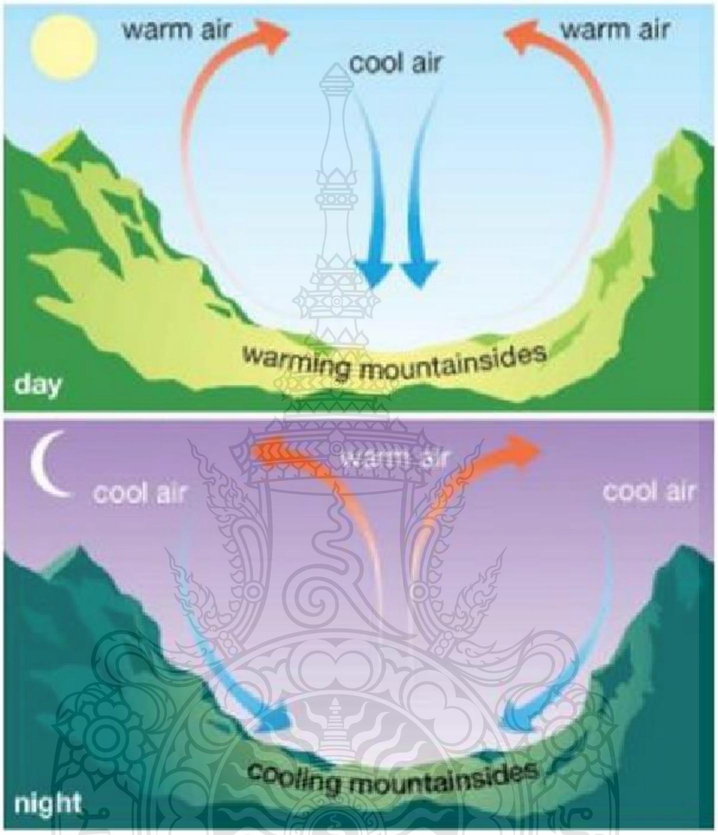

Figure 3.4 Valley and mountain breezes [65].

3.1.3 Topographical Effects

When seeking to determine the ideal location for wind turbines, the topography of the site must be taken into account. The best sites are able to generate increased air speeds through the shape of the hills acting as wing sections. In contrast, a poor site may generate significant levels of turbulence which can cause damage to the wind turbines. One basic rule to follow is that a wind turbine should be positioned at a distance no less than 10 times the height of the wind turbine tower away from any potential obstruction [65].

3.1.4 Wind Shear

When the surge of the mean wind speed swells with height, wind shear follows. Both the valuation of wind resources and wind turbines designs are impacted by wind shear. Initially, the evaluation of wind resources over a large area may involve anemometer data from various sources fixed to a familiar elevation. Next, from the layout, the fatigue life of the rotor blade will be impacted by the cyclic loads arising from spinning through the wind field, which changes in the vertical plane. Therefore, a wind speed deviation model with height is needed for wind energy functions [66].

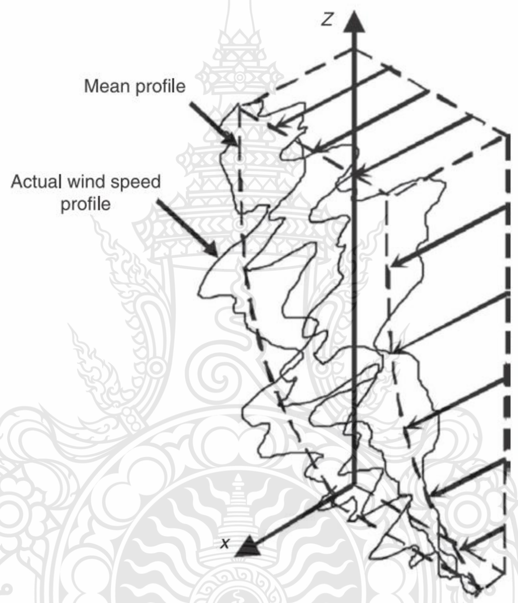

Figure 3.5 Actual wind speed profile [66].

In Figure 3.5 wind gets slowed at low heights caused by friction between moving air and the earth's surface, providing variation in mean wind speed with height. The mean wind speed reduces from roughly 2 km above the surface, where the friction effects are marginal, down to the surface, where the value is (basically) zero. This layer is the boundary layer of the atmosphere. The vertical variance of the mean wind speed, the mean wind speed profile, can be described in various ways. The logarithmic profile is one of the most frequently used functions to express such a profile as:

$$V(z) = V_{ref}\frac{ln\left(\frac{z}{z_0}\right)}{ln\left(\frac{z_{ref}}{z_0}\right)} \tag{3.1}$$

Where $V(z)$ is average wind speed at height z (m/s) V_{ref} is average wind speed at the orientation height z_{ref} (m/s) z_{ref} is orientation height (m) and z_0 is surface roughness length (m)

3.1.5 Wind Rose

A wind rose is an effective instrument used to measure the wind profile (speed and direction) at a specific place. Wind roses are constructed by superimposing the data from anemometers and wind valves onto a 360-degree graph. The standard wind rose comprises evenly spaced concentric circles and a series of 16 radial lines. The circles are used as a measure that indicates the ratio of wind blowing in the direction away from the base measurement. The 16 radial lines reflect the 16 primary directions of the compass and, as well as direction, indicate the rate of wind speed (for given ranges) that way [67]. Figure 3.6 gives an example of a wind rose.

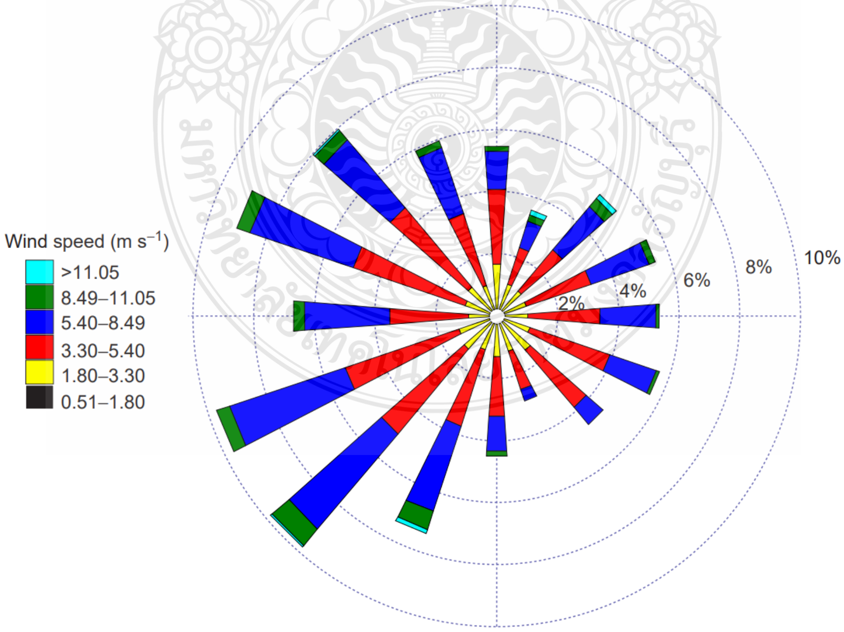

Figure 3.6 Illustration of wind directions on a wind rose [67].

3.1.6 Wind Turbine Description

The principal objective of a wind turbine is to generate mechanical energy from wind-provided kinetic energy, which can then be used to produce electricity [68]. The wind turbines themselves are operated using concepts which are similar to those applied in aviation. Aircraft wings are able to use aerodynamic forces to generate lift, while wind turbine blades are able to use the same forces to generate rotation which harnesses the wind energy [69]. A generator positioned within the rotor works to produce the electricity when the blades rotate. Furthermore, the speeds of the rotation are governed by the use of gearbox which can ensure that the right speeds are maintained to generate electrical power from the rotational energy within magnetic fields inside the generator [70]. The turbines will only be able to work, however, when the wind is actively providing the input energy [71].

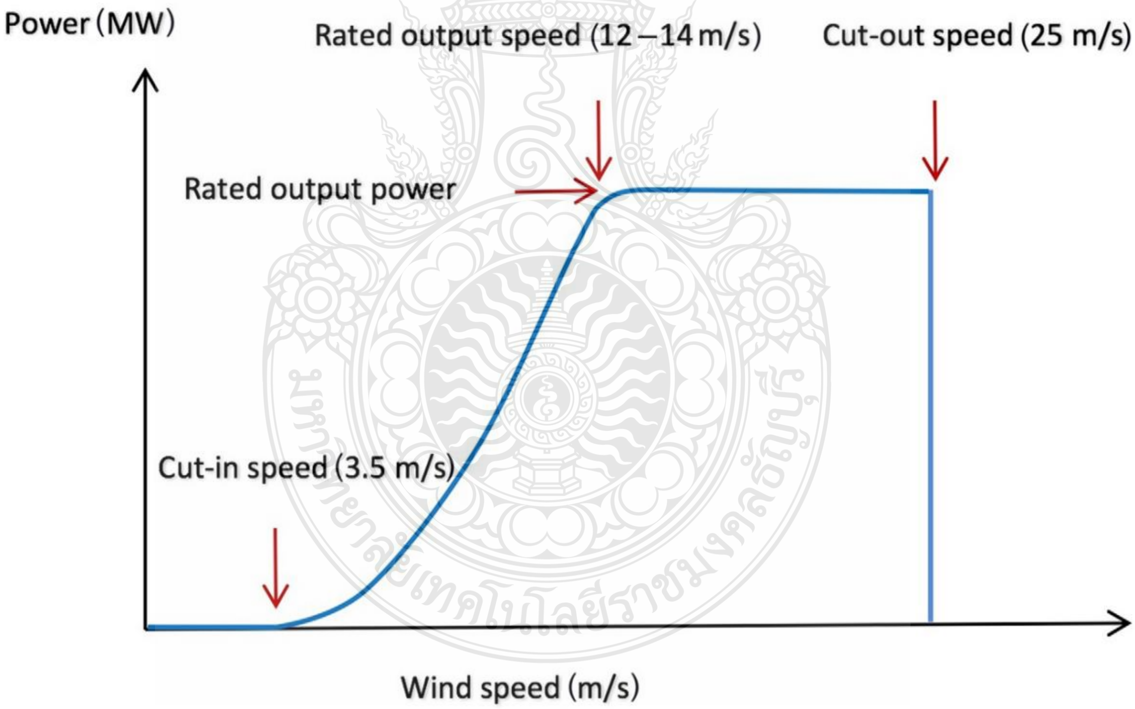

Figure 3.7 The typical wind turbine power curve [72].

Figure 3.7 displays a power curve which is typical of that generated by a wind turbine, so the links between steady wind speeds and electrical output are clearly displayed. Once the wind has accelerated to a speed of around 3.5 m/s, electricity will begin to be produced (cut-in speed). Maximum power is generated once the wind speed reaches a range of 12-14 m/s. However, if the wind accelerates to speeds in excess of 25 m/s, the wind turbine must be shut down (cut-out speed) in order to protect the blades and equipment from damage, furling, or stalling [73].

3.1.7 Statistical Analysis of Wind Data

The key methods used in wind energy are wind speed probability density projections and the equations that describe them quantitatively. Their usage covers a wide variety of uses, from the methods used to evaluate the parameters of the propagation functions to the use of those functions for the study of data on wind speed and the dynamics of wind energy. The Weibull distributions and Rayleigh distributions are two of the widely used mechanisms for fitting a calculated wind speed probability distribution at a certain position over a certain time period [74].

3.1.7.1 Weibull Distribution

A widely used utility for examining measured wind speed data in a given location over a given period is the two-parameter Weibull distribution. The two-parameter distribution of Weibull is a special case of the generic distribution of gamma. The two-parameter Weibull probability distribution equation is the most relevant, supported and endorsed distribution approach for the evaluation of wind speed results since it provides better fit and high precision for regular probability density distributions of calculated wind speed than any other distribution equation. The Weibull probability density equation can be written as [75]:

$$f(v) = \left(\frac{k}{c}\right)\left(\frac{v}{c}\right)^{k-1} exp\left[\left(-\frac{v}{c}\right)^{k}\right] \tag{3.2}$$

Where *f(v)* is the prospect of wind speed, *k* is the shape parameter and *c* is the scale parameter (in m/s). The correlating cumulative distribution task of the Weibull distribution is to integrate the probability density function, specified as [75]:

$$F(v) = 1 - exp\left[-\left(\frac{v}{c}\right)^k\right] \quad (3.3)$$

3.1.7.2 Rayleigh Distribution

For most wind circumstances, the k values range from 1.5 to 3.0. The Rayleigh distribution is an unique circumstance of the Weibull distribution where the shape value is 2.0. For the Rayleigh distribution, the probability density function can be shortened to [76]:

$$f(v) = \frac{2v}{c^2} exp\left[\left(-\frac{v}{c}\right)^k\right] \quad (3.4)$$

$$c = \frac{2}{\pi} V_m \quad (3.5)$$

Where V_m is the mean speed (m/s)

3.2 Technologies Used in Wind Turbines

3.2.1 Wind Turbine Types

It is possible to rotate a wind turbine horizontally or vertically, and this results in two different designs: the horizontal axis wind turbines (HAWT) and the vertical axis wind turbine (VAWT).

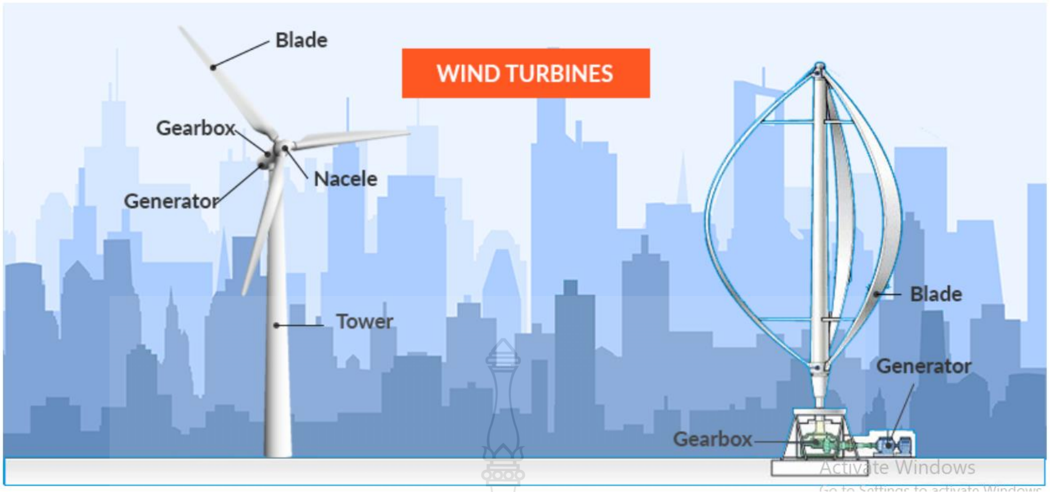

Figure 3.8 Wind turbine designs: left: horizontal axis wind turbines and right: vertical axis wind turbines [77].

3.2.1.1 Horizontal Axis Wind Turbines (HAWTs)

HAWTs are the most widely used type and can be seen in Figure 3.8. They typically have two or three blades, and the main rotor shaft and generator are located at the top of the wind turbine tower [78]. Axial flow devices are positioned inside HAWTs and will control the operation in terms of wind direction, using a wind flow sensor or tail vane to determine the wind direction and to turn the rotor to face the right direction [79][80].

3.2.1.2 Vertical Axis Wind Turbines (VAWTs)

VAWTs have a vertical rotor shaft, while the blades are attached to the top and bottom of this shaft, as can be observed in Figure 3.8. In this case, a cross-device system ensures that the blades will operate when the wind flows from any direction [79], so no sensors or tail vanes are required to manage the directional aspect of the wind turbine operation. It is therefore cheaper than the HAWT design [71]. VAWTs are commonly installed on rooftops or on the ground, and therefore it is easy for maintenance workers to gain access to the generators or gearboxes. The only drawback is that the VAWTs lack the efficiency of the HAWTs [77].

3.2.2 Applications of Wind Turbines

A majority of wind turbines are a part of the national power grid and are used to generate electricity. However, it is also possible for the mechanical power generated in the wind turbine shaft to be employed in a simple manner which can bring about economic benefits [81].

Some of these applications of mechanical power from wind turbines are listed as follows:

- Water pumps
- Saltwater desalination
- Water aeration in agricultural ponds or reservoirs
- Wastewater circulation
- Water heating by means of fluid turbulence

3.2.3 Components of a Wind Turbine

Wind turbines need a number of different components in order to function effectively. These are illustrated the components of a wind turbine for electricity generation in Figure 3.9. Further details can be explained as follows:

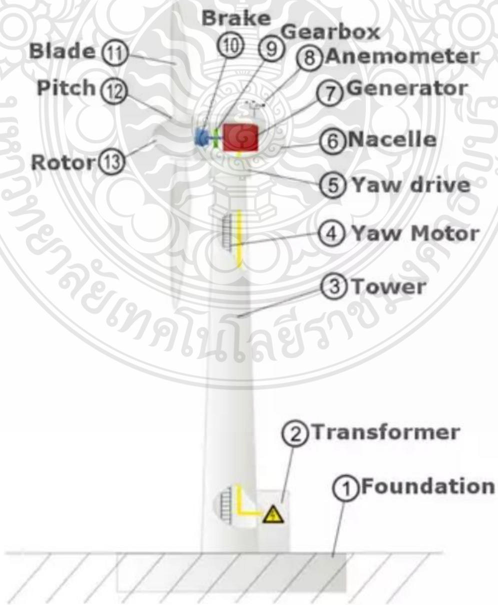

Figure 3.9 Wind turbine components [82].

3.2.3.1 Foundations

Wind turbines must be built upon foundations which can support the load of the wind turbine. The type of foundation required will be dependent upon the type of soil and the position of the water table at the wind turbine location. All construction projects require a safe foundation design which is also cost effective. Typical foundation designs for wind turbines include the slab foundation, for which the foundation materials sit predominantly very close to the surface, or the pile foundation, which is necessary when the ground is weaker and unable to readily offer support to the construction. Foundations of either type must be able to withstand the vertical load exerted by the wind turbine, as well as the shear force, vibration force, and overturning moments. They must also be designed to take into consideration the necessary tolerances for foundation settlement and tilt [83].

3.2.3.2 Transformers

The design of transformers relies upon the principle of developing a magnetic field which fluctuates by using a uniform sinusoidal input alternating voltage source. This serves to induce the current flow within, as well as the voltage potential across, the separate conductor in that fluctuating field. Many wind turbines have step-up transformers which can increase the output voltage from the generator to fit the voltage requirements of the distribution network. Step-up transformers are typically designed to take into consideration a number of factors and requirements, such as harmonic and non-sinusoidal loads, variable loading, transformer sizing, voltage variation, and low voltage fault ride through, in addition to fire prevention activity, switching surges, transient over-voltages, step-up duty, gassing, and loss evaluation [84].

3.2.3.3 Towers

Three types of towers are commonly used for three wind turbines: lattice towers; tubular steel towers, and guyed pole towers. Tubular steel wind turbines are typically large, and are constructed in sections measuring 20-30 m which have flanges at each end. The sections are fixed together on location. The towers themselves are conical, with the base wider than the peak, which offers cost savings on materials, as well as greater strength with the broad base able to support the considerable height and weight of the wind turbine. The flexibility of the steel makes the conical shape feasible in constructing the tower without the danger of breaking. However, this design requires skillful manufacturing engineers in order to manage the welding and to control any deformation which might occur. Furthermore, such towers can be difficult to transport and also to install, especially because transport limitations are imposed by the vehicle size and conditions of the roads. Once on site, it is necessary to use large cranes to install the towers in a time-consuming process. The second type of towers are lattice towers which use welded steel profiles rather than steel sheets. Lattice towers re cheaper due to their lower material content for towers of similar size. However, such towers are just as stiff and reliable as a tubular tower. Steel is a very strong material, and hence allows towers to be built without the need to use large quantities of the metal. Furthermore, the wind is able to pass through the lattice tower, thus lowering the pressure which is exerted upon the construction. The main drawback of lattice towers, however, is the appearance, since they are not visually appealing, and are therefore not widely used for wind turbines today [85]. Guyed pole towers are the final design type. They cannot be tilted downwards once complete as they are held in place by four steel cables which offer superior strength. The advantages of such systems is that they are not expensive, although inspection and maintenance of this kind of tower is more difficult [86].

3.2.3.4 Ladders

Ladders are necessary to allow workers to reach the nacelles for maintenance. For wind turbines in Europe, it is mandatory for safety to install platforms at six-meter intervals to allow workers to rest when climbing. Ladders are typically made from aluminum and can be attached to the outside or the inside of the tower [87].

3.2.3.5 Yaw Mechanism

The yaw mechanism is a system which makes use of electric motors to turn the nacelle so that the rotor can face the right direction to operate in the wind. An electronic sensor or wind vane determines the wind direction and then controls the motor for the yaw mechanism [88].

3.2.3.6 Nacelles

Nacelles are particularly important since they house the vital equipment which enables the wind turbine to operate, such as the brakes, generator, and gearbox of the wind turbine. It is possible for workers to repair and maintain the equipment by entering the nacelle directly from the wind turbine tower [89].

3.2.3.7 Generators

All wind turbines require generators in order to produce electricity from the mechanical power of the turning turbine blades. Three kinds of generators are commonly used: AC induction generators; permanent magnet generators (PM), and DC generators [22]. Among these, wind turbines most commonly use PM generators, which make use of a magnetic field which is produced by turning magnets which are attached to the rotor. Most wind turbine operators prefer to use magnets which are made from rare-earth elements. These offer greater field strength but tend to be rather expensive. However, they offer excellent value because they eliminate the need for an external power source for the PM generator in order to initiate the magnetic field. This is a particular strength in the context of wind turbines located in remote regions [90].

3.2.3.8 Wind Vanes/Anemometers

Anemometers or wind vanes are used to measure the direction of the wind, and then to control the directional settings of the wind turbine to ensure that it can face the right direction to optimize the use of the available wind energy [91].

3.2.3.9 Brakes

Brakes are necessary in order to halt the rotor in emergency circumstances. These can work electrically, mechanically or hydraulically [92].

3.2.3.10 The Gearbox

The gearbox is able to facilitate the management of rotational speeds in order to ensure that the speed is suitable for driving the generator. In particular, the gearbox can raise the speed of a low-speed shaft to hat required of a high-speed shaft to serve the generator [93].

3.2.3.11 The Blades

The blades used by wind turbines are airfoil shaped and capable of capturing and utilizing the energy of the wind so that it can drive the wind turbine rotor. The use of an airfoil design enables the blade to produce lift which is a force exerted perpendicular to the direction of the wind. The resulting force vector drives the rotor, providing energy to the wind turbine. In this regard, the blades are the most crucial components of the wind turbine. Due to their role, they encounter high levels of stress and must be manufactured to exacting standards. In particular, their manufacturing tolerances must ensure their balance in order to avoid vibration which could damage or ultimately destroy the wind turbine. To optimize the aerodynamics of the blades, the design involves a thin blade, with close attention paid to the structural integrity of the oblique airfoil since this increases the speeds at which the blade can survive and extend the overall lifespan of the blade. It is necessary to find a suitable balance of all these attributes in order to have an efficient wind turbine which also offers longevity [94].

3.2.3.12 Pitch Controls

The blades are equipped with pitch controls in order that they might be adjusted in order to harness the right amount of wind energy available as the wind blows across the blades. It is essential not to exceed the maximum rotational speed parameters for the wind turbine, and this can be achieved in strong winds by rotating the blades to reduce the exposed surface area. This allows the blades to operate safely in high winds, or when other power outages arise which would otherwise allow the wind turbine to run without control [95].

3.2.3.13 Rotor Hub

The role of the rotor is to harness wind energy and then release this energy to the drivetrain. The rotor blades are linked to this system via the rotor hub, which ensures that the energy is passed efficiently to the rotor shaft [96].

3.3 Aerodynamics of Wind Turbines

3.3.1 One-Dimensional Momentum Theory

One basic model explains the link between wind power and thrust and the optimum rotor. This basic model was developed in 1919 by Albert Betz, a German physicist. The momentum theory is used to research the energy. For determining the most power that can be extracted from the wind through kinetic energy to mechanical energy conversion, the model can assist. Figure 3.10 reveals the concept of momentum theory.

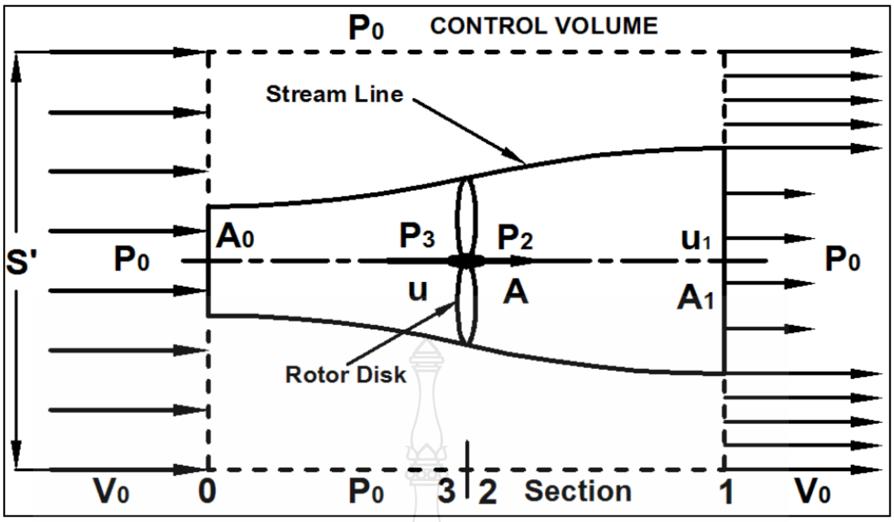

Figure 3.10 The concept of momentum theory [97].

Several postulations must be envisioned for the concept of momentum theory.

1) The wind flow assessment must be reliable.
2) There should be no obstacles in the inlet and outlet flow of the test tunnel.
3) For the wind turbine blade, there should be no turbulence in wind movement.
4) The wind flow assessment must be deemed an incompressible fluid. Thus, the temperature used in the study is not compromised.

To examine Figure 3.10, there are factors that require explanation:

S' is control volume

V_0 is the wind speed at the inlet and outlet of control volume (m/s)

u is wind speed prior to reaching the face of the examined rotor disc (m/s)

u_1 is wind speed after moving through the rotor disc (m/s)

P_0 is atmospheric pressure (N/m^2)

P_2 is the air pressure moving through the rotor disc (N/m^2)

P_3 is the air pressure prior to hitting the rotor disc (N/m^2)

A is the cross-sectional region of the rotor disc (m^2)

A_0 is the entrance cross-section region of the wind tunnel (m^2)

A_1 is the exit cross-section region of the wind tunnel (m^2)

Q is the airflow rate utilized for the examination (m^3/s)

To study the momentum theory, it is expected that air density is 1.225 kg/m^3 at normal air temperature. Further, flow must be even through the system based on the law of constant flow (continuity equation) that is $Q = AV$, which gets $V_0A_0 = uA = u_1A_1$. Likewise, only pressure was studied from section 0 to section 3 and from section 2 to section 1 in Figure 3.10, as from Bernoulli's law.

For the study of all wind turbines types, the required elements must be utilized, the results of which comprise:

$$\frac{1}{2}\rho V_0^2 + P_0 = \frac{1}{2}\rho u^2 + P_3 \tag{3.6}$$

$$\frac{1}{2}\rho u^2 + P_2 = \frac{1}{2}\rho u_1^2 + P_0 \tag{3.7}$$

Consequently, thrust at the rotor blade would be:

$$T_a = PA \tag{3.8}$$

Which is $$A(P_3 - P_2) \tag{3.9}$$

The energy from the wind transferred to the rotor disc is $(P_3 - P_2)$. Energy is kept in the blades. If wind speed is examined, the thrust force arising in the rotor blade can be expressed as:

$$T_a = \frac{\rho A(V_0^2 - u_1^2)}{2} \tag{3.10}$$

From wind, the kinetic energy equation is $KE = \frac{1}{2}\rho AV^2$. From Equation 2.9, however, the energy is transferred to the rotor blade, shown as $(Au - A_1u_1)$.

$$\text{Thus, if } u = \left(\frac{V_0+u_1}{2}\right) \tag{3.11}$$

When u is mean wind speed in the system. We suppose that losses are needed for the system to be described as the axial interference factor when examining the system; this measure is the ratio of the reduction in wind energy between the free air flow and the wind that reaches the rotor blade, that is

Wind power drop between the free incoming wind and the wind that strikes the wind turbine blade, that is:

$$a = \frac{v}{V_0} \text{ and from } v = V_0 - u \text{ thus, replace } v = V_0 - u \tag{3.12}$$

As the loss value will be $u = V_o(1 - a)$

Thus, replace the values into Equation 2.11 to get u_1 as

$$u_1 = V_o(1 - 2a) \tag{3.13}$$

In the measurement of the function of the wind turbine, if the decreasing trend of the wind energy is equal to 0, this means that there is no interference on the device which the wind at the inlet and outlet does not change the ratio of the reduction of the wind energy. However, it is difficult for the machine to run without failure at all. Around the same time, the percentage decrease of wind energy is equal to 1, meaning that there is no wind energy at all delivered to the wind turbine blades, which would not be appropriate, so that the significance of this analysis will decide how much wind energy is conveyed to the wind turbine blades per unit time.

Which is P_w by

$$P_w = \frac{1}{2}\rho A u V_0^2 - \frac{1}{2}\rho u_1^2 A u \tag{3.14}$$

Replace a for:

$$P_w = \frac{1}{2}\rho A u V_0^3 4a(1 - a)^2 \tag{3.15}$$

In order to evaluate the wind turbine system in general, wind energy is made by the free flow of the formula used to measure P_a through the air intake region, so

P_a = (Volume of flow) x (Kinetic energy of wind versus flow volume)

2.3.2 Betz Limit

Conceived by Albert Betz, the Betz limit was the product of attempts to develop a method for the rapid calculation of the power and load parameters of the HAWTs.

There is a vector to be regarded for the output of the wind turbine to evaluate the productivity of wind turbines, which is power coefficient (C_p). C_p is derived by evaluating the energy transferred by the wind turbine (P_w) and the energy transported by the free-flowing wind turbine (P_w) (P_a). Thus, the power is proportional to the energy provided by the energy transferred to the system. Hence, peak wind turbine production can be expressed as:

$$C_p = \frac{P_w}{P_a} = \frac{\frac{1}{2}\rho A V_0^3 4a(1-a)^2}{\frac{1}{2}\rho A V_0^3} \tag{3.16}$$

Thus,
$$C_p = 4a(1-a)^2 \tag{3.17}$$

Hypothetically, the peak power coefficient that a wind turbine could take from wind energy can be obtained by distinguishing equation 2.17, hence:

$$C_p = 4a - 8a^2 + 4a^3 \tag{3.18}$$

By differentiating again with a value then:

$$\frac{dC_p}{da} = 4 - 16a + 12a^2 = 0$$

$$12a^2 - 16a + 4 = 0$$

$$3a^2 - 4a + 1 = 0$$

Therefore, the *a* value would be:

$$a = \frac{4 \pm \sqrt{(-4)^2 - 4 \times 3 \times 1}}{2 \times 3}, a = \frac{4 \pm \sqrt{4}}{6}$$

Thus, *a* values are:

$$a = \frac{2}{3} \pm \frac{1}{3}$$

$$a = 1 \text{ and } a = \tfrac{1}{3}$$

Hence

$$C_{P,max} = \frac{16}{27} = 0.5926$$

Based on the Betz limit, an optimal wind turbine is unable to accomplish higher rates of conversion than 59.2% of the kinetic energy to become mechanical power at a = 1/3. In this circumstance, flow via the disk corresponds to that of the stream tube, which gives an upstream cross-section area of two-thirds of the disk area, which can be extended to twice the disk area downstream. This result implies that the greatest power generation would be attained if the ideal rotor was planned and used so that the wind speed at the rotor was equal to 2/3 of the free-stream wind speed. Therefore, the basic physical laws dictate that this is the highest power generation level that could ever be realized.

3.3.3 Tip Speed Ratio (TSR)

The TSR is an important factor which is not related to the dimensions of the wind turbine, but instead describes the relationship between rotor rotation and wind speed. Wind turbine design must take TSR into consideration in order to achieve both efficiency and safety [98].

The TSR is given as:

$$TSR = \lambda = \frac{speed\ of\ rotor\ tip}{wind\ speed} = \frac{U}{V} = \frac{\omega r}{V} = \frac{2\pi rN}{V60} \quad (3.19)$$

In which: V = wind speed (m/s)

U = speed of the rotor tip (m/s)

r = radius of the rotor (m)

ω = angular velocity (rad/s)

N = rotational rotor speed (rpm)

In order to maximize the power generation from the available wind, it is necessary to design the wind turbines to operate at the optimized tip speed ratio. A wind turbine which turns slowly will allow the airflow to pass between the blades and will not maximize the power extraction from the wind energy available. In contrast, when the blades spin too quickly, they can effectively become a solid barrier, resulting in turbulence and causing high levels of stress and potential damage [98].

Figure 3.11 displays the various different power coefficients resulting from different kinds of wind turbine. As a result of the Betz limit, the maximum efficiency of an ideal wind turbine is approximately 59 percent. If the tip speed ratio is high, the

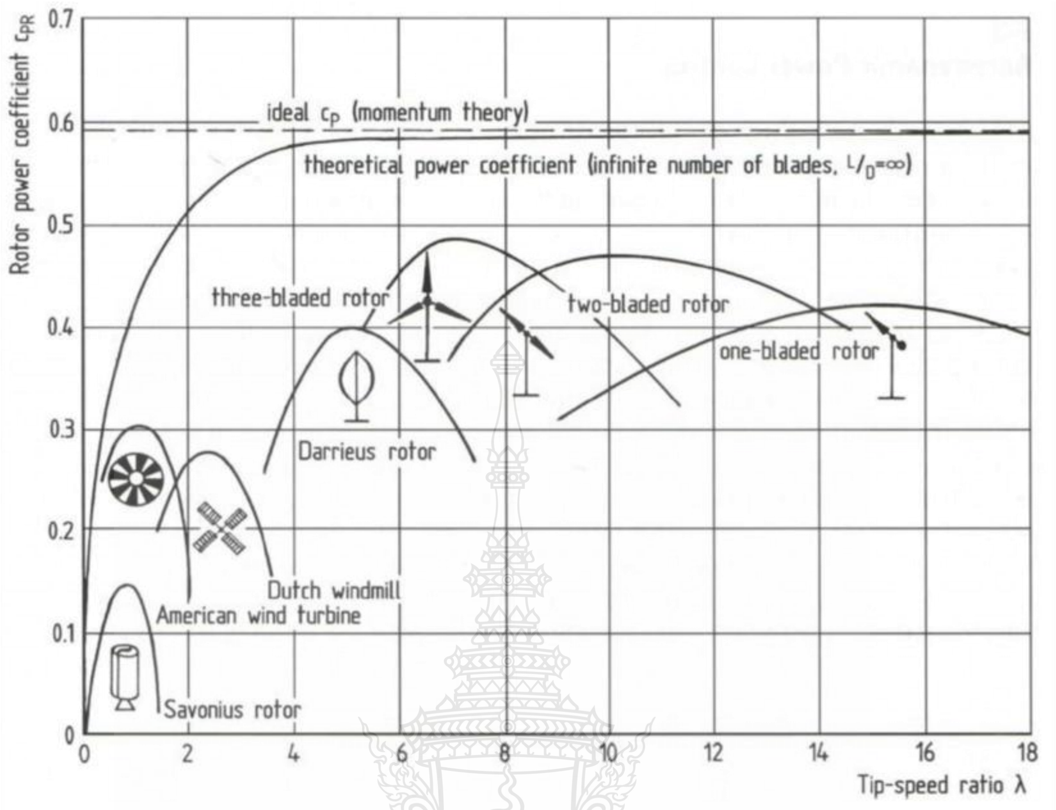

Figure 3.11 The power coefficients for various types of wind turbines [100].

3.3.4 Airfoils

Airfoils are geometric shapes which are constructed in such a way as to be able to generate mechanical forces from their own motion within an airflow. When the cross-section of a wind turbine blade is designed, the airfoil shape is critical, since the blades make use of the airfoil design in generating mechanical energy from the wind. The blade dimensions are critical in terms of the required aerodynamic performance, the necessary strength and properties, and the maximum power required of the rotor [101].

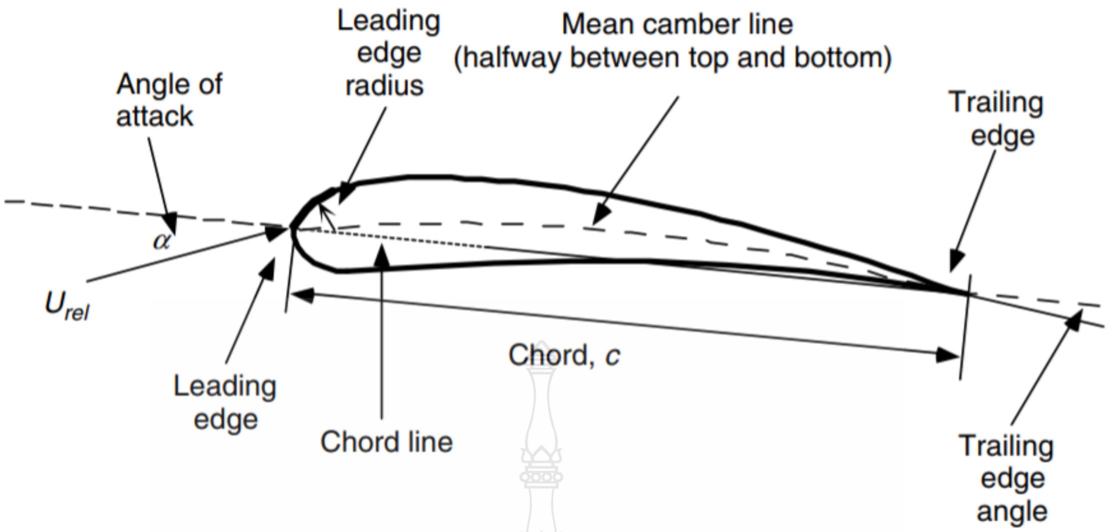

Figure 3.12 Airfoil nomenclature [101].

Airfoil terminology is explained as follows [101]:

- Mean camber line: This line is located at the midpoint between the upper and lower airfoil surfaces.
- Leading and trailing edge: These are the foremost and rearmost points of the mean camber line.
- Chord line: This straight line links the leading and trailing edges.
- Chord (c): The chord line distance.
- Camber: The distance from the chord line to the mean camber line, with measurements taken perpendicular to the chord line.
- Thickness: The distance from the upper surface to the lower surface, with measurements taken perpendicular to the chord line.
- Angle of attack (α): The angle between the chord line and the relative wind (U_{rel}).
- Span: The airfoil length measured perpendicular to the cross-section.

3.3.5 Coefficients of Lift, Drag and Moment

Two forces and one moment typically arise around the airfoil as a consequence of the pressure and friction exerted by the air as it flows over the airfoil, thus causing the forces to be distributed. Around the convex airfoil surface, the velocity of the airflow increases, thus reducing the average pressure. In contrast, a concave airfoil surface has the effect of slowing the airflow and increasing the pressure. Furthermore, viscous friction arises where the air meets the airfoil surface, and this can slow the airflow at the surface. The forces and moment which have been identified to act upon the airfoil are lift force, drag force, and pitching moment [101].

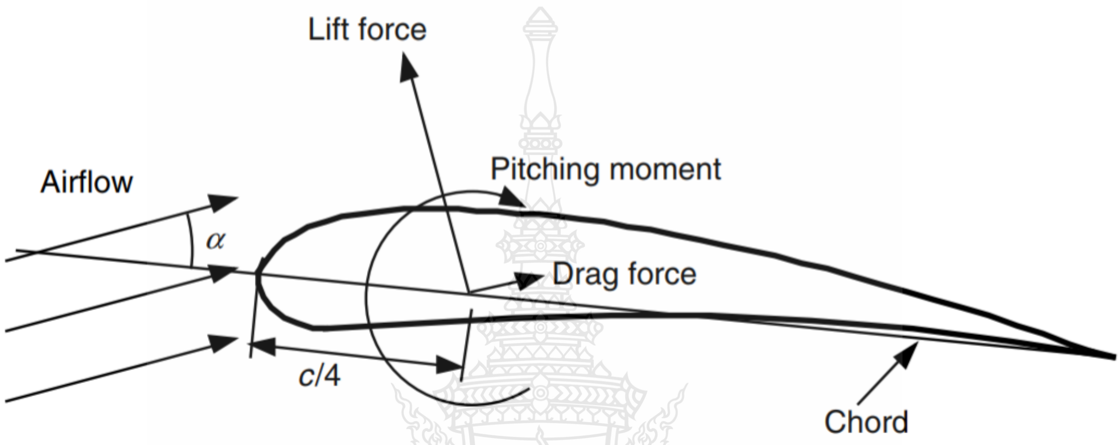

Figure 3.13 Forces and moments exerted upon the airfoil section [101].

The force of lift acts perpendicular to the oncoming flow of air, as illustrated in Figure 3.13. This lift results from the difference in pressure at the upper and lower surfaces of the airfoil. An increase in airflow speed over the curved leading edge causes the pressure to drop, creating a negative pressure gradient. When the air reaches the trailing edge, it then begins to slow, raising the surface pressure and creating a pressure gradient which is positive. Depending on the design of the airfoil shape as well as the angle of attack, the air might accelerate more rapidly across the upper surface than the lower surface, hence creating lift. Drag is then defined as a force operating parallel to the oncoming airflow which can be seen in Figure 3.13. This occurs as a consequence of the differences in pressure acting upon the surfaces of the airfoil which face into or away from the wind flow. The two factors which cause drag are therefore the distribution of pressure over the airfoil surface, and the friction arising between the airfoil and the airflow at the surface. Net pressure in the direction of the airflow direction therefore causes drag. The component of drag which is caused by friction results from fluid viscosity and causes the dissipation of energy into the airflow. Meanwhile, the pitching moment can be defined as movement about an axis running perpendicular to the cross-section of the airfoil, and thus the moment is a function of the integral of pressure force moments acting about the quarter chord over the airfoil surface [102].

It is normal to define the lift, drag, and moment coefficients as shown below [101]:

$$Lift\ coefficient, C_l = \frac{L/l}{\frac{1}{2}\rho U^2 c} = \frac{Lift\ force/Unit\ length}{Dynamic\ force/Unit\ length} \tag{3.20}$$

$$Drag\ coefficient, C_d = \frac{D/l}{\frac{1}{2}\rho U^2 c} = \frac{Drag\ force/Unit\ length}{Dynamic\ force/Unit\ length} \tag{3.21}$$

$$Pitching\ moment\ coefficient, C_m = \frac{M}{\frac{1}{2}\rho U^2 Ac} = \frac{Pitching\ moment}{Dynamic\ moment} \tag{3.22}$$

In which: ρ = Air density (kg/m^3)

U_a = Undisturbed air flow velocity (m/s)

A = Projected area of the airfoil (chord × span) (m^2)

c = Chord length of the airfoil (m)

l = Span of the airfoil (m)

3.3.5 Theory of Blade Element Momentum (BEM)

The Theory of BEM combines moment theory and blade element theory in order to explain the way the shape of the blades will affect the capacity of the rotor to harness wind energy. Momentum theory takes into consideration the control volume analysis of the force at the blade in the context of the conservation of linear and angular momentum. Meanwhile, blade element theory considers the effects of forces exerted upon particular sections of the blade in the context of blade geometry [101].

3.3.6 Momentum Theory

To determine the conditions of flow and force upon the blades of the wind turbine, the conservation of moment can be employed, since force can be defined as the rate of change in momentum. The ideas of conservation of linear and angular momentum play a key role in momentum theory when analyzing the control volume of forces exerted upon the blade [101].

3.3.7 Blade Element Theory

It is possible to explain the forces which are exerted upon a wind turbine blade in terms of lift and drag coefficients along with the angle of attack. Figure 3.14 illustrates this approach, dividing the blade into N sections, also known as elements. Two key assumptions must be taken into account: there is no aerodynamic interaction arising between blade elements, and the forces acting upon the blades are solely the product of the drag and lift characteristics resulting from the airfoil design. When the forces on the blade section are analyzed, lift will be perpendicular to the wind direction, while drag will be exerted parallel to the wind [101].

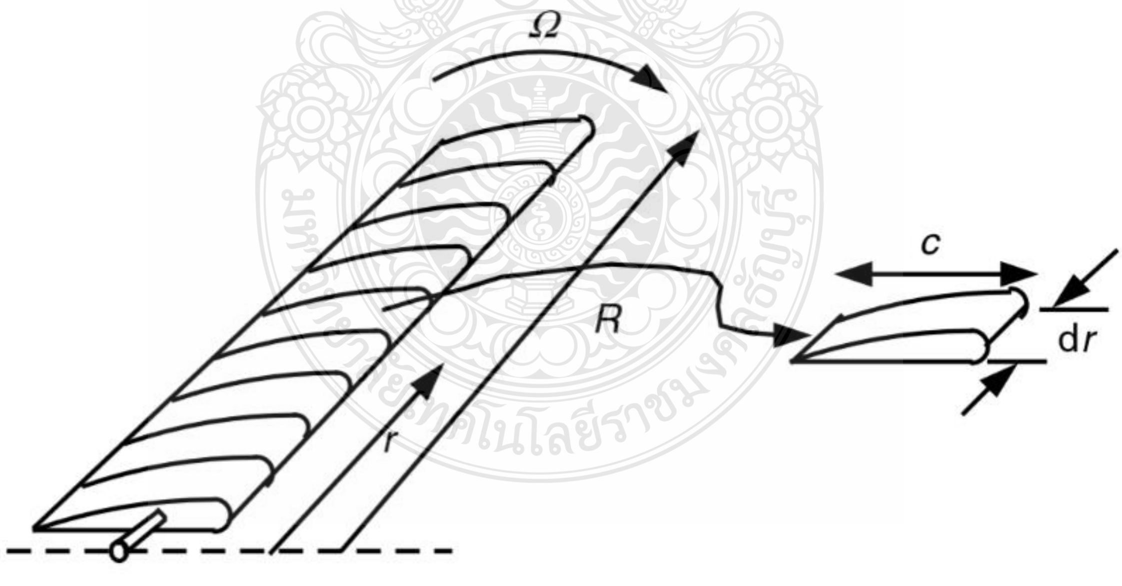

Figure 3.14 Diagram of the blade elements [101].

Figure 3.15 presents the relationships between the different forces, angles, and velocities involving the blades and the blade tips. In this case, θp denotes the section pitch angle, defined as the angle between the plane of rotation and the chord line, while $\theta p,0$ indicates the pitch angle of the blade at the tip, and θ_T represents the blade twist angle. Furthermore, α is the angle of attack, while the angle of relative wind is given by φ, and dF_L indicates the incremental lift force while dF_D indicates the incremental drag force. Finally, dF_N shows the incremental force normal to the plane of rotation, which is important in the context of thrust, while dF_T represents the incremental force at a tangent to the circular path followed by the rotor. It is this force which is responsible for the generation of useful torque. Then U_{rel} shows the relative wind velocity. The definition of the blade twist angle, θ_T, is given with reference to the blade tip [101]. Thus:

$$\theta_T = \theta_p - \theta_{p,0} \tag{3.23}$$

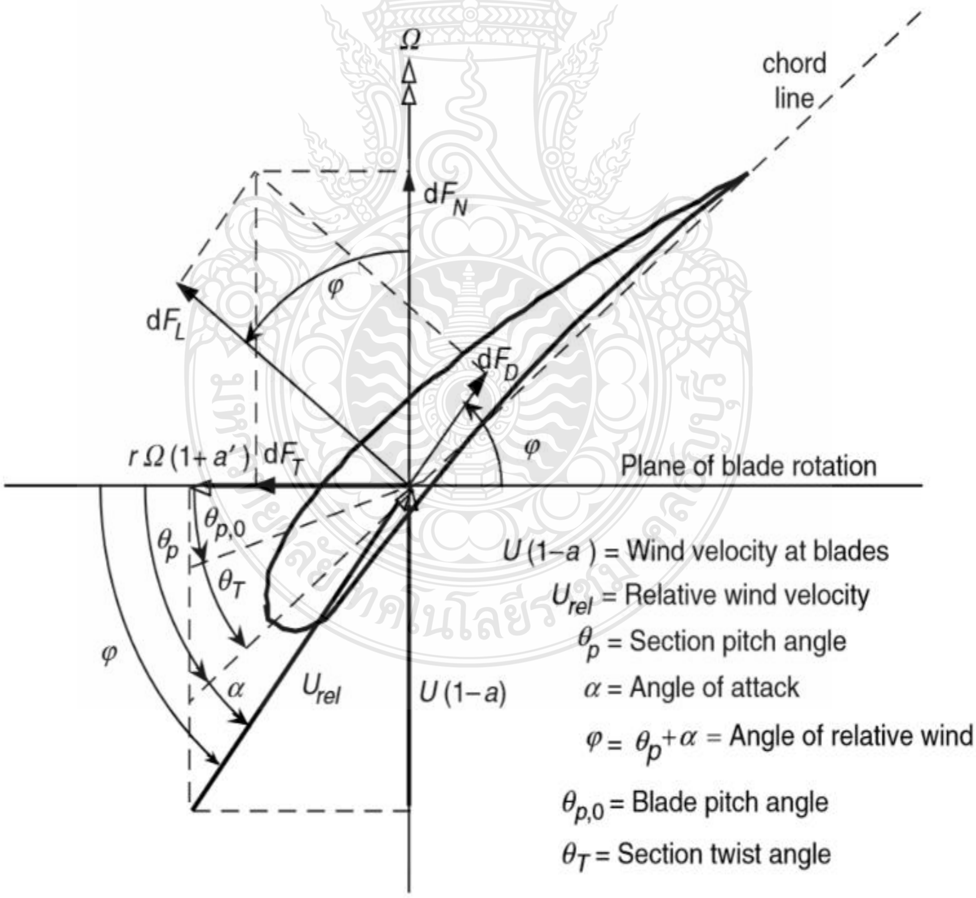

Figure 3.15 Blade geometry of a HAWT [101].

Furthermore, the relative wind angle will be derived from the sum of the angle of attack and the section pitch angle, given below:

$$\varphi = \theta_p + \alpha \tag{3.24}$$

From Figure 3.15 allows the following relationships to be inferred:

$$tan\varphi = \frac{U(1-a)}{\Omega r(1+a')} = \frac{1-a}{(1+a')\lambda_r} \tag{3.25}$$

$$U_{rel} = U(1-a)/sin\,\varphi \tag{3.26}$$

$$\mathrm{d}F_L = C_l\frac{1}{2}\rho U_{rel}^2 cdr \tag{3.27}$$

$$\mathrm{d}F_D = C_d\frac{1}{2}\rho U_{rel}^2 cdr \tag{3.28}$$

$$\mathrm{d}F_N = \mathrm{d}F_L cos\,\varphi + \mathrm{d}F_D sin\,\varphi \tag{3.29}$$

$$\mathrm{d}F_T = \mathrm{d}F_L sin\,\varphi - \mathrm{d}F_D cos\,\varphi \tag{3.30}$$

In the case where the rotor is equipped with B blades, the total normal force exerted upon the section at a distance from the center given by r is:

$$\mathrm{d}F_N = B\frac{1}{2}\rho U_{rel}^2(C_l cos\,\varphi + \mathrm{d}F_D sin\,\varphi)cdr \tag{3.31}$$

The differential torque to the tangential force when operating at a distance from the center given by r is:

$$\mathrm{d}Q = Br\mathrm{d}F_T \tag{3.32}$$

so

$$\mathrm{d}Q = B\frac{1}{2}\rho U_{rel}^{2}(C_l sin\,\varphi + \mathrm{C}_d cos\,\varphi)cr\,dr \tag{3.33}$$

Drag has the effect of reducing both torque and power so that thrust loading can be increased. From the perspective of blade element theory, two equations are obtained (Equations (2.33) and (2.35)) which can be used to explain both the normal (thrust) and tangential forces (torque) which are exerted upon the annular rotor section in terms of the flow angles measured at the blades and the attributes of the airfoil design [101].

3.4 Wind Turbine Management

To make sure that the wind turbine operates efficiently in terms of reliability, safety and maximum power output, a wind turbine control system is needed. Including pitch control systems and stand control systems, there are two major types of control systems for wind turbines [103]

For current wind turbine technology, a pitch control system is a critical tool. As shown in Fig. 3.16, this type of device is controlled by changing the angle of pitch of the blade, based on the direction and speed of the wind. As a result, the pitch control mechanism enhances wind turbine efficiency in terms of wind energy transmission and the reliability of power generation at any wind speed. In addition, this system type can act as an emergency system by controlling the wind turbine at high wind speeds in order to prevent any wind turbine damage [104].

The stall control mechanism is controlled by shutting down the blades after the wind turbines exceed the rated wind speed as illustrated in Figure 3.17. Passive control systems and active control systems are the two types of stand control systems. The passive control mechanism is mounted on the wind turbine by attaching the rotor blade to the hub at a set angle. As a result, the wind turbine runs at almost optimum performance at low wind speeds and is controlled by breaking the blades to monitor rotational speed and power output in order to minimize the possibility of damage and restrict rotational speed in high winds. This control plan is prepared specifically for small to medium-sized wind turbines. The active control system, on the other hand, works by stalling blades in combination with pitch control. At high wind speeds, the blades are rotated to a stand while the pitch control mechanism works in the reverse direction. It is called negative pitch power. This type of control system is primarily used for big wind turbines due to the ability of the pitch controller to sustain the rated capacity at high wind speeds and because of the precision of the power output controls. The use of the pitch adjustment system contributes to the expense of the wind turbine [103].

Figure 3.16 Pitch control wind turbine [105].

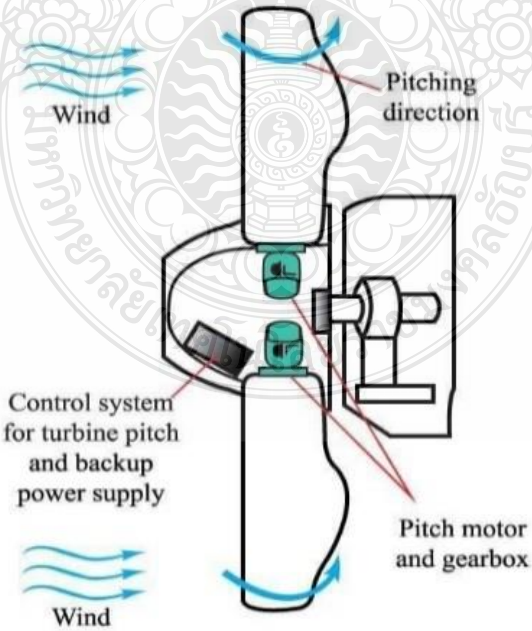

Figure 3.17 Explanation of airfoil stall [101].

3.5 Wind Turbine Control Strategies

Manipulating the pitch angle and generator is the most operative control plan for a wind turbine. Including the angle of attack and the power coefficient, many factors may impact the efficiency of wind turbines control strategies. Likewise, the efficiency of the wind turbine can be controlled by pitch, yaw and rotational speed modulation. These control measures are crucial for optimizing the output of wind turbines and ensuring the safe design and operation of wind turbines [106]. Fixed-speed fixed-pitch (FS–FP) control, fixed-speed variable-pitch (FS–VP) control, variable-speed fixed-pitch (VS–FP) control, and variable-speed variable-pitch (VS–VP) control are the four kinds of wind turbine control approaches. These regulation approaches are developed to monitor the power curve of the wind turbine. As seen in Figure 3.18, each control strategy offers unique power curve performance [107].

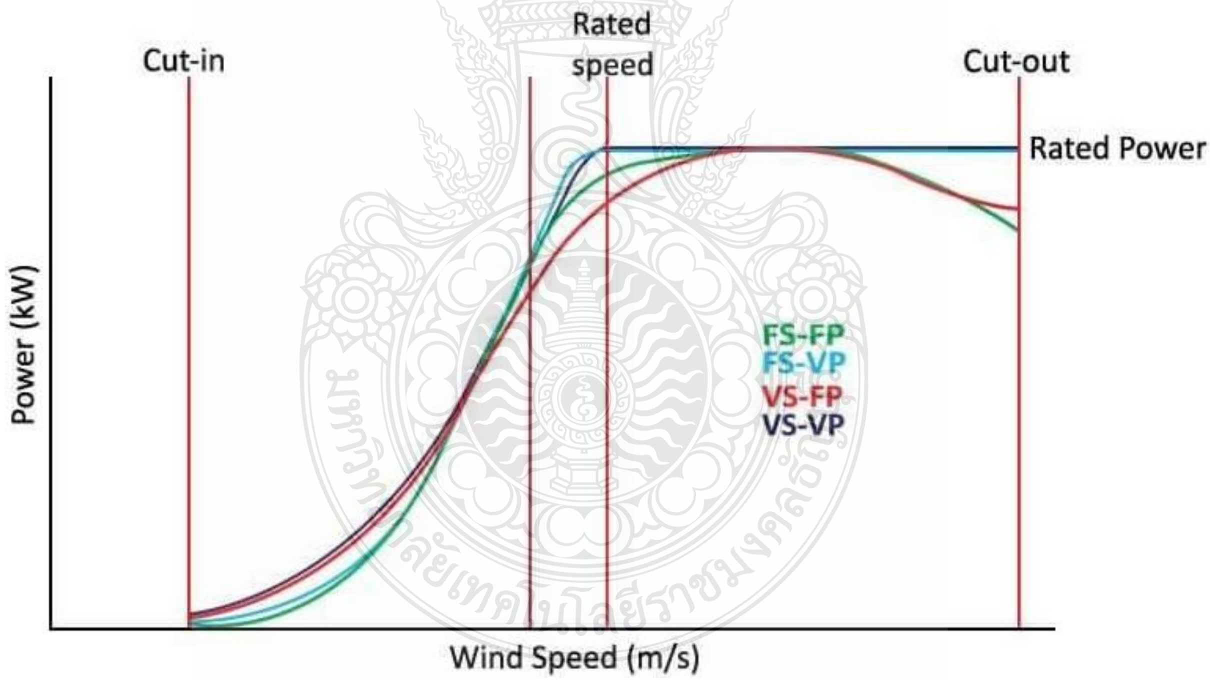

Figure 3.18 Power curves for different control strategies [106].

FS–FP management cannot boost operation by active control. The high-speed passive stall system is then used to monitor the output of the wind turbine. The frequency of the power line and the rotational speed are fixed by the speed of the generator since the generator is clearly linked to the power grid. In addition, passive control is used with the gearbox ratio to prevent power overstepping. The energy capture is lower, which allows the real power to be lower than the optimal power, as a result of the highest efficiency obtained at just one wind speed, as shown in Fig. 3.18. Therefore, the rated capacity only corresponds to one wind direction [106].

FS–VP is a management tool that enables optimum power efficiency at a single wind speed. This technique entails adjusting the blade pitch angle at wind speeds higher than the rated wind speed, while the pitch angle is constant at wind speeds below the rated wind speed. Feather control and stall control are two FS–VP control approaches that can be used to restrict power. The feather approach boosts the difficulty of the control design, while stall control can enhance unnecessary thrust forces. Below the rated wind speed, the energy efficiency of the region 2 is almost optimally efficient, as shown in Fig. 3.18. Thus, the pitch angle must be continuously changed to preserve power efficiency at speeds higher than the rated wind speed to avoid loss of power [107].

VS–FP is a management technique that uses power supervision to regulate the speed of the engine, which corresponds to wind speed. The configuration of the airfoil blade is a critical element in the regulation of fixed-pitch strength by passive stalling. Maximum power output is obtained at low wind speeds, as shown in Fig. 3.18. Consequently, there is only one wind speed capable of producing rated wind power. Passive stand control is essential for the management of electricity, as it prevents the rated power from being achieved. Under certain circumstances, this may be an inappropriate solution to power management. The VS–FP control technique is sufficient for the extraction of resources and the achievement of high energy quality in low wind speed regions. VS–FP is well-known for its use in the design of small to medium-sized wind turbines as it is basic, inexpensive and highly efficient [106][108].

VS-VP is a blend of VS-FP and FS-VP. At wind speeds below the rated wind speed, VS–FP can be used to increase power quality and boost power output. In addition, FS–VP can be applied at wind speeds above the rated wind speed to increase the reliability of the power management at the rated wind level. This control technique is the only solution to balance the optimal power curve [106].

3.6 Wind Turbine Capacity Factor

Wind turbines cannot make power all the time since wind is sporadic by nature. Consequently, the energy factor of the wind turbine may be used to calculate the actual power output of the wind turbine for a certain duration (e.g. one year) determined by its power output if the wind turbine has run for the entire time. A fair capacity factor would be 25% – 30% and a very strong capacity factor would be roughly 40%. The power factor of the wind turbine is very susceptible to mean wind speed [103].

3.7 Wind Turbine Vibration Properties

The vibrational qualities of wind turbines include the natural propensity to bend related to the tower and the components of the rotor. It is also possible for the vibrations of the tower, rotor, and nacelle to interact in certain circumstances, which can lead to the wind turbine sustaining damage or becoming impossible to operate. One problem is that harmonic rotor loads can lead to excessive vibration when they occur at exact multiples of the speed of the rotor itself. This problem is known as resonance, where the frequency of the system is driven by the harmonic load of the rotor. Resonance can lead to serious structural weaknesses and damage. It is therefore necessary to ensure that the rotor does not turn at a critical speed which would induce resonance and potentially destroy the wind turbine system [109]. The issue of vibration can generally determine the overall performance and stability of a wind turbine system, and ultimately determine its lifespan. When monitoring the condition of a wind turbine or diagnosing any potential faults, vibration analysis plays a major role. Consideration of the vibration signals from different wind turbine components allows the dynamic analysis of the wind turbine to be improved. While modeling a wind turbine in detail can be challenging, the overall structure can be simplified and modeled in terms of a number of major substructures. Some of these substructures are involved in the vibration of the wind turbine, such as blades flapping, the tower oscillating, and the shaft of drive train rotating, as indicated in Figure 3.19 [110].

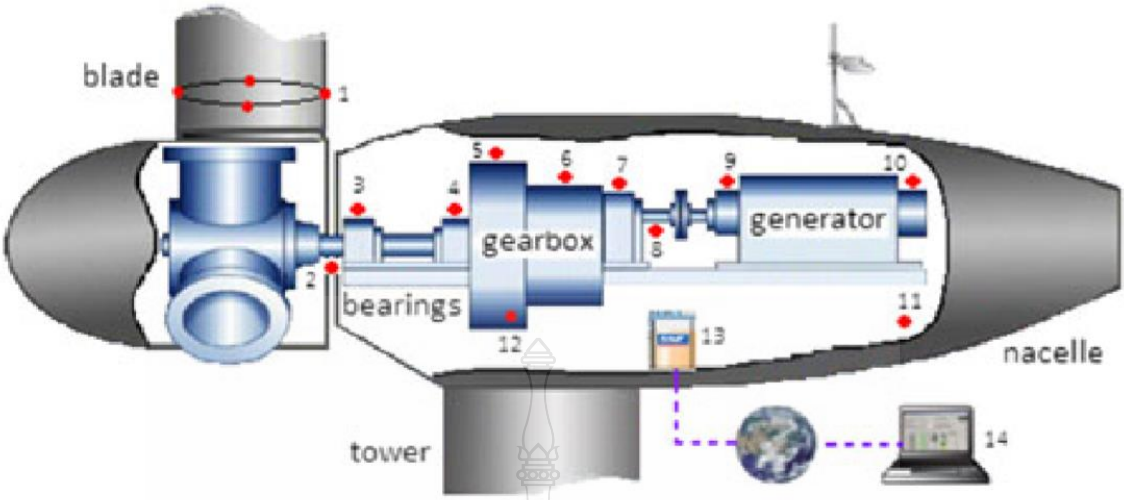

Figure 3.19 Vibration-based system for wind turbine condition monitoring [111].

There are several methods which can be employed to manage the problem of vibration in wind turbines. One approach is to install vibration isolators at the gearboxes, generators, and mounting devices, so that the amplitude of vibrations will be controlled, reducing noise and lengthening the lifespan of the wind turbines. The role of an isolator is to provide a soft padding between the nacelle, gearbox, and tower structure so that the noise path is interrupted and the components are subjected to lower stress levels than would otherwise be the case. This can reduce the potential for severe damage which can be caused by certain types of vibration. A second method involves the rotating parts of the wind turbine, by attaching torsional vibration isolators. This can be helpful since the rotational components present significant problems related to reliability. Torsional vibration isolators serve to limit the effects of variable torque and alter the influence of dangerous resonances. Noise is also lowered and the lifespan of the components can be prolonged [112].

3.8 Offshore Wind Farms

Wind farms developed in offshore locations are an increasingly important means of harnessing energy. The energy industry based on fixed offshore installations has developed significantly in recent years, providing both social and political solutions to the questions of using renewable energy resources. However, when selecting suitable locations for FOWTs, there are a number of factors to consider, such as fishing and shipping, the impact upon wildlife and the seabed, the existence of underwater archeological sites and the presence of pipelines or undersea cables [113]. The advantage of offshore wind energy is that the winds over the sea have preferable characteristics in comparison to onshore winds due to the smoother sea surface and absence of obstacles to block the airflow. The wind speed is thus stronger and more consistent, with better horizontal uniformity and less turbulence. It is also easier to find available space for wind turbines in the sea. FOWTs do face some problems, however, such as the need to withstand the sea, which is a difficult environment both for installation and maintenance, when compared to locating onshore wind turbines [114].

OWTs come in two main design types: Non-floating and floating offshore wind turbines.

3.8.1 Non-Floating Offshore Wind Turbines

These designs are also known as fixed foundation OWTs and can be used when the sea is relatively shallow, at less than 50 m in depth. The various foundation types can be explained as follows:

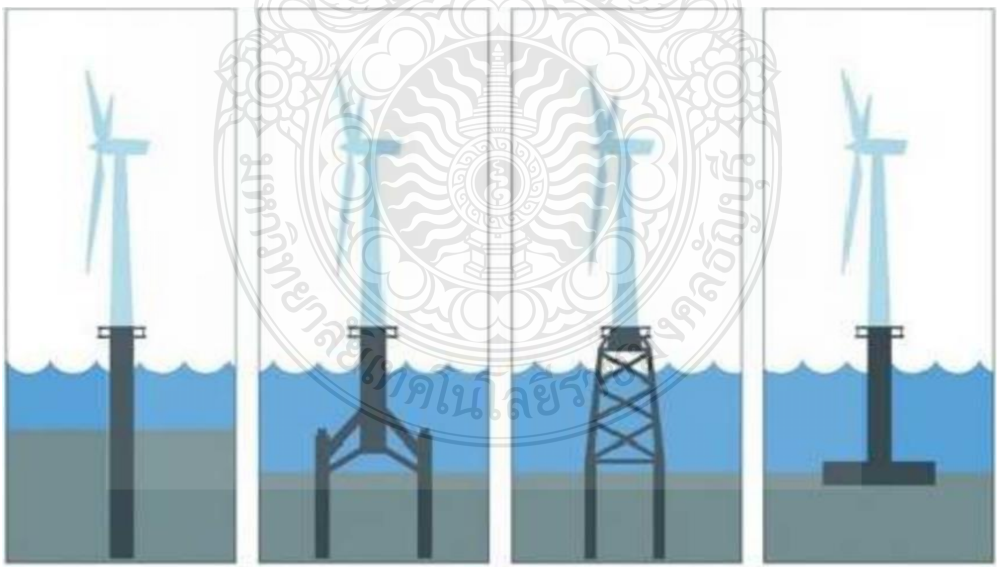

Figure 3.20 Illustrations of different fixed foundation wind turbine types. From left: monopile, three footed jacket, four footed jacket, and gravity based structure [115].

3.8.1.1 Monopile Foundations

Monopile foundations are the most widely used for OWTs due to their simplicity and suitability for shallow waters [116]. The design involves a single tube of diameter 4-5 m which is driven straight into the seabed toa depth of 15-30 m in accordance with the conditions of the seabed. This can be seen in Figure 3.20. For additional strength, it can be helpful if the seabed sediment is allowed to enter the end of the tube [115].

3.8.1.2 Jacket Foundations

The two principal types of jacket foundations are the three-legged and four-legged jackets. Three-legged jackets can be sued in water with a depth of up to 25 m, while the four-legged version is better for deeper water of up to 100 m [54]. The jackets will undergo piling into the seabed so that they will not be overturned. Furthermore, the steel pipes are connected with bracing sections which ensure that the necessary stiffness is achieved, as can be observed in Figure 3.20 [117].

3.8.1.3 Foundations using Gravity Based Structures

Gravity based designs have a broad and flat base which can be lowered on to the seabed, where it will be able to sit securely without overturning, as can be seen in Figure 3.20. However, it can only be used in shallow water up to a depth of 30 m [116].

3.8.2 Floating Offshore Wind Turbines (FOWTs)

FOWTs use floating platforms which support the wind turbines. A system of moorings is used to hold the floating platforms in position, and it is crucial that the platform offers sufficient buoyancy to support the weight of the wind turbines. A number of different platform designs exist at both the operational and developmental stages, but Figure 3.21 shows the three principal design concepts for floating platforms which are currently most commonly used for deep sea offshore locations [118].

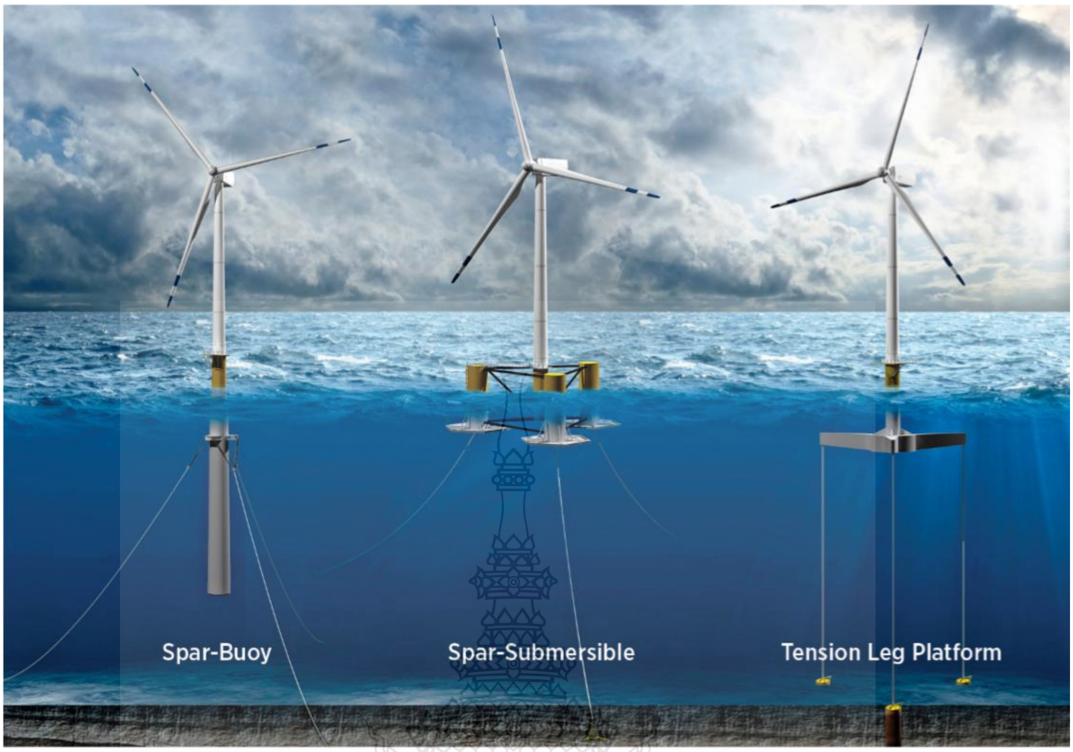

Figure 3.21 Floating offshore wind turbine platform conceptual designs [118].

3.8.2.1 Spar-Buoy Platforms

These platforms are designed as cylinders in shape, while there is ballast positioned on the underside of the platform to ensure that the platform continues to float in an upright position. This will occur because a significant righting moment is created, which offers resistance via inertia to rolling and pitching in the water. The stability is enhanced by the design which ensures that the center of gravity sits below the center of buoyancy. Furthermore, the upper part of the structure is constructed from lightweight materials, while the base remains much heavier. Platforms of this type should be installed in deep water because the draft of the platform must be relatively deep, exceeding the hub height above mean sea level, so that the platform will be stable, and any heaving motion will be minimized. One other issue is that sufficient vertical seabed space must be available in order to meet the spar-buoy type platform needs in terms of mooring systems to achieve operational effectiveness [119].

3.8.2.2 Semi-Submersible Platforms

The platforms are connected via column tubes, upon one of which the wind turbine can be mounted, so that it sits exactly at the geometric center of the platform, with the support of the lateral bracing members. In addition, the column tubes can provide ballast when they are partly filled with water, which can help to stabilize the platform when it is floating [120]. The structure therefore is able to act as a semi-floating platform which is attached to the seabed via the catenary mooring cables. It is important that the structures have bulk and considerable mass to aid stability, but if the draft can be minimized, this allows greater flexibility in usage as well as greater ease of installation [119].

3.8.2.3 Tension Leg Platforms (TLP)

The TLP design involves a semi-floating structure which derives its stability from taut mooring lines which are fixed to the seabed. These structures can be relatively small and light since the draft is shallow and stability results from the tension. However, the approach using a vertical tendon and anchor system is subject to greater stress. One further issue with TLP types is that their response tends to be less dynamic than is the case for other types which are semi-submersible [120].

3.8.3 Floating Offshore Wind Turbine Applications

FOWTs are primarily designed to take advantage of the stronger winds offshore by harnessing the energy and then transmitting it via cables back to land. In addition to this basic role, however, there are other ways to use FOWTs which are more economical and do not risk the loss of energy when the transmission lines are used [121]. These are some of the applications which are suitable:

- Provision of electrical power to islands or offshore rigs.
- Provision of power for desalination plants.
- Serving as a power source for fishing or exploration vessels at sea.

3.8.4 Floating Offshore Wind Turbines and their Loading Supplies

Shallow or deep offshore settings a few miles offshore are the typical locations for wind turbines designed for fixed or floating support platforms. As revealed in the figure 3.22, the loads on these systems are ruled by aerodynamic and hydrodynamic influences. in the actual design phase, the impact of sea ice, varying mean sea level and marine growth are peripheral burdens that must be addressed. The next section gives a description of the different loads used in the construction of a FOWTs.

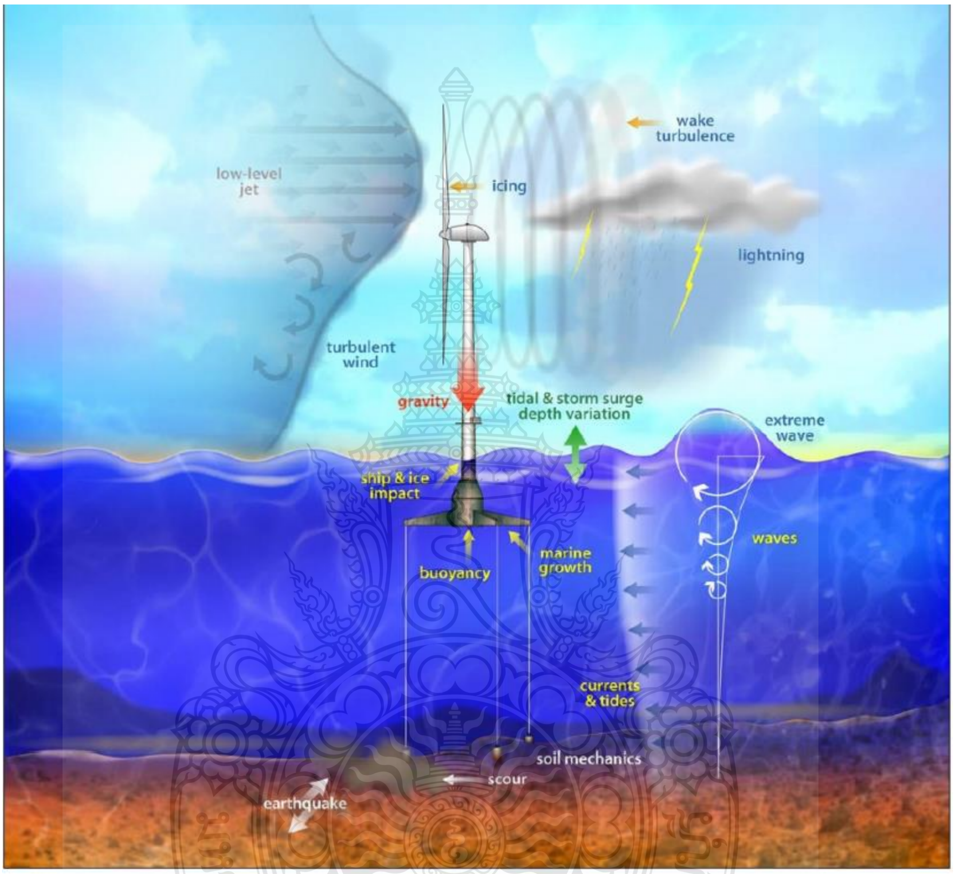

Figure 3.22 Floating offshore wind turbines and loading supplies [122].

3.8.4.1 Aerodynamic Loads

The interface between the airfoils of each rotor blade and the wind affect the power made by a wind turbine. Aerodynamic lift and drag are created by air streaming through the airfoil of the blades. The ensuing aerodynamic forces on the blades and wind turbine can be categorized into 3 groups, including 1) Stable aerodynamic forces caused by the average wind speed, 2) Recurrent aerodynamic forces caused by wind shear, rotation of the rotors, off-axis winds, and tower shadow, and 3) Arbitrarily shifting aerodynamic influences caused by gusts, turbulence, and dynamic properties. Wind loading technology for OWTs most frequently applies the BEM concept. The BEM theory is based on the theory of the blade factor, together with the concept of momentum. This theory deconstructs the arrangement into small, isolated components that support the model. The momentum principle suggests that the work done in moving the blade components through the rotor plane would lead the device to lose momentum [123].

3.8.4.2 Hydrodynamic Loads

Nonlinear and linear viscous drag effects, currents, radiation (linear potential drag) and diffraction (wave scattering), buoyancy (restoring forces), mixing of dynamic pressure over the wetted surface (Froude–Krylov) and inertia forces comprise the hydrodynamic loads on the floater. For hydrodynamic loading, a variation of the pressure integration method, the boundary element method, and the Morison formula can be used. Linear wave theory may be used in deep water environments, although linear wave theory is not valid in shallow water, since waves are usually nonlinear. For OWTs, it is apparent that nonlinear (second-order), random waves are better description of waves in shallow water. The immediate location of the framework when it comes to locating loads adds some variability. These hydrodynamic distortions are especially involved in resonant reactions, which affect power generation and structural reactions at low natural concentrations. Given the size and form of the support system and wind turbine, wave loading can be important and could be a major source of fatigue and extreme loads to be explored in the coupled examination. The identification of an effective method for evaluating hydrodynamic loads can therefore have a substantial impact on the expense of the device and its capacity to endure atmospheric and operating loads. To measure the hydrodynamic forces, the panel method, the Morison formula, the pressure integration method or a mixture of these methods can be used. The approach used should rely on the concept. Some of the hydrodynamic features of the FOWTs that could be considered based on the definition and site design are described below [124]:

- Suitable wave kinematics mockups
- Hydrodynamic models taking into account water depth, sea conditions, and support assemblies
- High hydrodynamic loading, counting breaking waves, via nonlinear wave

theories and proper amendments

- Stochastic hydrodynamic loading by linear wave theories with practical adjustments
- Significance of slender and large-volume constructions subject to the FOWTs support structure

Morison's equation is typically used to assess wave loads on slim structures, such as for a monopile. This formula consists of two parts, the first allowing for the forces of inertia and the second adjusting for the consequences of drag. The cumulative measured force is considered to be similar to the direction of flow. This load relies on the considerable wave height, wave period, and wave intensity, which can vary significantly at moments in calm seas relative to severe load levels. According to the evaluation being done (e.g. decisive versus fatigue loading situations), this must be considered [123].

3.8.4.3 Drag Loads

Drag loads result from the effects of the wind directly impacting upon the tower, along with the potential vortex shedding loads [125].

3.8.4.4 Inertial Loads

Inertial loads are related to the various systemic vibrational modes resulting from turbulence or wind shear and influenced by the inertial attributes and aerostructural properties of rotor [125].

3.8.4.5 Current Loads

Current loads refer to the currents generated by the wind and the tides, including those in the form of storm surges, which any design must take into consideration. When the waters are shallow, a much higher proportion of the total hydrodynamic load will come from currents [126].

3.8.4.6 Dead Loads

Dead loads are the loads which arise due to gravity, and will incorporate the weight of the structure itself, and weight of the internal tower components, in addition to all of the other machinery, such as cranes, transformers, platforms or landings for boat access which are affixed to the monopole or deck [125].

3.8.5 Floating Offshore Wind Turbines Six Degree of Freedom

Materially, the flow-field around the spinning wind turbine blade is inherently dynamic due to the presence of wind shear, vibration, gust, and yaw motion of the nacelle. Flow dynamics become more complicated than those of a fixed OWTs in the case of a floating offshore, HAWT. The added influence of the wind input, which is conveyed to the rotor due to the platform motion, needs to be taken into account since the motion of a floating platform comprises three translational components (heave in the vertical, sway in the lateral, and surge in the axial) and three rotational components (yaw about the vertical axis, pitch about the lateral, and roll about the axial), as revealed in the Figure 3.23. In such movements, platform pitch and yaw degrees of freedom dramatically contribute to uncertain aerodynamic forces on spinning blades incorporating the influence of wind shear, angle around the rotor disk, dynamic stall, rotor blade–wake impact, and distorted flow [58].

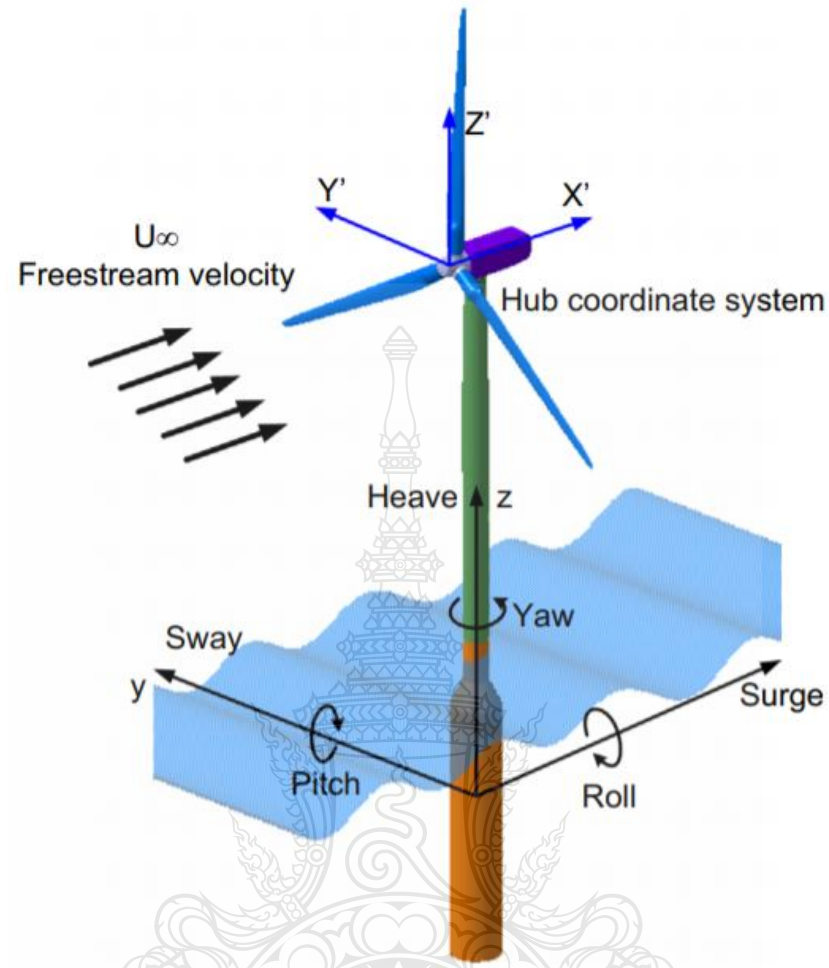

Figure 3.23 Floating offshore wind turbine platform showing degrees of freedom [58].

3.9 Activities of a Floating Platform

3.9.1 Buoyancy

Buoyancy can be understood using the concepts of Archimedes, according to which a structure which is completely submerged in a liquid shall have a force proportional to that of gravity acting on the quantity of material which has been displaced. The concept is based on the idea of harmony between forces, where the force acting on the body is buoyancy. This can be determined from the center of the body, which is known as the center of buoyant force [127]. Whether fully or only partly immersed, this force will act upon the body. As the force which occurs is the same as the mass of the liquid shifted, the body's weight is unimportant.

The buoyancy force can be indicated as [128]:

$$F = mg = \rho gV \tag{3.34}$$

In which: m = object mass (kg)

ρ = object density (kg/m^3)

g = force of gravity (9.81 N/kg)

V = object volume (m^3)

As shown in Figure 3.24, many buoyant forces will be applied on an object under varied situations. The object would be partly submerged under the provision that the mass of the object is not more that of the liquid, thereby causing the object to float as the volume of the object passes that of the liquid. The object will be completely immersed because the volume of the object is the same as the volume of the liquid and the weight of the object is equivalent to that of the liquid. In comparison, the target will plunge and become fully immersed if it is more dense than the liquid [129].

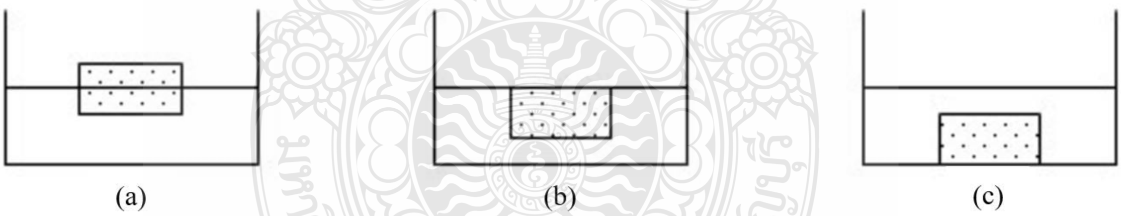

Figure 3.24 Buoyancy performance under unique circumstances: (a) partly immersed, (b) fully immersed, (c) completely submerged [129].

The weight and volume of the object would be in an acceptable ratio to balance the exact weight of the liquid in such cases. The result is neutral buoyancy, enabling the object to keep stationary when put in the liquid. As seen in Figure 3.24, an object that floats can oppose the condition in which it is put, on the other hand, and will turn over if the prospect is presented. These objects are statically unbalanced. Any disruption to the object or liquid can trigger displacement to a separate location that provides stability.

3.9.2 Static Stability

Usually, it is crucial to implement a strategic approach for a partly immersed body of arbitrary form, relative to arbitrary broad inclination angles in order to approximate all the required hydrostatic features, which is the synthesis of the pressure distribution on the immersed region. Still, the accompanying simplification theories are considered in the present work in order to gain better comprehension of the static stability of FOWTs systems: the fluid in which the body is submerged is at rest, the body is still in motion, and thus the sum of immersed volume is stable while (quasi-static) turning, and the inclination angle of the body is minimal (small angle calculation). 'Initial stability' analysis is the typical name for this. The examination is likewise limited to the pitch rotational d_f. (rotation about the y axis), though extension to roll rotational shifts is also possible [130].

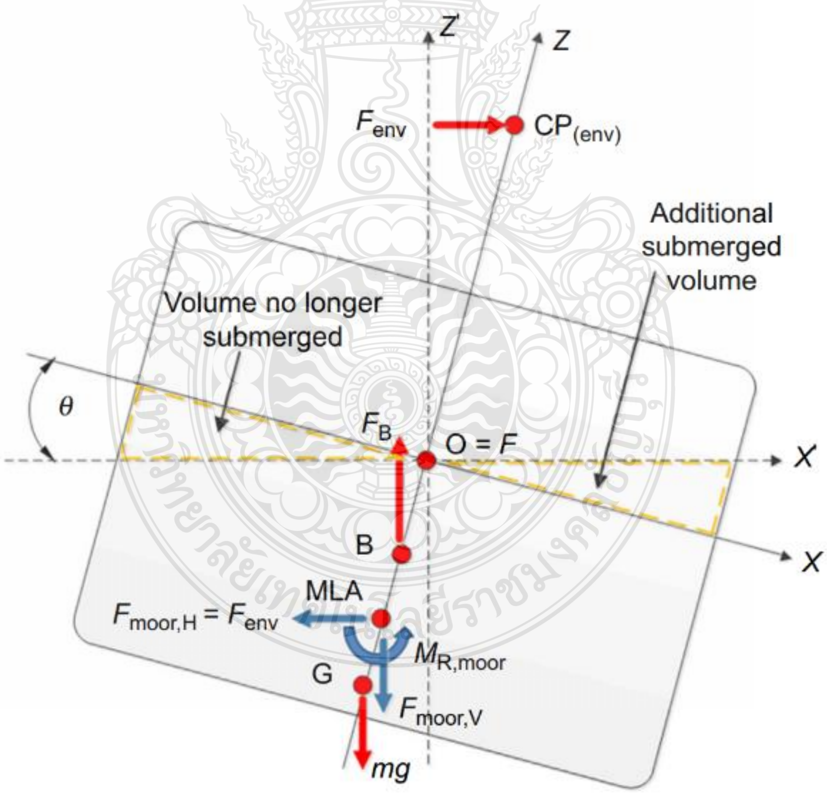

Figure 3.25 Forces and moments impacting a floating offshore wind turbine system, longitudinal plane [131].

With the floating body in the figure, the subsequent definitions are specified [130]:

- Axis system. The system of the orthogonal axis is specified, with x oriented with the wind direction, z perpendicular to x and vertical upward, and the origin concurrent with F (thus, z = 0 at the waterline level).
- Focal point of buoyancy (B). The geometric centroid of the immersed volume of a body in which the total buoyancy can be expected to act.
- Focal point of flotation (F). The geometric centroid of the waterplane region of any waterline. A waterline is the juncture line of the free water surface and the molded body surface.
- Centre of gravity (G). The center through which all weights involved in the system can be expected to act.
- Middle of mooring line action (MLA). The reference point of the mooring line action is the intersection of the line of action for the horizontal element of the mooring force with the z axis.
- Middle of pressure of environmental forces ($CP_{(env)}$). The elements operating on the FOWTs device include aerodynamic forces, hydrodynamic forces and existing forces. If equilibrium is assumed (no waves, only steady wind and existing forces), the pressure center of the environmental forces is measured from the point at which the total of the natural influences (F_{env}) is operating.

The centroid of the immersed volume of a body through which the overall buoyancy can be expected to act is the focal point of buoyancy (B). The centroid of the waterplane area, such as the area surrounded by a waterline, is the focal point of flotation (F). The juncture line of the free water surface with the molded body surface is a waterline. The center through which all the weights forming the system can be expected to act is the center of gravity (G). The juncture of the line of action for the horizontal component of the mooring force with the z axis is the middle of mooring line action (MLA), which is the orientation site of the mooring line action. Aerodynamic forces, hydrodynamic forces, and current forces comprise the forces impacting on the FOWTs system. The center of pressure for environmental forces ($CP_{(env)}$) is expressed as the point where all environmental forces (F_{env}) act on, if an equilibrium state is reflected with no waves, constant wind speed or current forces [131].

3.10 Maximum Inclination Angle

Although FOWTs structures may encounter comparatively broad angles of orientation (in roll and/or pitch), onshore and offshore wind turbines do not face such angles. As a result, very little expertise has been obtained in calculating the output of wind turbines at broad angles of inclination. Further, very few details have been published in literature. Besides, considering the fact that numerous offshore wind turbine subsystems (bearings, gearboxes, engines, etc.) have been designed to work in close proximity to the upright state, it is important to enforce a peak angle inclination for roll/pitch. The precise value of this optimum inclination angle is still subject to debate, but the literature states the starting value is 10 degrees. It is worth noting that this is the overall inclination angle, the sum of the static and dynamic angles of the oscillations due, respectively, to the average value (largely due to the wind) and the oscillation intensity (mainly due to waves) of the inclination incidents. In terms of architecture, this criterion can be converted into the minimal rotational stiffness of the floating support system [131].

3.11 Computational Fluid Dynamics (CFD)

CFD involves the modeling of the behavior of fluids within systems as shown in Figure 3.26. This requires the mathematical formulation of physical problems, which can be addressed by numerical methods, such as the discretization method, grid generation, or the use of numerical parameters. The calculations can then be performed by computers to simulate the way liquids and gases will interact, while boundary conditions are employed to define the surface interactions.

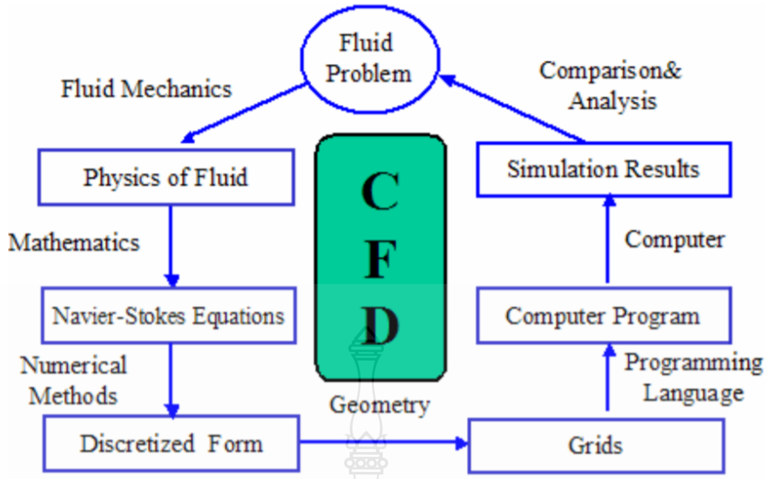

Figure 3.26 Computational fluid dynamics procedures [132].

Problems involving fluids can be addressed with a knowledge of the properties of those fluids derived from an understanding of fluid mechanics. The physical properties can be explained mathematically, using techniques such as the Navier-Stokes Equations which serve as the foundation of CFD. It is necessary to convert these Navier-Stokes equations to a discretized form if a computerized solution is to be reached. In this case, the translators will be techniques for numerical discretization, including the finite element, finite difference, and finite volume approaches. As a result, large problems must be subdivided into much smaller components due to this discretization. The problems can then be solved, and the simulation results analyzed, and comparisons drawn with the experimental outcomes. If the results prove to be inadequate, the process can be performed once again to rectify the matter [132][133].

3.11.1 Boundary Conditions

Boundary conditions serve as limits which can set the unique nature of the flow field for each particular problem under the equations which govern fluid motion. The type of boundary conditions necessary for a partial differential equation will be governed by the equation and also by the discretization approach which has been employed. Boundary conditions can be defined either as a numerical value or on the basis of its physical type [134].

3.11.2 Mesh Generation

Meshing is one of the key steps in finding solutions to CFD problems, although its difficulty is dependent upon the nature of the problem itself. Mesh generation is the name given to the process of discretizing the computational domain. For finite difference methods, the mesh will be a set of points, known as nodes as shown in Figure 3.27. In the finite volume method, points are used to form a set of volumes known as cells. Finite element methods make use of sub-volumes known as elements, for which the variables are defined at the nodes. The dependent variable values will be given for pressure, temperature, velocity, and so forth [134].

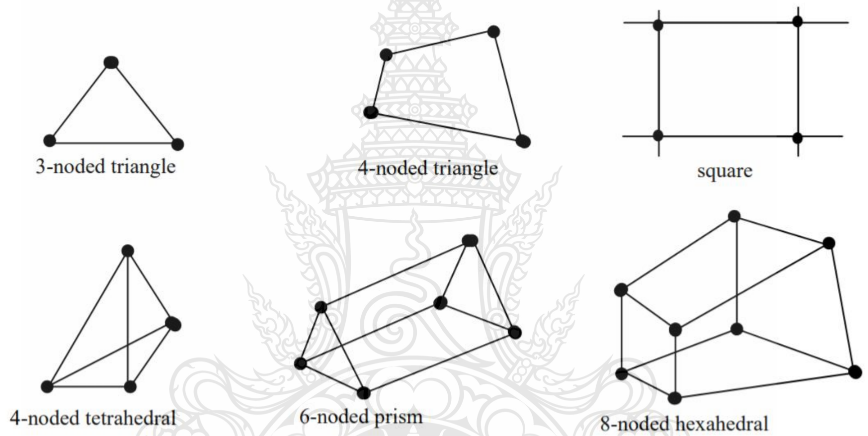

Figure 3.27 Common computational aspects [134].

Prior to generating the mesh, it will be necessary to identify the flow behaviors, which will include the boundary layers in the flow field, the vortices, and the existence of any substantial gradients in velocity or pressure. The size and shape of the mesh must be adequate for the determination of the physical conditions which arise within the flow. For large gradient regions it is necessary to use a high number of meshing points because there is very simple variation of parameters within each of the elements. The validation of the linear approximation between each pair of points therefore requires smaller mesh [134].

3.11.3 Convergence

Convergence describes the solution of a system of algebraic equations which tends towards the same initial and boundary conditions. Both consistency and stability will be necessary in order to explain the satisfactory numerical approach [135]. Figure 3.28 presents multiple iteration analysis. One iteration can be considered as a numerical pass through the whole model. Convergence of each of the degrees of freedom can then be plotted on the Convergence Monitor. In the initial stages of the analysis there are significant changes in outcomes from one iteration to the next, with the convergence lines tending to fluctuate widely. Once these convergence lines become horizontal, this can indicate that the results are no longer changing and that a converged solution has been reached [136].

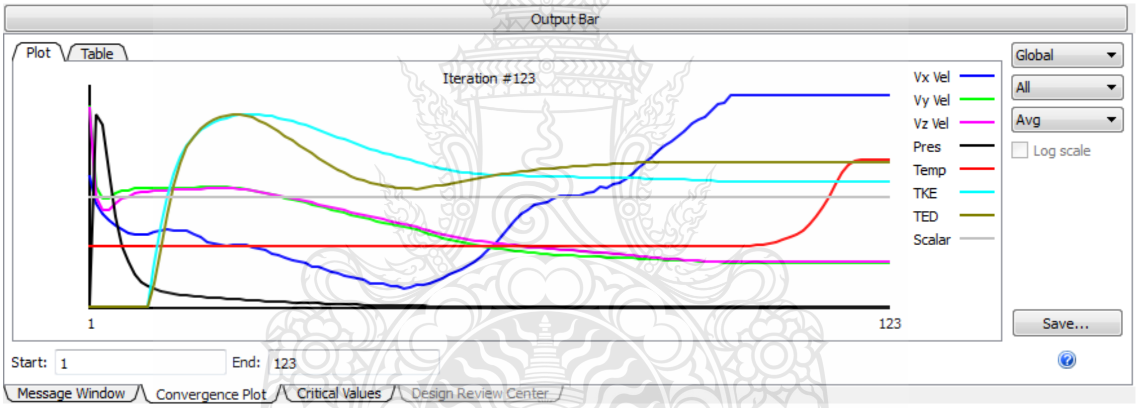

Figure 3.28 Convergence sample from multiple iterations [136].

3.11.4 Turbulence Models

To solve problems in CFD will typically demand that four key aspects are addressed. These are the issues of geometry and generating a grid, the development of a physical model, finding the solution, and finally conducting the post-processing of the computerized data. The geometry and grid are produced initially, and the set problem is computed, and it is well understood how the acquired data are presented. The theory is well known, but this is not the case when a physical model is set up to model the turbulence flows. It is difficult to model complex phenomena when the aim is to have as simple a model as possible. The ideal model should be designed to minimize complexity in the equations employed, while simultaneously describing the necessary physical processes, which can be complex.

The level of complexity involved in a model of turbulence will depend on the level of detail to be included, and the level of complexity to be examined via numerical simulation. It is the Navier-Stokes equations which introduce the complexity, since these equations are time-dependent, nonlinear, three-dimensional partial differential equations. In this context, turbulence can be described as a lack of stability in the laminar flow arising at high Reynolds numbers (Re). In the Navier-Stokes equations, the instabilities develop interactions between the nonlinear inertial terms and the viscous terms. Those interactions can be described as rotational, wholly time-dependent and fully three-dimensional. These interactions can be connected through vortex stretching. It is not possible to stretch the vortex when the space is two-dimensional, and this also explains why it is not possible to determine satisfactory two-dimensional approximations which can be applied to the phenomenon of turbulence. Turbulence is treated as a random process which occurs during a particular time period, and it is therefore not possible to apply a deterministic approach. The use of statistical techniques can, however, allow certain turbulence properties to be better understood. For example, flow variables may induce certain correlation functions, but these cannot be predetermined. One further key aspect of a turbulent flow is the movement of vortex structures along the flow. They typically have a long lifespan, and it is not therefore possible to specify some turbulent quantities as local. For this reason, the upstream history of any flow will be highly significant [137].

3.11.4.1 Semi-Implicit Method for Pressure-Linked Equations (SIMPLE)

This is the core algorithm used in a majority of CFD codes which are employed in commercial engineering. This technique offers robustness with coarse grids, although the rates of asymptotic convergence tend to be rather low. For this reason it can be readily applied to determine approximate solutions to many problems, including ones which are quite complex, but as grids are refined in an attempt to boost spatial accuracy, the approach become less effective. The method is developed in the form of a time stepping process, similar to the other algorithms explained, but it lacks the efficiency to be applied to solve problems which are time-dependent and which have a substantial spatial grid [138].

3.11.4.2 Large Eddy Simulation (LES)

LES is an approach to calculation in which large vortices, or eddies, can be directly computed, whereas smaller vortices can be modeled. The aim is to achieve convergent evolution. On a larger scale, eddies behave as directed by the forces which are exerted upon the flow and on the boundary conditions. The eddies are therefore dependent upon the flow. In contrast, eddies on the smaller scale act independently of the trends on the larger scale. Attempts have been made to find a universal model which can be applied to eddies of all sizes. The second key point concerning LES is that of filtering, since filtering functions can be used to address sub-grid fluctuation which might be resolving. These sub-grid fluctuations can be modeled by a process of averaging. One simple filtering function involves the central-difference approximation [138].

3.11.4.3 k-omega (k-ω) SST model

This model is one of the most frequently used and applies a pair of further transportation equations which govern the properties of flow turbulence and take into consideration the past effects of convection and the diffusion of energy from turbulence. Determining the energy of the turbulence is the transport variable k, while the scale of the turbulence is given by ω. The simple k-ω model may be applied to address problems of boundary layers, whereby the function works from the internal part and through the sticky sub-layer until it reaches the walls, and therefore this k-ω SST model may serve for low Reynolds flow applications which do not have extra damping functions. SST refers to Shear Stress Transport, while the SST formulation is switched to a k-ϵ behavior within the free-stream, thus eliminating one common k-ω problem whereby the model can show high sensitivity to the turbulence properties of the inlet free-stream. The k-ω SST model is also effective under conditions of adverse pressure gradients and separating flow. Some large turbulence levels are produced by the k-ω SST model in those areas which have a significant normal strain, such as stagnation regions or those with powerful acceleration. However, the effect in this case is not as strong as it would be with the normal k-ϵ model. It is possible for the SST model to take into consideration the transport of the principal shear stress appearing within adverse pressure gradient boundary-layers [139].

3.11.4.4 k-epsilon (k–ε) model

The k–epsilon (k–ε) model is the most widely used model for describing the mean flow features in a turbulence model. This type of model is used in a two-equation system as an adjunct to the Navier–Stokes equations. There are two variables in this type of model that describe the ordinary features of turbulence characteristics in a two-equation system: the turbulence kinetic energy (k) and the dissipation rate of turbulence kinetic energy (ε). This type of model is applicable to free-shear flows with relatively small pressure gradients. In addition, this type of model is quite simple to use as it only requires inputs for the initial values and/or boundary conditions [140].

The k–ε model equation cam be written as follows:

k-transport equation

$$\rho\frac{Dk}{Dt}=\frac{\partial}{\partial_{x_j}}\left[\left(\mu+\frac{\mu_t}{\sigma_k}\right)\frac{\partial_k}{\partial_{x_j}}\right]+\mu_t S^2-\rho\varepsilon; S=\sqrt{2S_{ij}S_{ij}} \tag{3.35}$$

ε-transport equation

$$\rho\frac{D\varepsilon}{Dt}=\frac{\partial}{\partial_{x_j}}\left[\left(\mu+\frac{\mu_t}{\sigma_k}\right)\frac{\partial_k}{\partial_{x_j}}\right]+\frac{\varepsilon}{k}(C_{1\varepsilon}\mu_t S^2-\rho C_{2\varepsilon}\varepsilon) \tag{3.36}$$

Coefficient

$$\sigma_k,\sigma_\varepsilon,C_{i\varepsilon},C_{\varepsilon 2} \tag{3.37}$$

Note: Air and water are used in simple flow experiments to determine the values of these constants.

Turbulent viscosity

$$\mu_t=\rho C_\mu\frac{k^2}{\varepsilon} \tag{3.38}$$

3.11.5 Governing Equations

CFD is based on the governing equations of fluid dynamics, which are derived from the mathematical equations of continuity, the conservation laws of physics, and the Navier–Stokes equations. There are three main physical laws underlying the governing equations: the continuity equation (the conservation of mass), the conservation of momentum according to Newton's second law, and the conservation of energy according to the first law of thermodynamics [141].

The general forms of the governing equations are as follows [142]:

Continuity equation

$$\frac{\partial \rho}{\partial t} + \nabla \cdot (\rho \vec{V}) = 0 \tag{3.39}$$

Conservation of momentum

$$\rho \frac{\partial \vec{V}}{\partial t} + \rho(\vec{V} \cdot \nabla)\vec{V} = -\nabla \rho + \rho \vec{g} + \nabla \cdot \tau_{ij} \tag{3.40}$$

Conservation of energy

$$\frac{\partial}{\partial t}\int e * \rho \, d\forall + \int (\breve{u} + \frac{p}{\rho} + \frac{V^2}{2} + gz)\rho V \cdot \breve{n} \, \mathrm{dA} = \dot{Q}_{net\ in} + \dot{W}_{net\ in} \tag{3.41}$$

The solutions can be calculated using partial differentials, which is the numerical method employed in CFD. There are several techniques for simplifying the problems by making some assumptions, such as is steady, isothermal, and incompressible fluid flow. In addition, some problems can be simplified by eliminating certain variables. A finite volume is used in CFD for simulation and spatial discretization of the governing equations. The numerical method must be verified.

CHAPTER 4
METHODOLOGY

In this chapter, the details of analyzing the tilt angle that occurred on the FOWTs in both experimental model and CFD simulation model would be described. The objective of this research was to study the effect of the rotor tilt angle on the performances; such as, rotational speed, power coefficient and tip speed ratio, and to compare and analyze the results between the experimental model and simulation model to define the different value between the two models.

4.1 Offshore Wind Energy Resources in Thailand

Located in the center of Southeast Asia, Thailand experiences low to moderate winds that are a speed of approximately 3-5 m/s on average. Furthermore, the areas of the country that offer the greatest potential for wind energy comprise the Gulf of Thailand coast and the Upper South on the west coast of the Gulf of Thailand as shown in Figure 4.1. These areas that are located 50 m above mean sea level have an average wind speed of 4.4 m/s per year. Additionally, it should be noted that offshore winds have much higher speeds, reduced turbulence, and are more constant with regard to the opportunities of wind flows when compared with those winds located onshore. This is because of the gentle sea surface and lack of impediments [143].

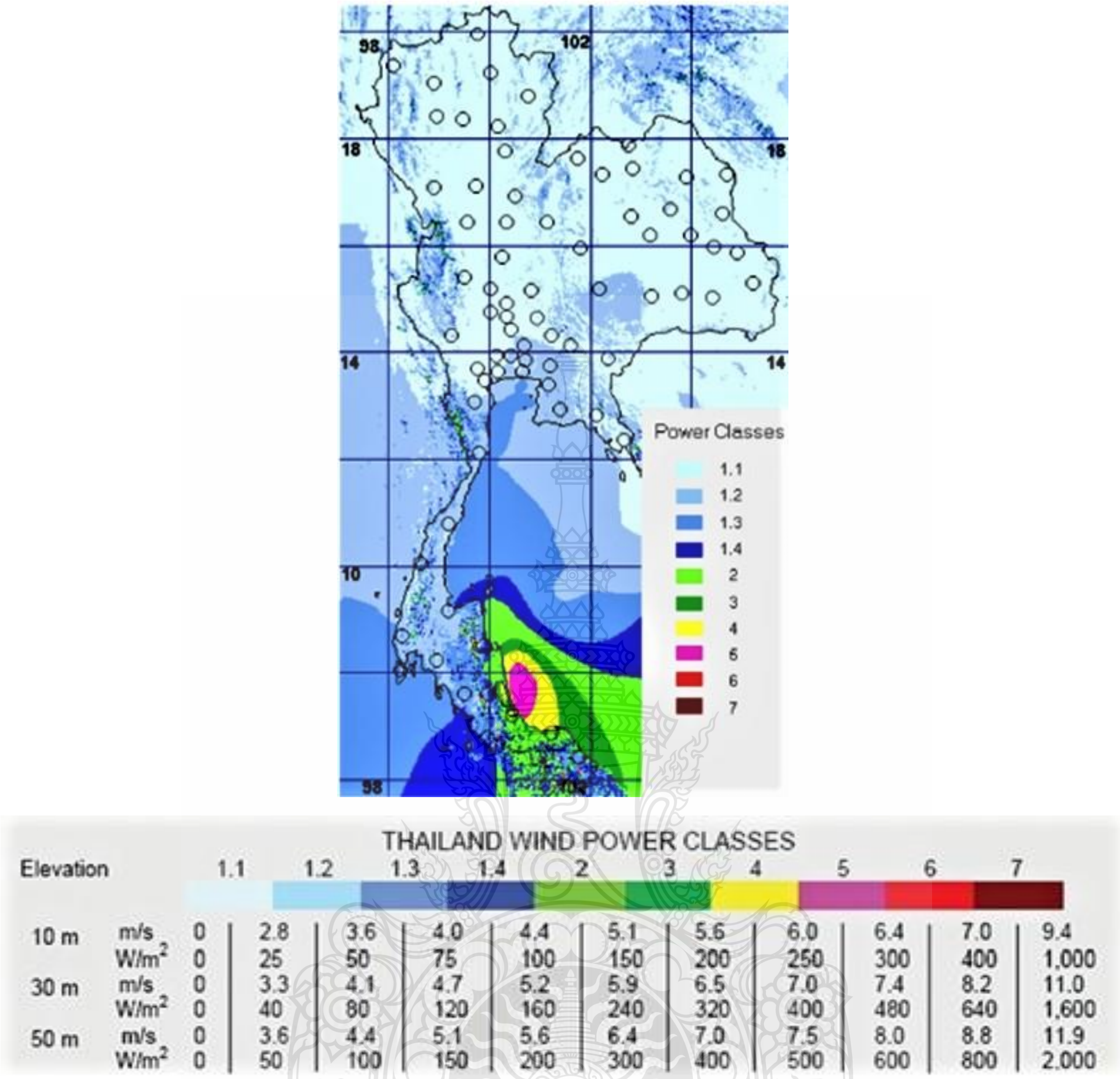

THAILAND WIND POWER CLASSES

Elevation			1.1		1.2		1.3		1.4		2		3		4		5		6		7	
10 m	m/s	0		2.8		3.6		4.0		4.4		5.1		5.6		6.0		6.4		7.0		9.4
	W/m^2	0		25		50		75		100		150		200		250		300		400		1,000
30 m	m/s	0		3.3		4.1		4.7		5.2		5.9		6.5		7.0		7.4		8.2		11.0
	W/m^2	0		40		80		120		160		240		320		400		480		640		1,600
50 m	m/s	0		3.6		4.4		5.1		5.6		6.4		7.0		7.5		8.0		8.8		11.9
	W/m^2	0		50		100		150		200		300		400		500		600		800		2,000

Figure 4.1 Map of the annual average wind power potential in Thailand [143].

However, in areas around the Gulf of Thailand at an elevation of 40 m. above mean sea level, the wind speed ranges between 3-6 m/s as shown in Figure 4.2.

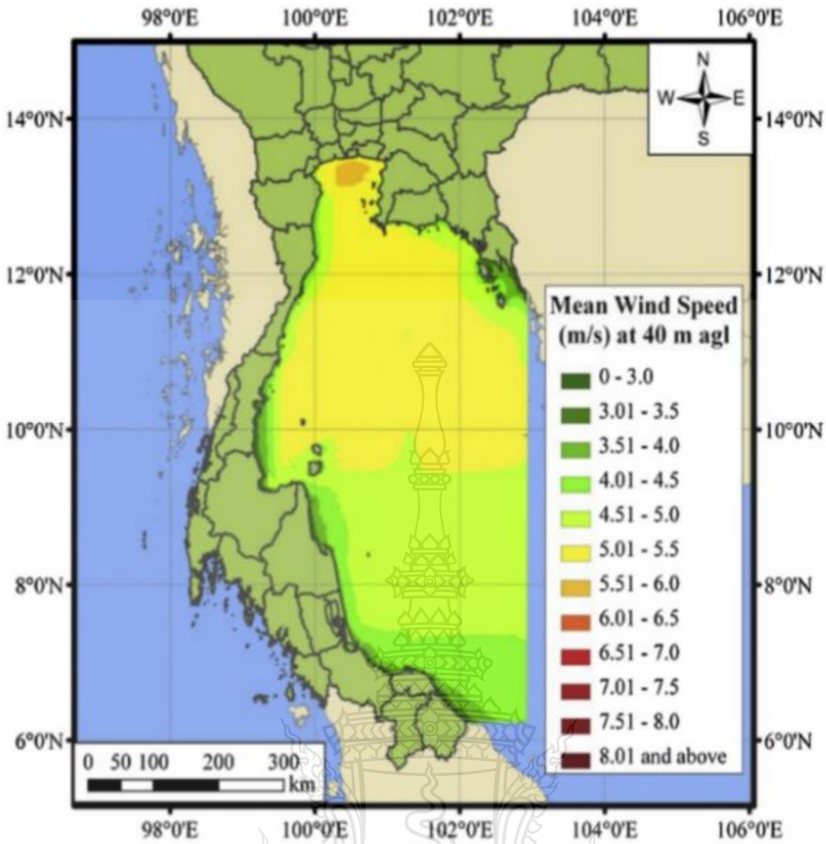

Figure 4.2 Wind speed of areas around the gulf of Thailand at an elevation of 40 m above mean sea level [144].

4.2 Conceptual Design

The objective of this study was to conduct a comparison of the performance of the rotor tilt angle of fixed tower wind turbines and FOWTs. R1235 airfoil blades with a diameter of 82 cm were utilized, which evaluated the actual experiment, theoretical equations, and CFD simulation. A comparison of the FOWTs versus the fixed tower wind turbines was conducted to evaluate their aerodynamic effectiveness empirically and numerically.

4.2.1 Floating Platform Calculations

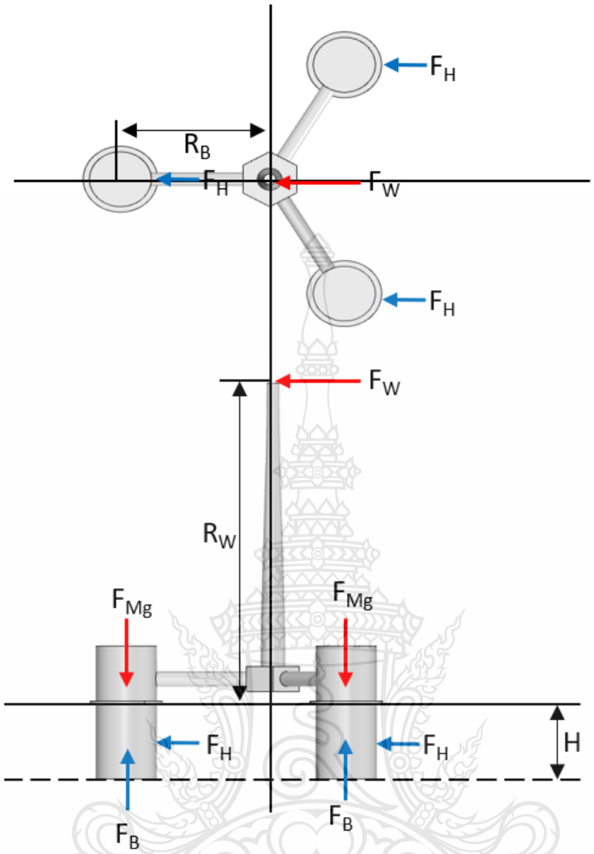

Figure 4.3 Forces acting on floating platform.

The sum of the external forces must also be zero in order for the object to balance and upright the object.

$$\sum M_{xyz} = 0 \tag{4.1}$$

Therefore, considering the total moment around the center of the base of the float from Figure 4.3.

$$F_W R_W + F_{Mg} R_B + 2F_B R_B \cos 60^{\circ} = 2F_{Mg} R_B \cos 60^{\circ} + F_B R_B + 3F_H \frac{H}{2} \tag{4.2}$$

Therefore,

$$F_B = F_{Mg} \tag{4.3}$$

$$F_W = \frac{1}{2}\rho_{Air}A_{Turbine}V_W^2 \tag{4.4}$$

$$F_H = \rho_{Water}g\frac{H}{2} * 2R_{Buoy}H = \rho_{Water}gH^2R_{Column} \tag{4.5}$$

When,

$$F_WR_W = 3F_H\frac{H}{2} \tag{4.6}$$

$$\frac{1}{2}\rho_{Air}A_{Turbine}V_W^2R_W = 3\rho_{Water}gH^2R_{Column}\frac{H}{2} \tag{4.7}$$

$$\rho_{Air}A_{Turbine}V_W^2R_W = 3\rho_{Water}gH^3R_{Column} \tag{4.8}$$

$$H = [\frac{\rho_{Air}A_{Turbine}V_W^2R_W}{3\rho_{Water}gR_{Column}}]^{\frac{1}{3}} \tag{4.9}$$

Also, from equation

$$F_B = gM_{Total} \tag{4.10}$$

$$\rho_{Water}g\nabla = gM_{Total} \tag{4.11}$$

Where: ∇ is the volume under the waterline of the buoy (m^3)
Therefore,

$$\rho_{Water}g(3 \times \pi \times R_{Column}^2 \times H_{Final}) = gM_{Total} \tag{4.12}$$

Hence, the total mass could be found as:

$$M_{Total} = \rho_{Water} \times 3 \times \pi \times R_{Column}^{2} \times H_{Final}$$

The calculated floating platform concepts could be showed in Figure 4.4.

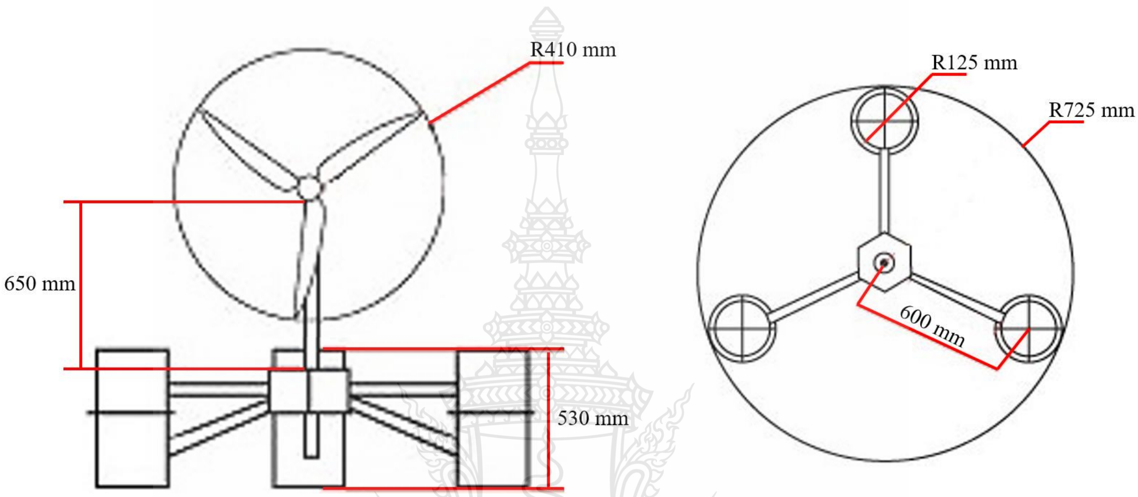

Figure 4.4 Calculated floating platform designs.

The actual weight of floating platform and monopole tower are shown in Figure 4.5-4.6

Figure 4.5 The actual weight of floating platform.

Figure 4.6 The actual weight of monopole tower.

Table. 4.1 The results obtained from equations.

	Calculated Parameters		Actual Parameters	
Parameter	Value	Unit	Value	Unit
$R_{Turbine}$	0.410	m	0.410	m
$A_{Turbine}$	0.528	m	0.528	m
R_W	0.650	m	0.650	m
R_B	0.600	m	0.625	m
R_{Column}	0.125	m	0.125	m
ρ_{Air}	1.225	kg/m^3	1.225	kg/m^3
ρ_{Water}	1000	kg/m^3	1000	kg/m^3
V_W	10	m/s	10	m/s
g	9.810	m/s^2	9.810	m/s^2
Draft, H	0.225	m	0.185	m
Buoy Volume	0.011	m^3	9.08×10^{-3}	m^3
Buoy Mass	11.045	kg	9.080	kg
Safety Factor	2		2	
H_{Final}	0.450	m	0.370	m
Final Mass	22.089	kg	18.166	kg
Total Mass	66.268	kg	54.500	kg

The result by calculated and actual parameters of floating platform designs could be showed in table 4.1 found that it requires higher draft (h) and total platform mass than the actual floating platform design as 0.450 m and 66.2 kg respectively. Whereas, the actual floating platform design values of draft (h) was 0.366 m. and the total platform mass was 54.5 kg. However, the actual floating platform still operated at the wind tunnel wind flow conditions even the design parameters were below the criteria design of calculated floating platform. In addition, the extra mass could be added to the actual floating platform to increase the platform stability, however, it is unnecessary in this research case. The actual floating platform dimensions could be showed in Figure 4.7. There were differences in column tube height and bracing tube length compared to the calculated floating platform concept to improve the stability and safety of the actual floating platform design.

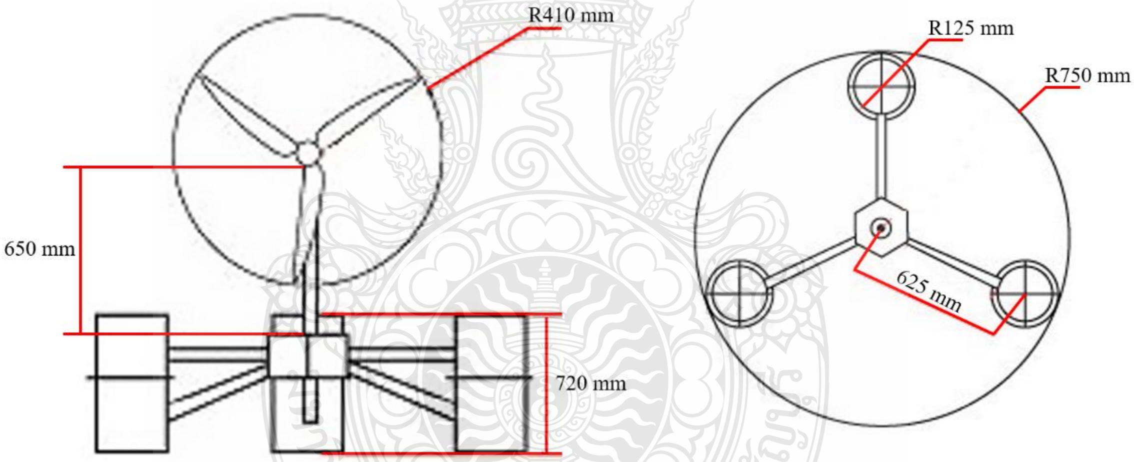

Figure 4.7 Actual floating platform dimensions.

4.2.2 Floating Platform Model Installation

The installation processes of the platform, wind turbine blades, monopole tower, and the water tank in the wind tunnel are shown in Figures 4.8-4.11

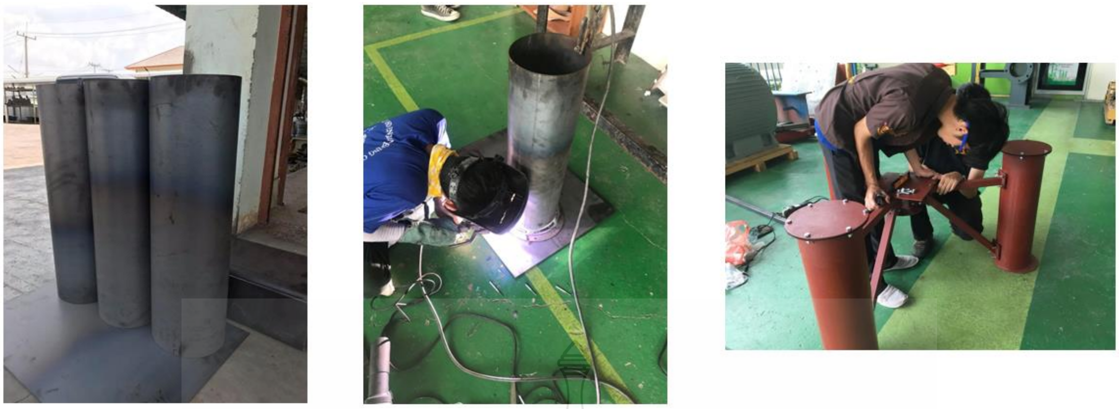

Figure 4.8 The installation process of the semi-submersible platform.

Figure 4.9 The installation process of the monopole tower.

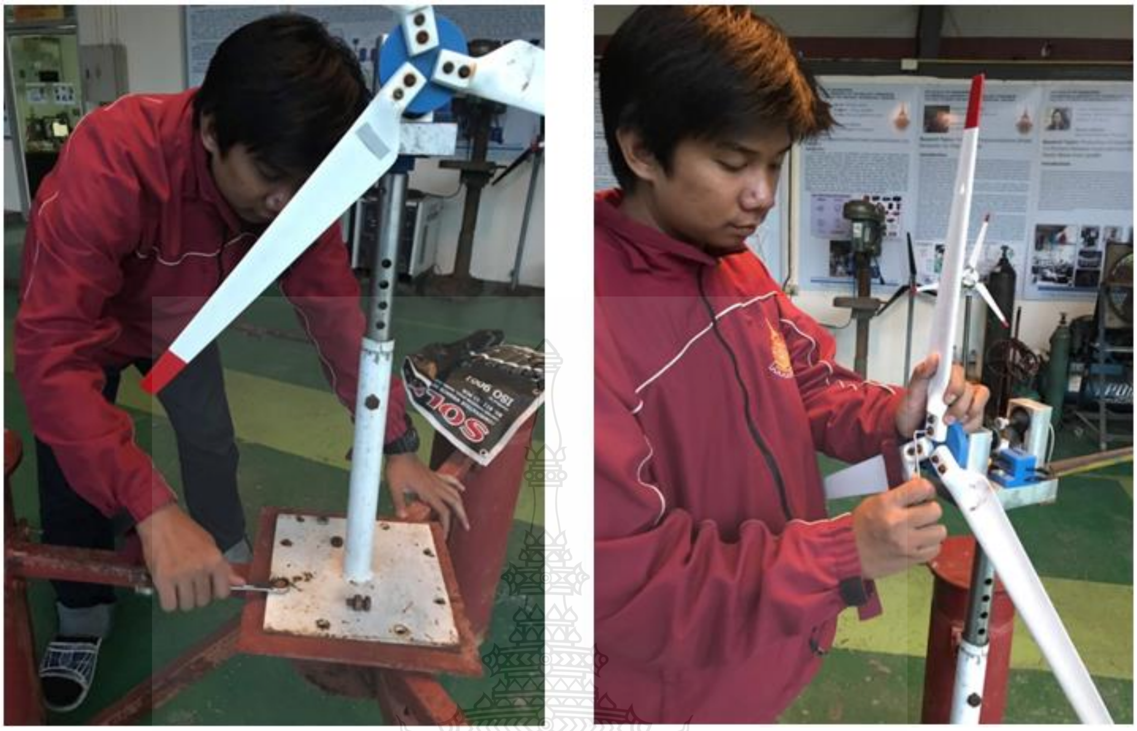

Figure 4.10 The installation process of the wind turbine blades.

Figure 4.11 The installation processes of the water tank.

The completed FOWTs components are shown in Figures 4.9-4.12 including the semi-submersible platform, R1235 airfoil blades, monopole tower and water tank.

Figure 4.12 Semi-submersible platform.

Figure 4.13 Monopole tower.

Figure 4.14 R1235 airfoil blades.

Figure 4.15 Water tank.

4.2.3 Experimental Setup

A wind tunnel at the Rajamangala University of Technology Thanyaburi (RMUTT) Energy Research and Service Center was utilized for undertaking the experiment. The wind tunnel, which was 3 m in height, 4 m in width and 4.5 m in length with a square airflow duct measuring 1 m^2 located in the center of the tunnel, had a 20,000 CFM centrifugal fan that was powered by a three-phase, 11 kW motor, a fan speed controller and a wind flow suction system for providing laminar flow as show in Figure 4.16.

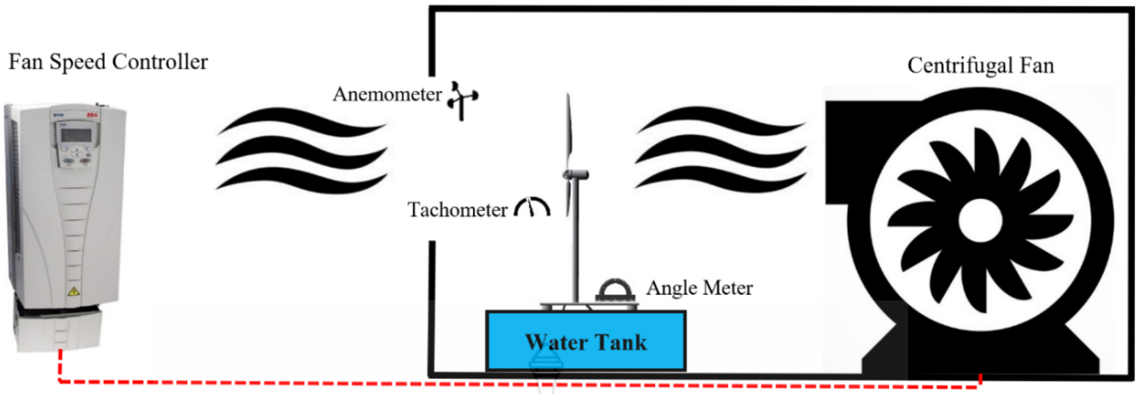

Figure 4.16 Schematic diagram of the wind tunnel.

The model used a semi-submersible platform, as it was easy to install, had a low draft and exceptional strength, as well as because of the space constraint of the wind tunnel. The FOWTs consisted of R1235 airfoil blades with a diameter of 820 mm, the tower height was 650 mm, and the platform floater was 720 mm as shown in Figure 4.7. The floating platform was placed in the water tank dimensions of 0.8 m high, 1.3 m wide, and 1.4 m long with water level of 0.75 m as shown in Figure 4.17-4.18. In addition, the fixed tower wind turbines had R1235 airfoil blades with a diameter of 820 mm and tower height of 1050 mm as shown in Figure 4.19.

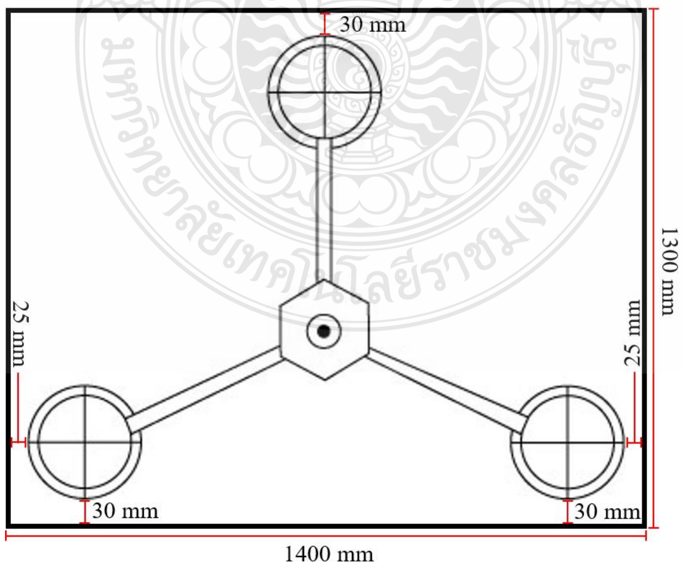

Figure 4.17 FOWTs in the water tank.

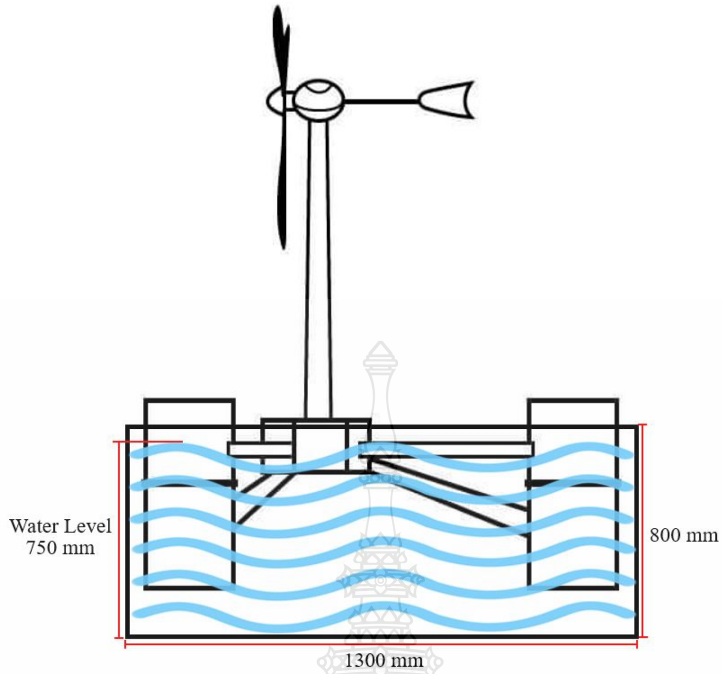

Figure 4.18 FOWTs in the water tank.

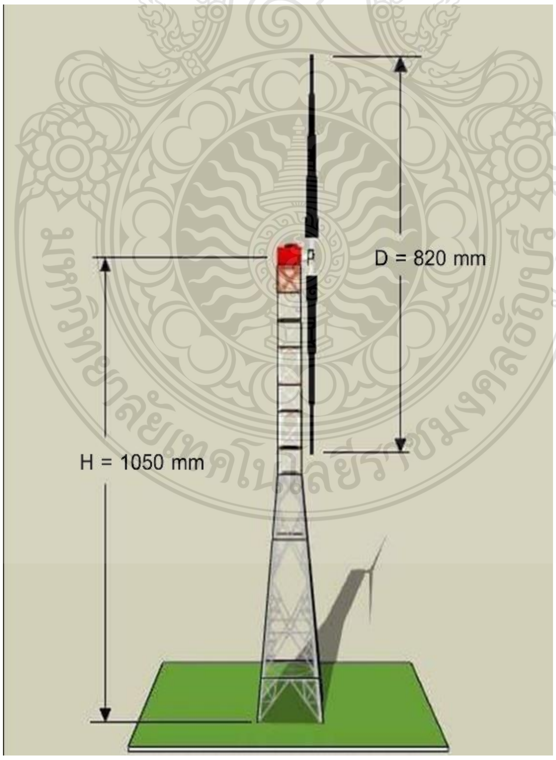

Figure 4.19 Dimensions of the fixed tower wind turbine.

4.2.3.1 Wind Tunnel Experimental Setup

In this study, the performance of the FOWTs and fixed tower wind turbine were analyzed by comparing the results obtained via wind tunnel testing of an experimental model and the FOWTs' CFD simulation model results. Winds with a speed of 2-5.5 m/s were the measurement for testing the model. The set up for the wind tunnel for the FOWTs and fixed tower wind turbines is shown in Figure 4.20.

Figure 4.20 Left: FOWTs and right: fixed tower wind turbines.

There were two possible FOWTs platform positions in the artificial pool: two-legged columnar tubes at the front facing the wind flow, and one-legged columnar tubes at the front of the platform as shown in Figure 4.21. The platform position with the two columnar tubes at the front was used in this experiment because the platform position with the one-legged columnar tubes at the front could potentially provide a higher buoyant force, which would infer that it would provide more support at the column tubes to reduce the effect of the tilt angle. As such, the platform position with the two-legged column tubes at the front was affected more by the tilt angle because the columnar tubes at the back provided less buoyant force. Thus, this experiment investigated the critical effect of the tilt angle in the analyses of the worst-case scenario for the FOWTs.

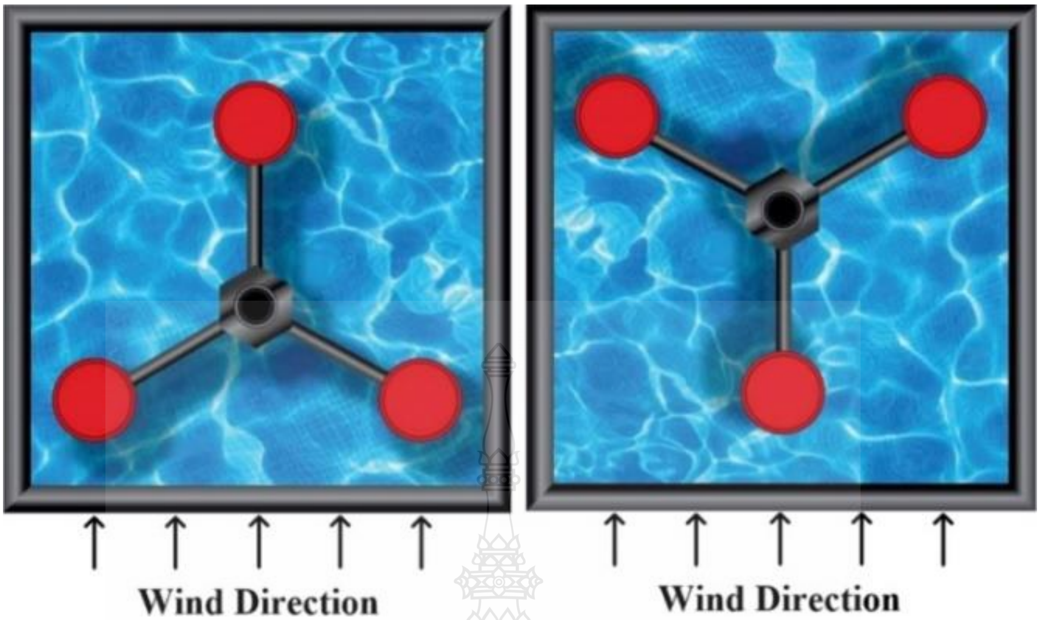

Figure 4.21 FOWTs platform positions: left: two-legged columnar tubes at the front and right: one-legged columnar tubes at the front.

4.2.3.2 Measurement Methods

Experimental data were obtained using three measurement tools: an anemometer for measuring the wind speed, a tachometer for measuring the rotational speed, and an angle meter for determining the tilt angle as shown in Figure 4.22. Moreover, to measure the wind speed, the fan speed controller was changed, which powered the motor of the centrifugal fan to reach the required speed 2-5.5 m/s. In order to obtain an appropriate result of the wind speed, 10 iterations were conducted on each blade rotation as shown in Figure 4.23.

Figure 4.22 From left: tachometer, anemometer and angle meter.

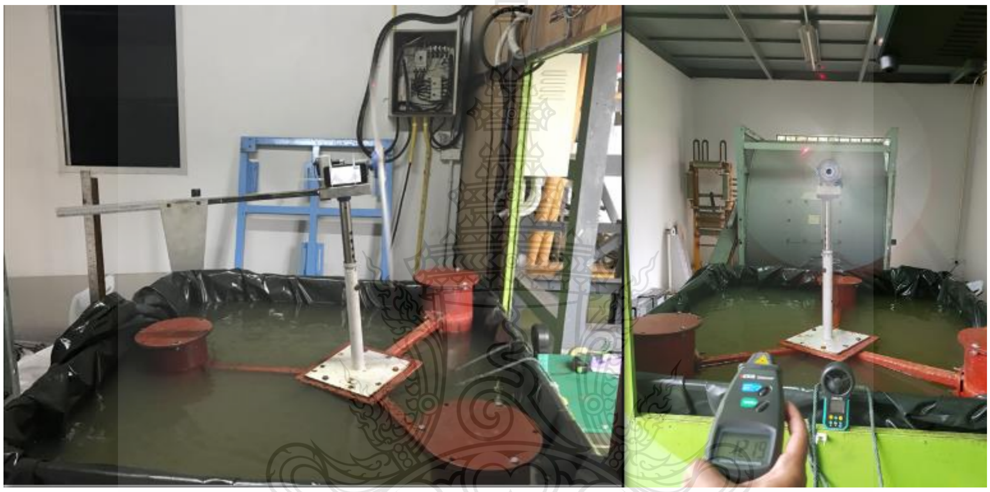

Figure 4.23 Measurement methods.

In order to establish the power productivity of the wind turbines at different wind speeds, it would be necessary to have a report of the various airfoil blades for appropriateness, which this study utilized the R1235 airfoil. This was because this airfoil has the capability of functioning in areas that experienced low wind speeds and could generate a higher lift force in low Reynolds number flows. As a consequence, the cut-in wind speed of the R1235 airfoil would be as low as 2 m/s, thus proving its suitability for the aforementioned areas that could have average wind speeds of 4-5 m/s. The findings of the experiment found that the R1235 blade produced a greater tip speed ratio in comparison to the theoretical wind turbine blade. The R1235 blade had a maximum power coefficient of 0.36 as shown in Figure 4.24.

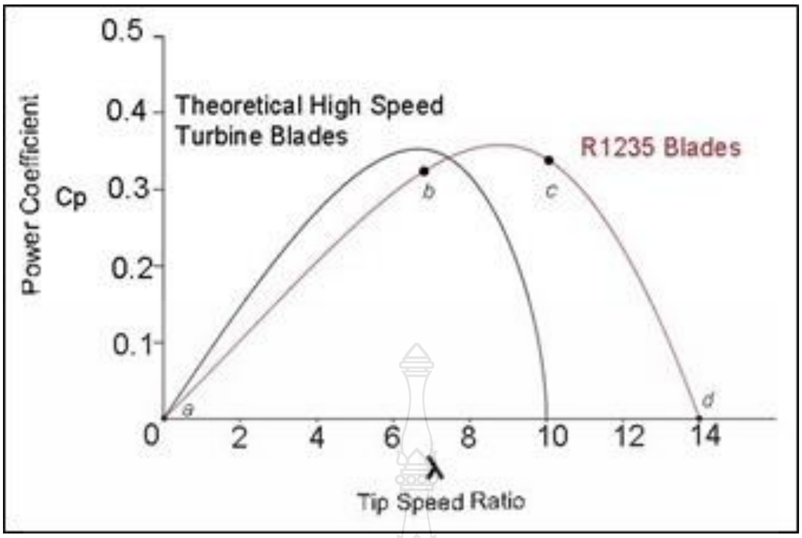

Figure. 4.24 Comparison of the blade tip speed ratio of the R1235 airfoil and theoretical wind turbine blade [145].

4.3 Wind Turbine Parameters

4.3.1 Wind Speed

This was a significant element, which demonstrated the power output and the amount of times that the blade rotated. For this experiment, wind speeds of 2-5.5 m/s were evaluated, as this equaled that of the range reached in Thailand.

4.3.2 Rotational Speed

This was the total sum of the revolutions per minute, which was used to determine the tip speed ratio of the wind turbine. The more and faster revolutions per minute, the greater the power output.

4.3.3 Tilt Angle

This would arise because of the vertical misalignment of the wind turbine axis, which would be a result of the movement of the rotor by the wind to be further apart from the axis. Thus, this would cause the defectiveness of the rotor's capability to capture a sufficient amount of energy.

4.3.4 Tip Speed Ratio (TSR)

This is the difference in the proportion of the rotor tip's speed and the real wind speed. Furthermore, this would incorporate the outcome of the aerodynamic performance of the wind speed, rotor size, and rotor angular speed combined with the power coefficient of the wind turbines rotor. Hence, this would be a significant element in generating the necessary wind energy. The TSR can be shown in equation 4.14:

$$TSR = \frac{U}{V} = \frac{\omega r}{V} = \frac{2\pi r N}{60V} \tag{4.14}$$

where U is the rotor tip's speed (m/s), V is the wind speed (m/s), ω is the angular velocity (rad/s), r is the rotor radius (m), and N is the rotational speed of the rotor (rpm).

4.3.5 Power Coefficient (C_p)

This comprises the evaluation of the total amount of wind energy that is transformed into electrical power. It was found that only 59.3% of the kinetic energy of the wind from the theoretical maximum C_p was able to be transformed into mechanical power that could operate a rotor.

4.3.6 FOWTs' Power Output

Kinetic energy is transformed into electrical power through the use of wind turbines; however, this production of power would rely on two major aspects: 1. wind speed and 2. the swept area of the wind turbine. The production of the power can be shown in equation 4.11:

$$P_w = \frac{1}{2}\rho A V^3 C_p \tag{4.15}$$

where ρ is the air density (1.225 kg/m^3), A is the swept area (m^2), V is the wind speed (m/s), and C_P is the power coefficient of the wind turbine.

In addition, the FOWTs performance could be adversely affected by the tilt angle. This would be caused by the vertical misalignment of the original positioning of the wind turbine that would correspond with the wind flow. Thus, this could affect the effective area available to capture energy from the wind flow. Figure 4.25 shows that the reduction factor would be the greatest at sin (90°) = 1, when the wind turbine blade would be positioned at a stationary point and would be perpendicular to the direction of the wind.

Moreover, the reduction factor would decrease as the tilt angle increased, which would degrade the performance of the wind turbine. Hence, the reduction factor could be determined as sin (90°+tilt angle), which would be assumed to be Sinβ in the FOWTs power output in equation 4.15:

$$P_w = \frac{1}{2}\rho A V^3 C_p sin\beta \tag{4.16}$$

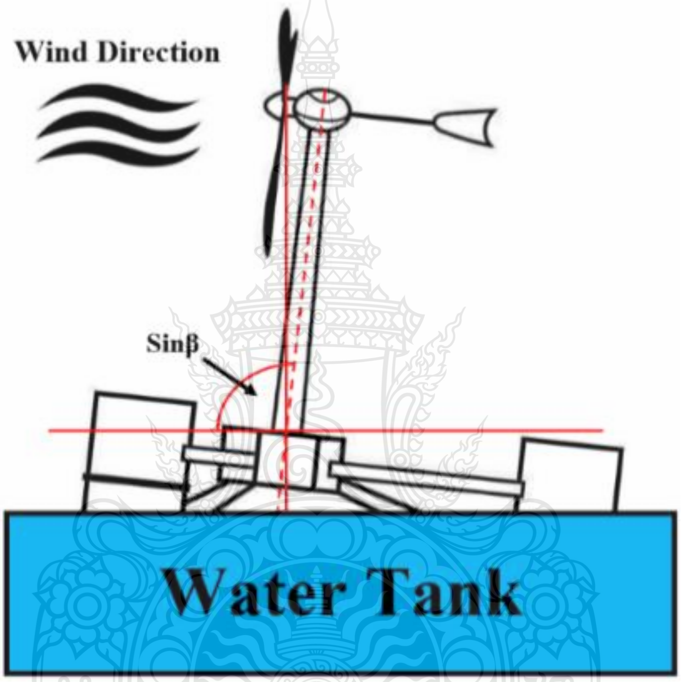

Figure 4.25 Assumption of tilt angle of FOWTs.

4.4 CFD Simulation Model Setup

The 3D model was the first step of this process. The part of the 3D model included all components of the FOWTs experimental model in the required dimensions, and the total weight of the FOWTs and rotating region. The materials of the wind turbine simulation included the static region and dynamic region. The former region comprised the wind turbine hub, wind turbine tower and floating platform, whereas the latter region consisted of the wind turbine blades and wind turbine rotating region. The rotating region used the free spin type. The boundary condition set up for the inlet was selected by the condition of the wind flow velocity, and the outlet side was selected by the pressure. The incoming wind speed direction would be selected depending on the value of the tilt angle. Additionally, the grid and mesh were created for the different parts of the study model. The mesh was also determined by a grid-dependent check using coarse, medium, and fine mesh to acquire the rotation speed as shown in Figure 4.26.

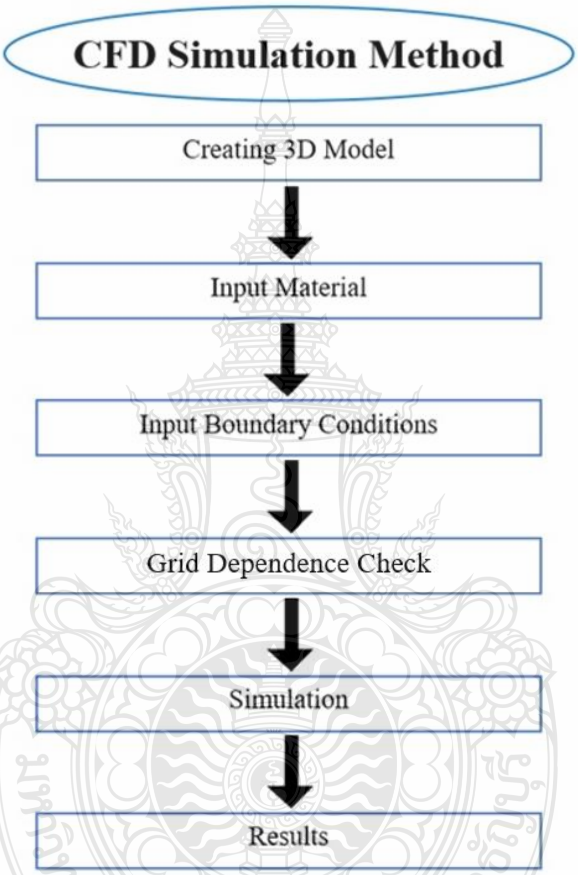

Figure 4.26 CFD simulation method.

4.4.1 CFD Boundary Conditions

The CFD simulation program, CFDesign v7, was used in this study. The experimental test results obtained were compared with those obtained via the CFD modeling. Figure 4.27 shows the boundary conditions applied to the CFD model for a wind tunnel with the dimensions of 5 m wide and 10 m long, and a rotating region 1 m wide. The set distance was required before the wind turbine could have a marked impact on the rotor blade; therefore, the rotor blade was positioned 7 m away from the velocity inlet to permit a laminar wind flow. The standard k–ε turbulence model was also applied in the simulation, and two types of boundary conditions were applied. The first type included the fixed conditions for the objects in the three-dimensional model that would be stationary when a force was applied, i.e., the wind tunnel's wall and edges. The second type constituted the moving conditions, which would be applied to objects that would move when acted upon by forces. In the experiments conducted in this study, the wind turbine blades (the rotating region) and moving air were subjected to moving boundary conditions. The rotating region was part of the motion module used for analyzing a rotating device and encompassed a spinning object.

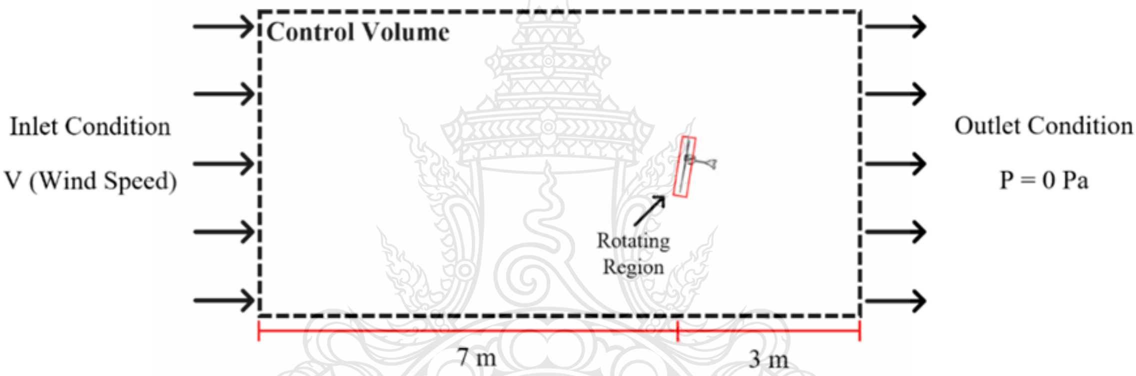

Figure 4.27 CFD boundary conditions.

Table 4.2 shows the CFD model parameters and values applied to the control volume model to solve the problem. The standard k–ε model was used as the turbulence model.

Table 4.2 CFD model parameters.

Parameter	Value	Units
Inlet: Wind Speed	2-5.5	m/s
Inlet Total Temperature	320	K
Angular Velocity	Free Spin	Rad/s
Working Fluid	Ideal Air	
Fluid Density	1.225	Kg/m^3
Turbulence Model	k-ε	
Outlet Pressure	0	Pa

Figure 4.28 displays both the rotating region and static region. The rotating region was part of the motion module, and was a region completely surrounded by a rotating object. The CFD rotating machinery capability would analyze the rotating devices using a locally rotating frame of reference. Hence, the rotating objects comprised the rotating region and wind turbine blade. The static region was the area in the model that were not rotating and analyzed in a static frame of reference. These regions are called static regions.

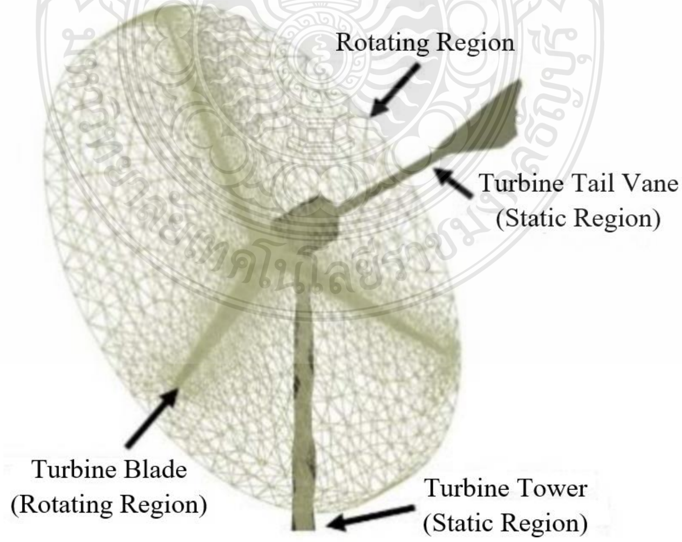

Figure 4.28 Rotating region and static region [146].

As shown in Table 4.2 above, the inlet condition of 2-5.5 m/s of the wind speed would be selected and the wind gauge pressure of 0 Pa would be selected for the outlet condition. The angular velocity was a free spin type with the working fluid of ideal air. Likewise, the turbulence model for simulation would be applied to the k-ε turbulence model.

4.4.2 Mesh Refinement

The Eulerian specification of the flow field was adopted in the CFD model to analyze the moving fluid at a particular location in the space through which the fluid would flow over the fixed mesh.

The cell-vertex numeric was applied to separate the domain, which could result in unstructured tetrahedral elements. Therefore, the complicated rotating geometry was detected; automatic meshing was used for further geometric improvements. As such, there were three steps for the mesh adaptation to adjust the high-volume velocity gradients in the problematic analyses: coarse meshing, medium meshing, and fine meshing as shown in Figure 4.29.

Table 4.3 shows the suitable amounts of meshing for the CFD wind turbine model for the various blade velocities. These were established through the examination of the model at an inlet wind speed of 5.5 m/s. As can be seen in Figure 4.30, the appropriate quantities of meshing for the CFD wind turbine model for numerous blade velocities could be concluded from analyzing the model at an inlet wind speed of 5.5 m/s. Furthermore, the correlation between the total sum of elements and the wind turbine's rotational speed was shown to be at intervals of 12,000-2,500,000 elements. Consequently, as could be observed, the slope would become constant when the number of the elements of the model reached 1,500,000. Therefore, 1,500,000 elements were used in the CFD simulation model. Figure 4.31 shows that the meshing of each part was not the same as the element size. The blade element size should be the most detailed due to the complexity of the curvature of the blade surface. The complex airfoil surface would thus need fine meshing to make the elements smooth along the surface of the airfoil.

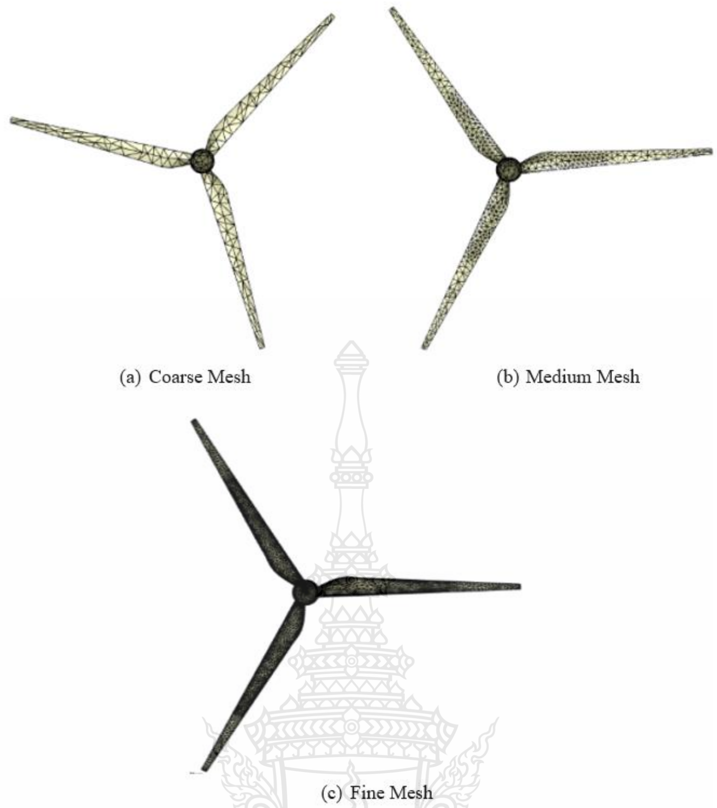

Figure. 4.29 Wind turbine blade meshing in the CFD.

Table 4.3 Number of elements and blade velocity.

Meshing Number	Blade Velocity (rpm)
0	0
12,000	1,000
70,000	1,050
200,000	1,150
300,000	1,201
600,000	1,300
1,000,000	1,669
2,000,000	1,785
2,500,000	1,802

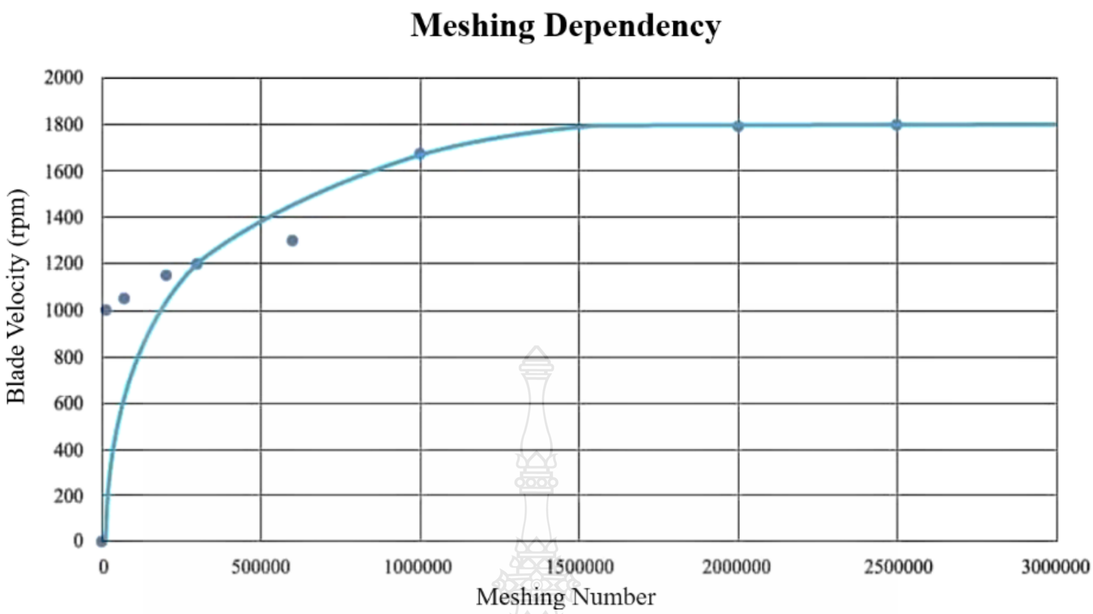

Figure. 4.30 Relationship between the meshing number and blade velocity.

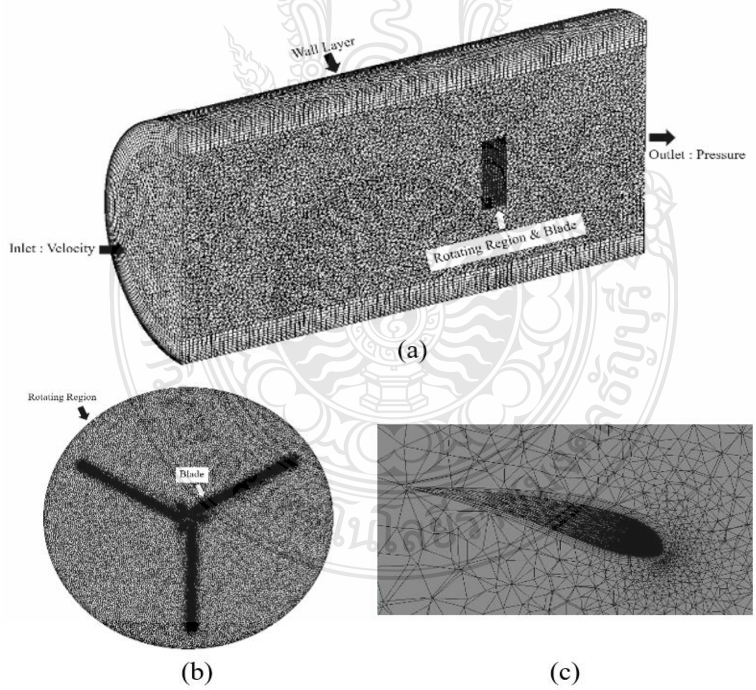

Figure. 4.31 CFD mesh structure: (a) meshing of the cross-section of the wind tunnel, (b) meshing of the blade rotation region, (c) meshing of the airfoil cross-section.

CHAPTER 5
RESULTS AND DISCUSSION

The analysis and comparison of FOWTs and fixed tower wind turbines using experimental models in wind tunnels and FOWTs based on CFD models are presented in this chapter. A wind speed in the range of 2-5.5 m/s was employed in both the wind tunnel experiments and the CFD simulation. The tilt angle values obtained in the wind tunnel experimental model were applied in the CFD simulation models. This chapter also explains the findings for the rotational speed of the turbines, the tip speed ratio, the power coefficient and the power output.

5.1 Results of the Two Floating Platform Positions

There were two possible FOWTs platform positions in the water tank that were tested for the stability of the floating platform in the wind tunnel. Firstly, the one-legged columnar tubes at the front, facing the wind flow, and the two-legged columnar tubes at the front of the platform as shown in Figure 5.1.

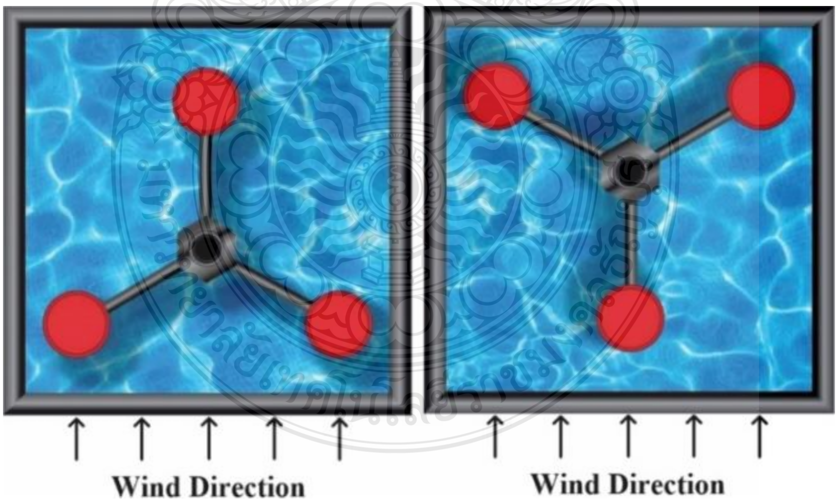

Figure 5.1 FOWTs platform positions: left: two-legged columnar tubes at the front and right: one-legged columnar tube at the front.

As shown in Table 5.1 and Figure 5.2 below, the one-legged columnar tube at the front could obtain the stability of the floating platform better than the two-legged columnar tubes at the front in terms of the floating platform tilting motion from the wind flow. The dotted lines in the figure are used to represent the values which are missing as no results were obtained from the experiment. The rotational speeds were reduced, and the tilt angles were increased in the two-legged columnar tubes. In Table 5.2 showed the rotational speed percentage differences and the tilt angle percentage differences at wind speed between 2-5.5 m/s. The average percentage difference between the two positions showed the rotational speed difference was 4.7%, while the tilt angle average difference was 43%. Hence, the platform position with the two-legged columnar tubes at the front was tested in the wind tunnel experiment due to its position with the two columnar tubes at the back that may potentially provide a higher buoyant force. This inferred that it would provide more support at the columnar tubes to reduce the effect of the tilt angle. The platform position with two columns at the front was affected more by the tilt angle because the columnar tubes at the back provided less buoyant force. Thus, this experiment investigated the critical effect of the tilt angle in an analysis of the worst-case scenario for the FOWTs.

Table 5.1 The results between the two floating platform positions.

	One-Legged Columnar Tube at the Front		Two-Legged Columnar Tube at the Front	
Wind Speed (m/s)	Rotational Speed (rpm)	Tilt Angle (Degree)	Rotational Speed (rpm)	Tilt Angle (Degree)
2.0	325.8	2.0°	307.1	3.5°
2.5	460.0	2.4°	437.7	3.8°
3.0	570.2	2.6°	534.6	3.9°
3.5	700.6	3.2°	655.6	4.3°
4.0	803.6	3.6°	781.1	4.7°
4.5	935.3	3.9°	891.2	5.0°
5.0	1025.0	4.4°	1010.8	5.8°
5.5	1183.5	4.5°	1144.7	6.1°

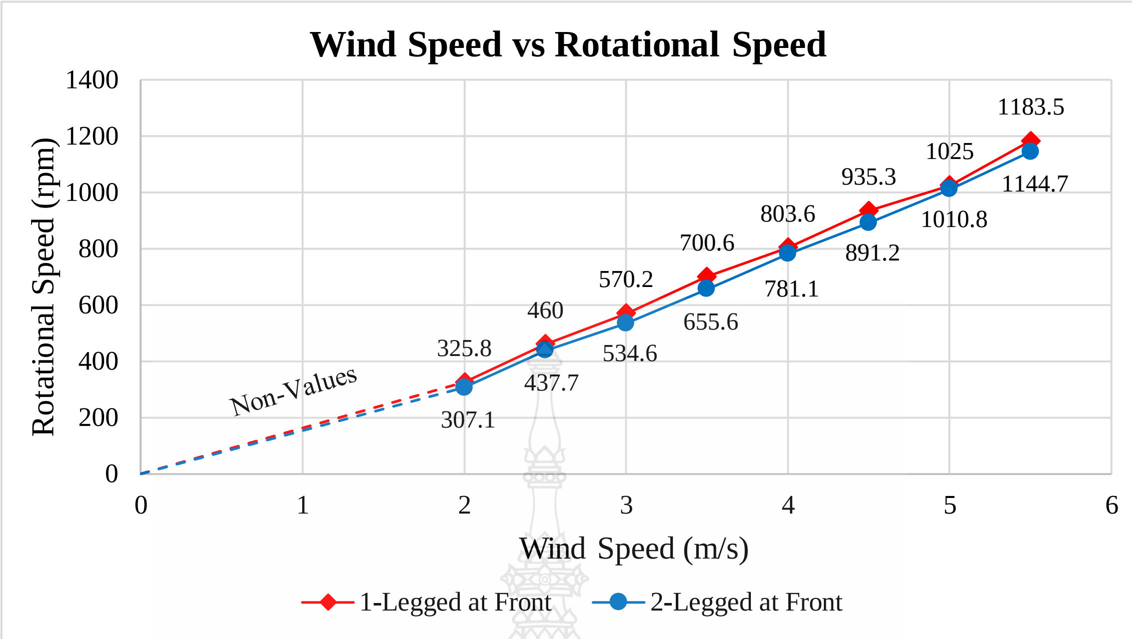

Figure 5.2 Comparison between the one-legged columnar tubes at the front and two-legged columnar tubes at the front floating platform positions.

Table 5.2 The rotational speed percentage differences between the one-legged columnar tubes at the front and two-legged columnar tubes at the front floating platform positions.

Wind Speed (m/s)	Rotational Speed Percentage Differences (%)	Tilt Angle Percentage Differences (%)
2.0	6.1	75.0
2.5	5.1	58.3
3.0	6.7	50.0
3.5	6.9	34.4
4.0	2.9	30.6
4.5	4.9	28.2
5.0	1.4	31.8
5.5	3.4	35.6

5.2 Wind Tunnel Results Comparison for FOWTs and Fixed Tower Wind Turbines

Table 5.3 shows the results obtained from the experiments in the wind tunnel involving the fixed tower wind turbines, with data provided for wind speeds, rotational speeds, tip speed ratios and power coefficients. In Table 5.4, the results concerning wind speed, rotational speed, tip speed ratio, power coefficient and tilt angles are shown for the experiments with FOWTs.

In both sets of experimental data, it was apparent that wind speed and rotational speed were in direct proportion; rising wind speed resulted in rising rotational speed. The rotational speeds for FOWTs remained consistently lower than those of the fixed tower wind turbines as a consequence of the way the tilt angle affects the performance of the rotor wind turbine.

Table 5.3 Experiment data in the wind tunnel for fixed tower wind turbines**.**

Wind Speed (m/s)	Rotational Speed (rpm)	Tip Speed Ratio (λ)	Power Coefficient (C_P)
2.0	393.1	8.4	0.36
2.5	591.6	10.2	0.33
3.0	736.4	10.5	0.32
3.5	904.0	11.1	0.29
4.0	1043.9	11.2	0.28
4.5	1241.6	11.8	0.24
5.0	1432.4	12.3	0.20
5.5	1608.9	12.6	0.17

Table 5.4 Experiment data in the wind tunnel for FOWTs**.**

Wind Speed (m/s)	Rotational Speed (rpm)	Tip Speed Ratio (λ)	Power Coefficient (C_P)	Tilt Angle (Degree)
2.0	307.1	6.6	0.32	3.5°
2.5	437.7	7.5	0.34	3.8°
3.0	534.6	7.7	0.35	3.9°
3.5	655.6	8.0	0.35	4.3°
4.0	781.1	8.4	0.36	4.7°
4.5	891.2	8.5	0.36	5.0°
5.0	1010.8	8.7	0.36	5.8°
5.5	1144.7	8.9	0.36	6.1°

In Figure 5.3 the rotational speeds of a FOWTs and a fixed tower wind turbine are compared when the wind speed is set in the range of 2-5.5 m/s. The dotted lines in the figure are used to represent the values which are missing as no results were obtained from the experiment. From the graph it can be seen that the FOWTs rotational speeds were not as high as those for the fixed tower wind turbine as a consequence of the rotor blade being vertically misaligned. In order maximize the use of the available wind energy it is important to optimize the direction of the wind flow arriving at the wind turbine through the optimal positioning of the wind turbine rotor. If the tilt angle is increased, moving further away from an ideal position, the amount of wind energy used by the turbine will be reduced. Table 5.5 shows the percentage decrease in rotational speed when comparing between the FOWTs and fixed tower wind turbines, revealing a mean difference of 36.8%. Where the rotor blade angle of attack was altered from its optimal position, this would affect the aerodynamic properties of the blade. In particular, the area effectively swept by the rotor would also change, and this had a direct influence on the performance of the wind turbine.

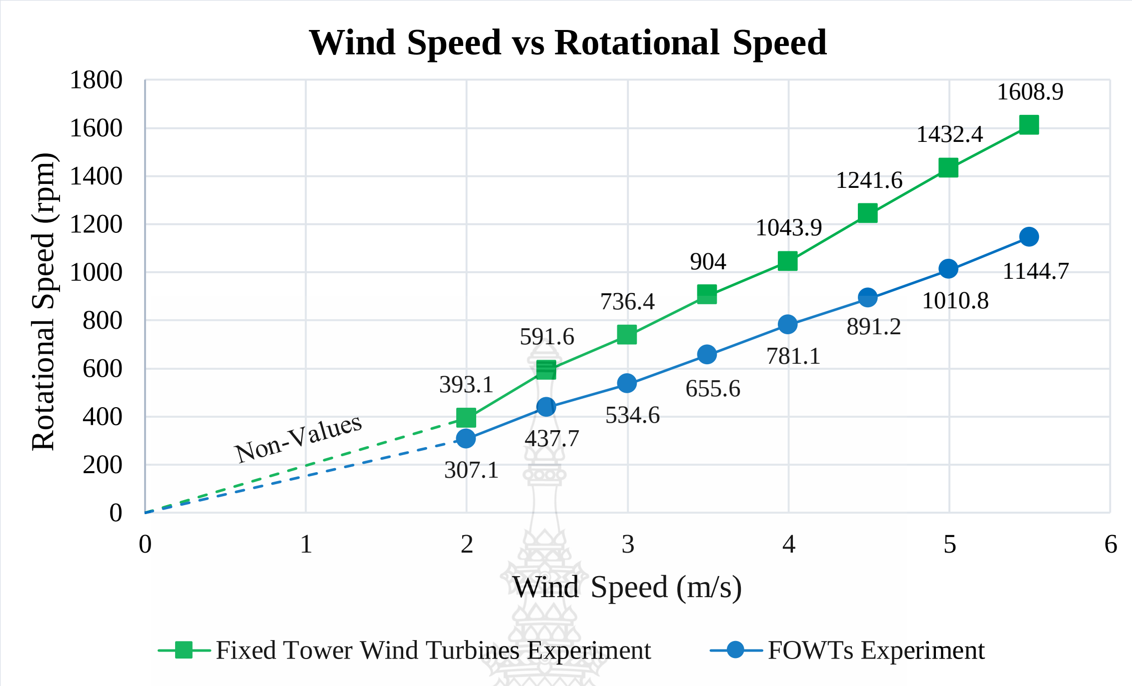

Figure 5.3 Comparison of rotational speeds at different wind speeds in a wind tunnel for a fixed tower wind turbine and a FOWTs.

Table 5.5 The rotational speed percentage differences of the fixed tower wind turbine and FOWTs in the wind tunnel experiment.

Wind Speed (m/s)	Rotational Speed Percentage Differences (%)
2.0	28.0
2.5	35.2
3.0	37.7
3.5	37.9
4.0	33.6
4.5	39.3
5.0	41.7
5.5	40.6

However, the tip speed ratio obtained by the calculation from tip speed ratio equation and power coefficient obtained from the R1235 airfoil blade tip speed ratio verses the power coefficient in Figure 4.24 could provide the results shown in Figure 5.4. The dotted lines in the figure are used to represent the values which are missing as no results were obtained from the experiment. This demonstrated that the FOWTs in the wind tunnel experiment could be maintained, and the power coefficient values could be enhanced further than those of the fixed tower wind turbine with optimum power coefficient values at wind speed of 3-5.5 m/s and tip speed ratio of 7.7-8.9. In addition, the majority of the FOWTs power coefficient values were found to be higher than 0.30 when there was a wind speed of 2-5.5 m/s, while the fixed tower wind turbine's power coefficient values began to decrease at wind speed of 2.5 m/s. This could have been a result of the rotor blades rotating quickly, thus gradually reducing the efficiency of the extraction of wind power, as the rotor blade would increasingly act as a solid wall preventing the wind flow when the blade spun quickly, therefore, the power coefficient values started to decrease after a tip speed ratio of 10.

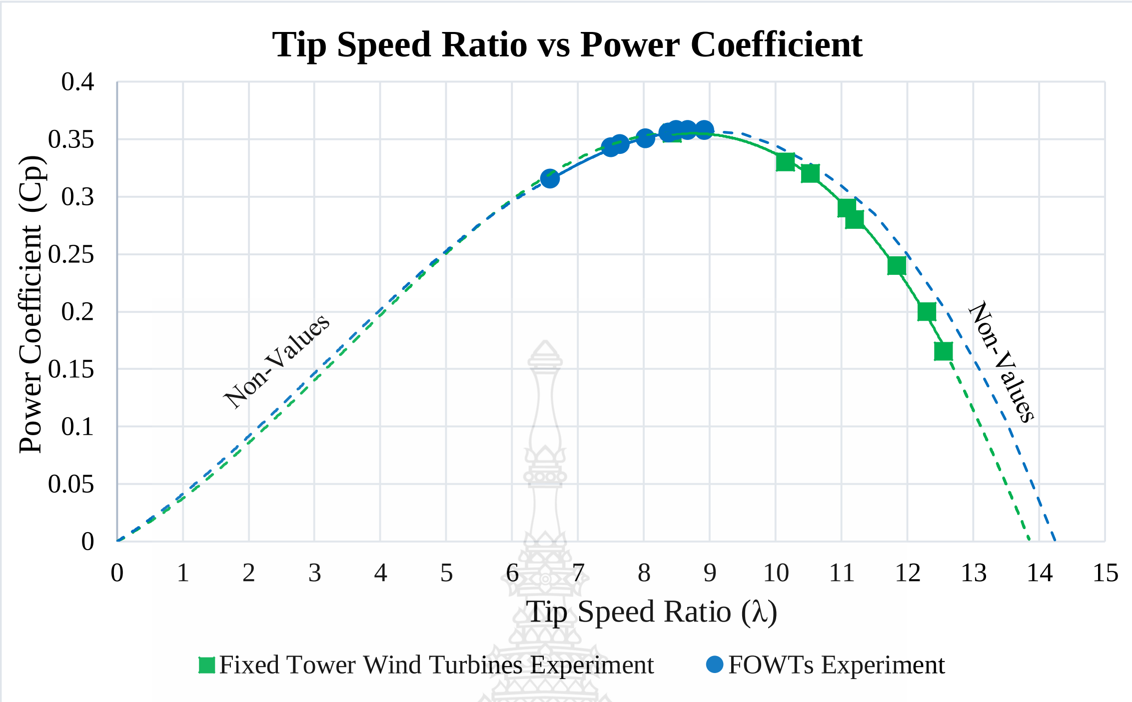

Figure 5.4 Comparison of the tip speed ratio and power coefficient of the fixed tower wind turbine and FOWTs in the wind tunnel experiment.

5.3 Results Comparison of the Fixed Tower Wind Turbines in a Wind Tunnel and FOWTs in the CFD

Table 5.3 presents the findings concerning wind speed, rotational speed, tip speed ratio and power coefficient for the fixed tower wind turbine, while Table 5.6 presents the results obtained from the CFD simulation involving the FOWTs, with data provided for wind speeds, rotational speeds, tip speed ratios, power coefficients and tilt angles from wind tunnel experiments.

As in the preceding section, the rotational speed and wind speed were once again in direct proportion for both the wind tunnel data and the simulated CFD data. Rising wind speed was matched by rising rotational speed. In this case, the rotational speeds for the FOWTs were not as high as those of the fixed tower wind turbine as a consequence of the way the tilt angle affects the performance of the rotor wind turbine.

Table 5.6 FOWTs in the CFD simulation data.

Wind Speed (m/s)	Rotational Speed (rpm)	Tip Speed Ratio (λ)	Power Coefficient (C_P)	Tilt Angle (Degree)
2.0	341.5	7.3	0.34	3.5°
2.5	543.5	9.3	0.36	3.8°
3.0	671.3	9.6	0.35	3.9°
3.5	714.1	8.8	0.36	4.3°
4.0	873.3	9.4	0.36	4.7°
4.5	999.3	9.5	0.35	5.0°
5.0	1198.4	10.3	0.33	5.8°
5.5	1363.9	10.6	0.32	6.1°

A comparison of the rotational speeds for a range of different wind speeds of 2-5.5 m/s is presented in Figure 5.5 for a CFD simulation of a FOWTs and a fixed tower wind turbine. The dotted lines in the figure are used to represent the values which are missing as no results were obtained from the experiment. From the graph it can be seen that the FOWTs rotational speeds were not as high as those for the fixed tower wind turbine as a consequence of the rotor blade being vertically misaligned. In order maximize the use of the available wind energy it is important to optimize the direction of the wind flow arriving at the wind turbine through the optimal positioning of the wind turbine rotor. If the tilt angle is increased, moving further away from an ideal position, the amount of wind energy used by the turbine will be reduced. Table 5.6 shows the percentage decrease in rotational speed when comparing between the FOWTs and fixed tower wind turbine, revealing a mean difference of 17.7%. Where the rotor blade angle of attack was altered from its optimal position, this would affect the aerodynamic properties of the blade. In particular, the area effectively swept by the rotor would also change, and this had a direct influence on the performance of the wind turbine.

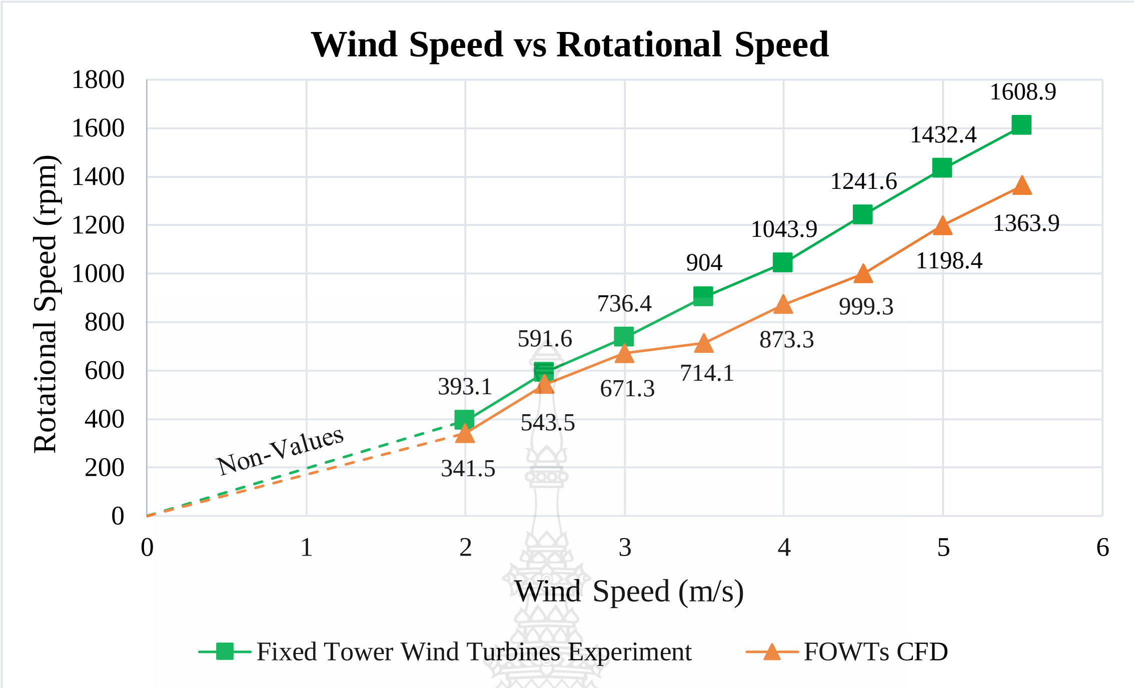

Figure 5.5 Wind speed and rotational speed comparison showing wind tunnel results for a fixed tower wind turbine and CFD results for a FOWTs.

Table 5.7 Percentage differences in the rotational speeds of fixed tower wind turbines in a wind tunnel and CFD simulated FOWTs.

Wind Speed (m/s)	Rotational Speed Percentage Differences (%)
2.0	15.1
2.5	8.9
3.0	9.7
3.5	26.6
4.0	19.5
4.5	24.2
5.0	19.5
5.5	18.0

The tip speed ratio obtained by the calculation from tip speed ratio equation and power coefficient obtained from the R1235 airfoil blade tip speed ratio verses the power coefficient in Figure 4.24 could provide the results shown in Figure 5.6. The dotted lines in the figure are used to represent the values which are missing as no results were obtained from the experiment. This demonstrated that the FOWTs in the CFD simulation could be maintained, and the power coefficient values could be enhanced further than those of the fixed tower wind turbine with optimum power coefficient values at wind speed of 2.5-4.5 m/s and tip speed ratio of 8.8-9.5. Furthermore, the majority of the FOWTs power coefficient values were found to be higher than 0.30 when there was a wind speed range of 2-5.5 m/s while the fixed tower wind turbine's power coefficient values began to decrease at wind speed of 2.5 m/s. This could have been a result of the rotor blades rotating quickly, thus gradually reducing the efficiency of the extraction of wind power, as the rotor blade would increasingly act as a solid wall preventing the wind flow when the blade spun quickly, therefore, the power coefficient values started to decrease after a tip speed ratio of 10.

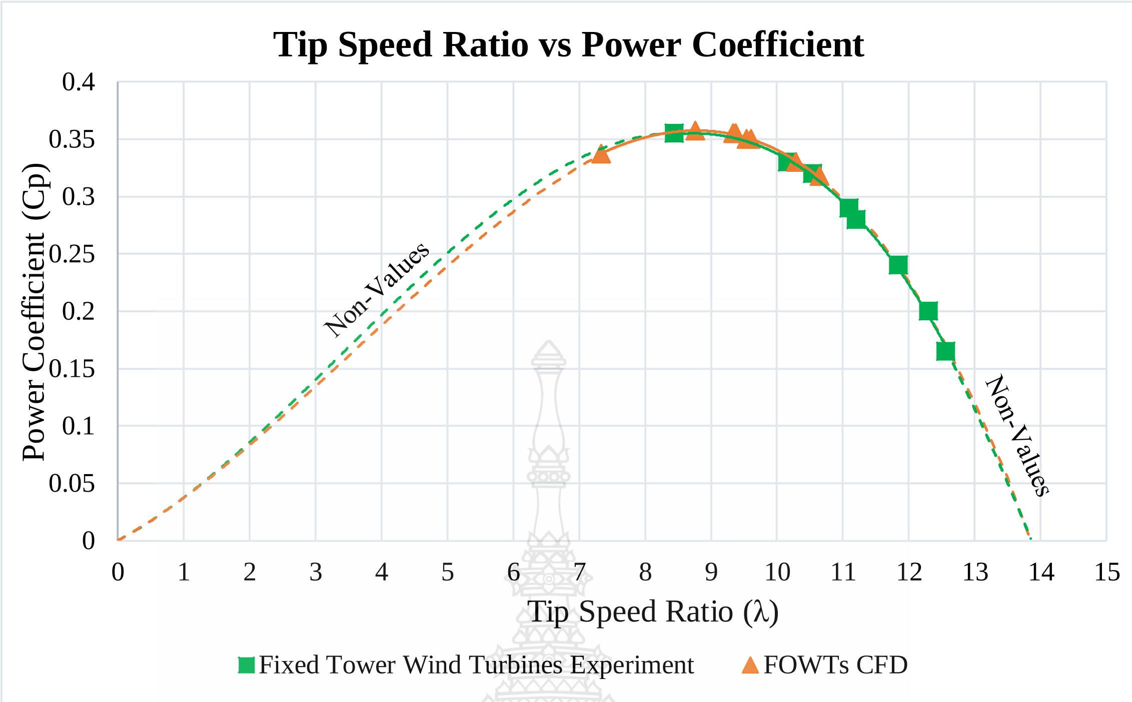

Figure 5.6 Comparison of the tip speed ratio and power coefficient of the fixed tower wind turbine of the wind tunnel and FOWTs in the CFD.

5.4 Comparison of FOWTs Results in CFD and in a Wind Tunnel

In Table 5.8, the various outcomes are presented for wind speeds, rotational speeds and tilt angles, allowing comparisons to be drawn between FOWTs in the wind tunnel experiment and in the CFD simulation. The measurements for the tilt angle were taken from the experiment findings when the wind speed was set in a range of 2-5.5 m/s. The tilt angles from the wind tunnel FOWTs experiment were used as the reference in the CFD simulation in order to assess the way the rotational speed might vary while maintaining a given tilt angle.

Table 5.8 The rotational speed results of the FOWTs in the wind tunnel and FOWTs in the CFD simulation.

Wind Speed (m/s)	Tilt Angle (Degree)	Rotational Speed Experiment (rpm)	Rotational Speed CFD (rpm)
2.0	3.5°	307.1	341.5
2.5	3.8°	437.7	543.5
3.0	3.9°	534.6	671.3
3.5	4.3°	655.6	714.1
4.0	4.7°	781.1	873.3
4.5	5.0°	891.2	999.3
5.0	5.8°	1010.8	1198.4
5.5	6.1°	1144.7	1363.9

The graph presenting the rotational speeds achieved at a range of wind speeds from 2-5.5 m/s for both the experimental and CFD models can be seen in Figure 5.7. The dotted lines in the figure are used to represent the values which are missing as no results were obtained from the experiment. It is clear from the graph that the rotational speeds achieved in the CFD simulation exceeded those of the experimental model. Table 5.9 shows the percentage differences between the models, revealing a mean difference of 16.4%. This happens because in the CFD simulation, only the rotation region of the wind turbine is taken into account, which refers only to the rotor blade rotation, while in the experimental version, the rotor blade is attached to the shaft axle and the bearings so that it is able to rotate when exposed to the wind. When the measurements are taken, it is likely that the shaft axle and bearings generate friction which lowers the rotational speed in the experiment.

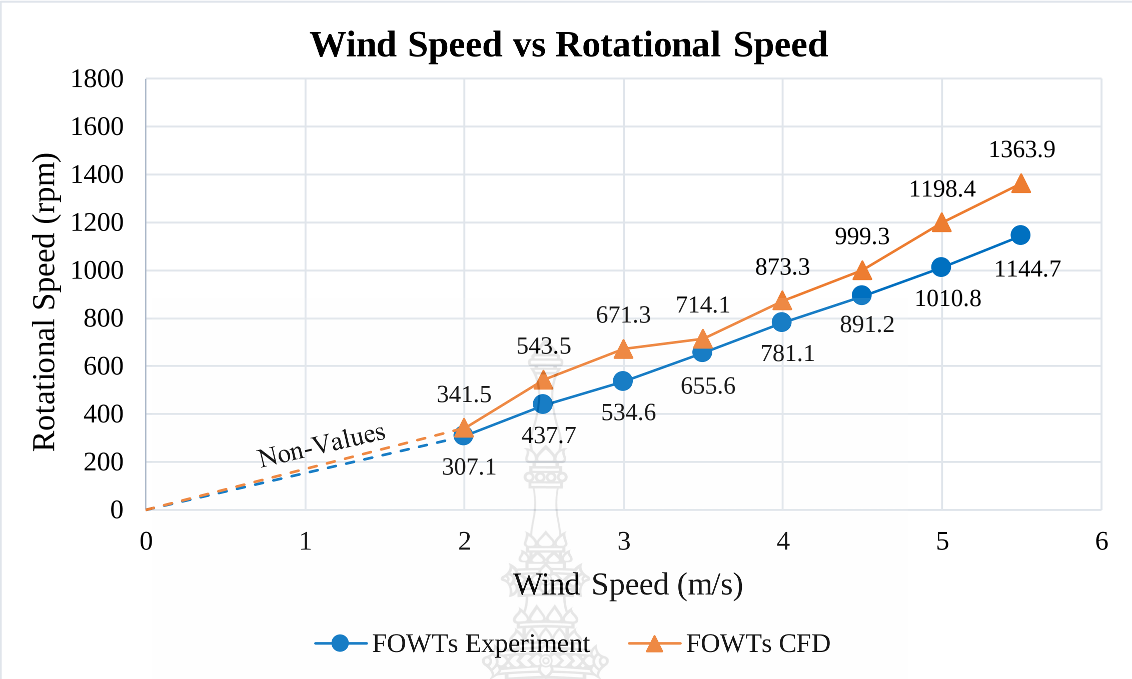

Figure 5.7 Rotational speeds for FOWTs comparing between the wind tunnel and the CFD simulation.

Table 5.9 Percentage differences in rotational speeds for FOWTs in the wind tunnel and in the CFD simulation**.**

Wind Speed (m/s)	Rotational Speed Percentage Differences (%)
2.0	11.2
2.5	24.2
3.0	25.6
3.5	8.9
4.0	11.8
4.5	12.1
5.0	18.6
5.5	19.1

In Table 5.10, the values for the tilt angle, tip speed ratio and power coefficient are shown for both the experiment in the wind tunnel and the CFD simulation. The value for the tip speed ratio is obtained via the tip speed ratio equation. Meanwhile, the power coefficient of the R1235 airfoil blade tip speed ratio can be compared to the power coefficient from Figure 4.24.

Table 5.10 Results of the FOWTs in the wind tunnel and FOWTs in the CFD simulation.

		FOWTs Experiment		FOWTs CFD	
Wind Speed (m/s)	Tilt Angle (Degree)	Tip Speed Ratio (λ)	Power Coefficient (C_P)	Tip Speed Ratio (λ)	Power Coefficient (C_P)
2.0	3.5°	6.6	0.32	7.3	0.34
2.5	3.8°	7.5	0.34	9.3	0.36
3.0	3.9°	7.7	0.35	9.6	0.35
3.5	4.3°	8.0	0.35	8.8	0.36
4.0	4.7°	8.4	0.36	9.4	0.36
4.5	5.0°	8.5	0.36	9.5	0.35
5.0	5.8°	8.7	0.36	10.3	0.33
5.5	6.1°	8.9	0.36	10.6	0.32

Figure 5.8 shows the tip speed ratio versus the power coefficient plots for the wind tunnel experiment and CFD models. The dotted lines in the figure are used to represent the values which are missing as no results were obtained from the experiment. The results were similar for the power coefficient values in the range of 0.32-0.36. However, the power coefficient values for the experiment and CFD models started to decrease after a tip speed ratio of 10, which could have been a result of the rotor blades rotating quickly, thus gradually reducing the efficiency of the extraction of wind power, as the rotor blade would increasingly act as a solid wall preventing the wind flow when the blade spun quickly. Furthermore, the optimum power coefficient values of 0.35-0.36 were able to be achieved when the tip speed ratios were between 7.7-9.6. This variance

in the power coefficient correlated with the tilt angles of 3.9-5.8° with wind speeds of 3-5 m/s that was the mean wind speed in Thailand. In addition, the tilt angle would behave as a variable pitch to maintain the optimal power coefficient. This in turn would decrease the budget of the pitch control systems for small to medium fixed pitch FOWTs.

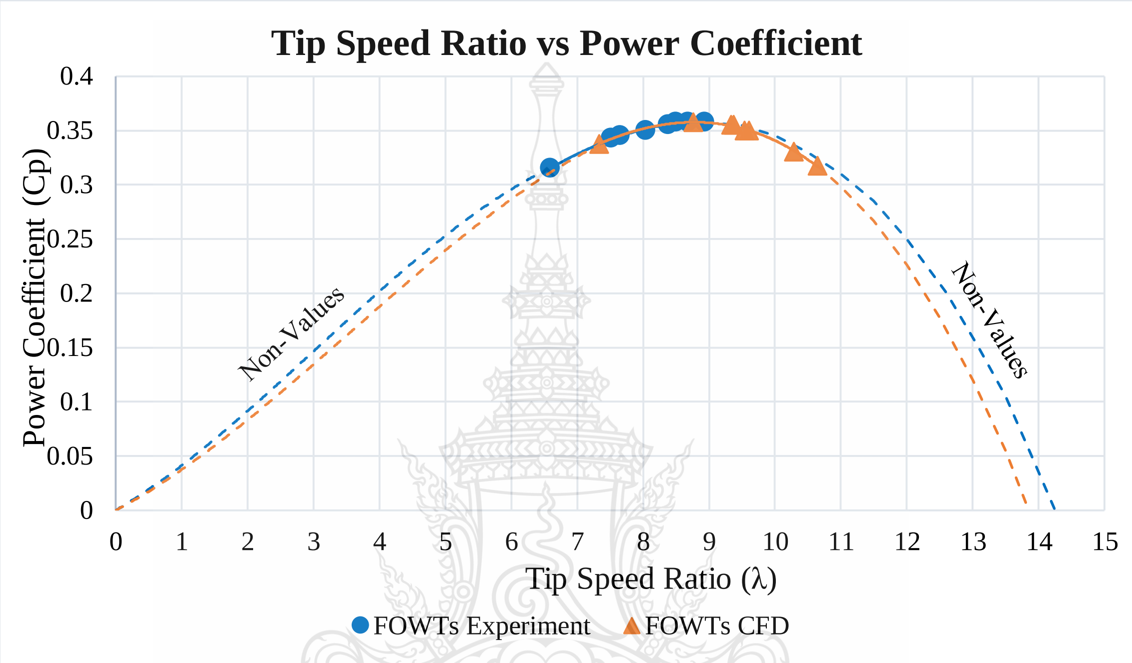

Figure 5.8 Comparison of the tip speed ratio and power coefficient of the FOWTs in the wind tunnel and FOWTs in the CFD.

The rotational speeds and the tilt angles for the FOWTs in both the experiment in the wind tunnel and in the CFD simulation are shown in Figure 5.9. The dotted lines in the figure are used to represent the values which are missing as no results were obtained from the experiment. It can be seen from the graph that in both models an increase in the tilt angle resulted in an increase in the rotational speed. Where the tilt angles in the CFD simulation were the same as those in the wind tunnel experiment, the rotational speeds for the CFD simulation were higher. This finding might be a consequence of the CFD simulation only taking into account the wind turbine rotation region, which refers to the rotor blade rotation. In the wind tunnel experiment, however, the rotor blade is attached to the shaft axle and bearings, ensuring its ability to rotate whenever there is an available wind. It is therefore possible that friction from the shaft axle and bearings may be lowering the rotor blade rotational speed.

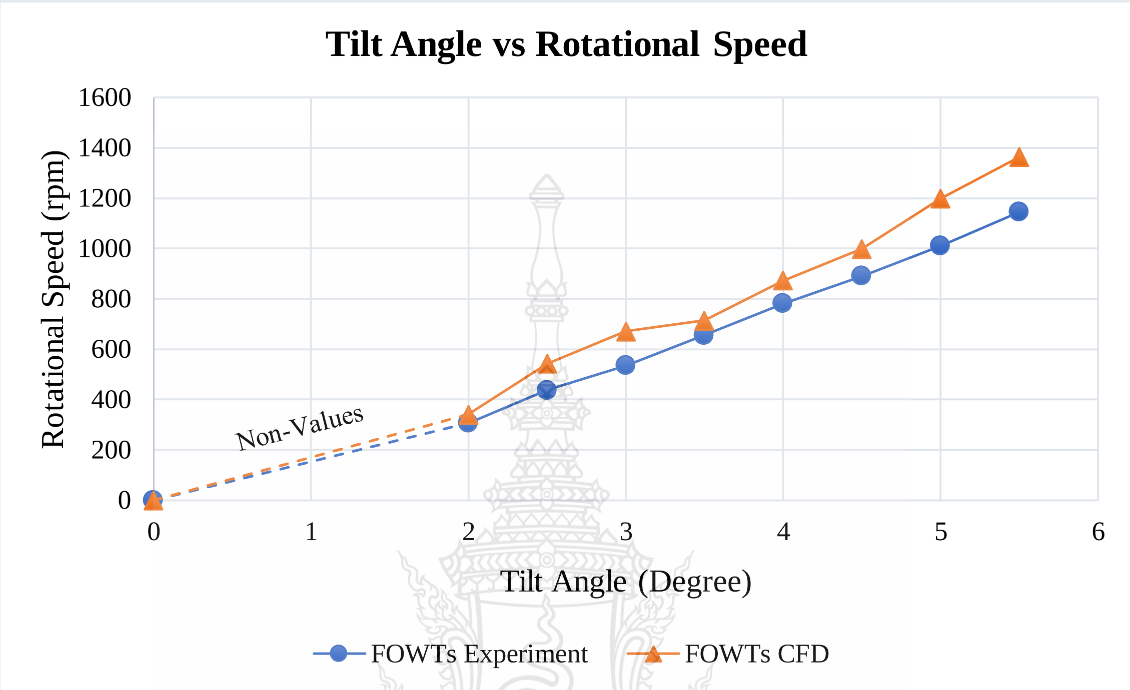

Figure 5.9 Rotational speed and tilt angle comparison between the wind tunnel FOWTs and the CFD Simulation FOWTs.

In Figure 5.10 there is a comparison of the tip speed ratios and tilt angles for the FOWTs in the wind tunnel experiment and the CFD simulation. The dotted lines in the figure are used to represent the values which are missing as no results were obtained from the experiment. From the graph it can be seen that as the tilt angle increases there is a similar rise in the value of the tip speed ratios. It can also be understood from the earlier section that the tip speed ratio is related to the rotational speed, so accordingly there is a higher value for the FOWTs in the CFD simulation than for the FOWTs in the experiment.

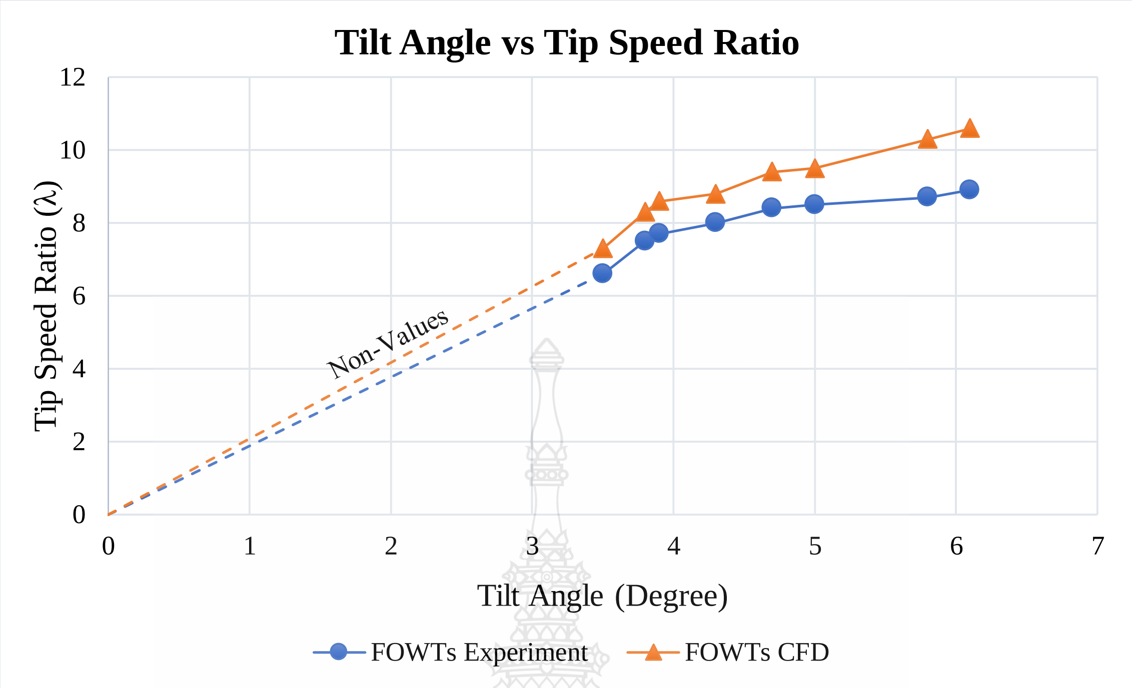

Figure 5.10 Tip speed ratio and tilt angle comparison between the wind tunnel FOWTs and the CFD simulation FOWTs.

In Figure 5.11 a comparison is shown for the wind speed and power output involving fixed tower wind turbines, the FOWTs in the wind tunnel experiment, and the CFD simulation FOWTs for wind speeds in the range of 2-5.5 m/s. The dotted lines in the figure are used to represent the values which are missing as no results were obtained from the experiment. It was possible to determine the power output via the use of the power output equation. In this case, the FOWTs both had higher power output values than the fixed tower wind turbines as a consequence of the FOWTs ability to maintain a high-power coefficient throughout the process, while the fixed tower wind turbines could not, which therefore reduced the power output.

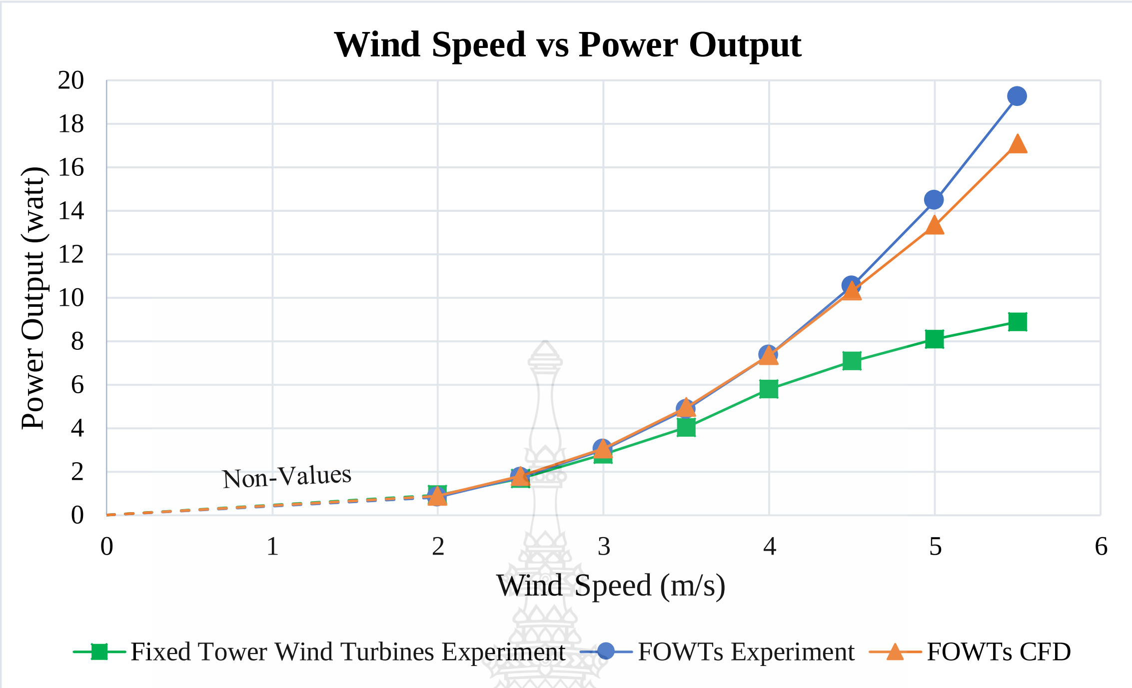

Figure 5.11 Wind speed and power output comparison for the fixed tower wind turbines and the FOWTs in the wind tunnel experiment and CFD.

5.5 FOWTs in the CFD Simulations

5.5.1 Velocity Magnitude

Figure 5.12 presents the velocity magnitude contour for CFD both prior to passing through the wind turbine as well as afterwards, where the wind speeds are varied in the range of 2-5.5 m/s while the tilt angles are in the range of 3.5-6.1°. In the areas above and below the wake area there was very little difference in the velocity contour. However, as the wind speed increased, the differences in speed after passing through the wind turbine became much more clearly apparent. Once the wind speed exceeded 3 m/s it was found that the streamline became separated as a consequence of the differences in the wind speed. This arose because of the turbulence caused when the wind flow strikes the wind turbine, and this phenomenon was more clearly apparent at higher wind speeds while the size of the wake area behind the wind turbine became larger as the wind became faster. The stagnation point, which is defined as the zone in which the wind speed drops to the point where it ceases to flow, then moves nearer to the wind turbine at higher wind speeds. The tilt angle is then altered by the higher wind speed which causes the streamline to be pushed downwards, leading to streamline separation behind the wake area of the turbine at the bottom.

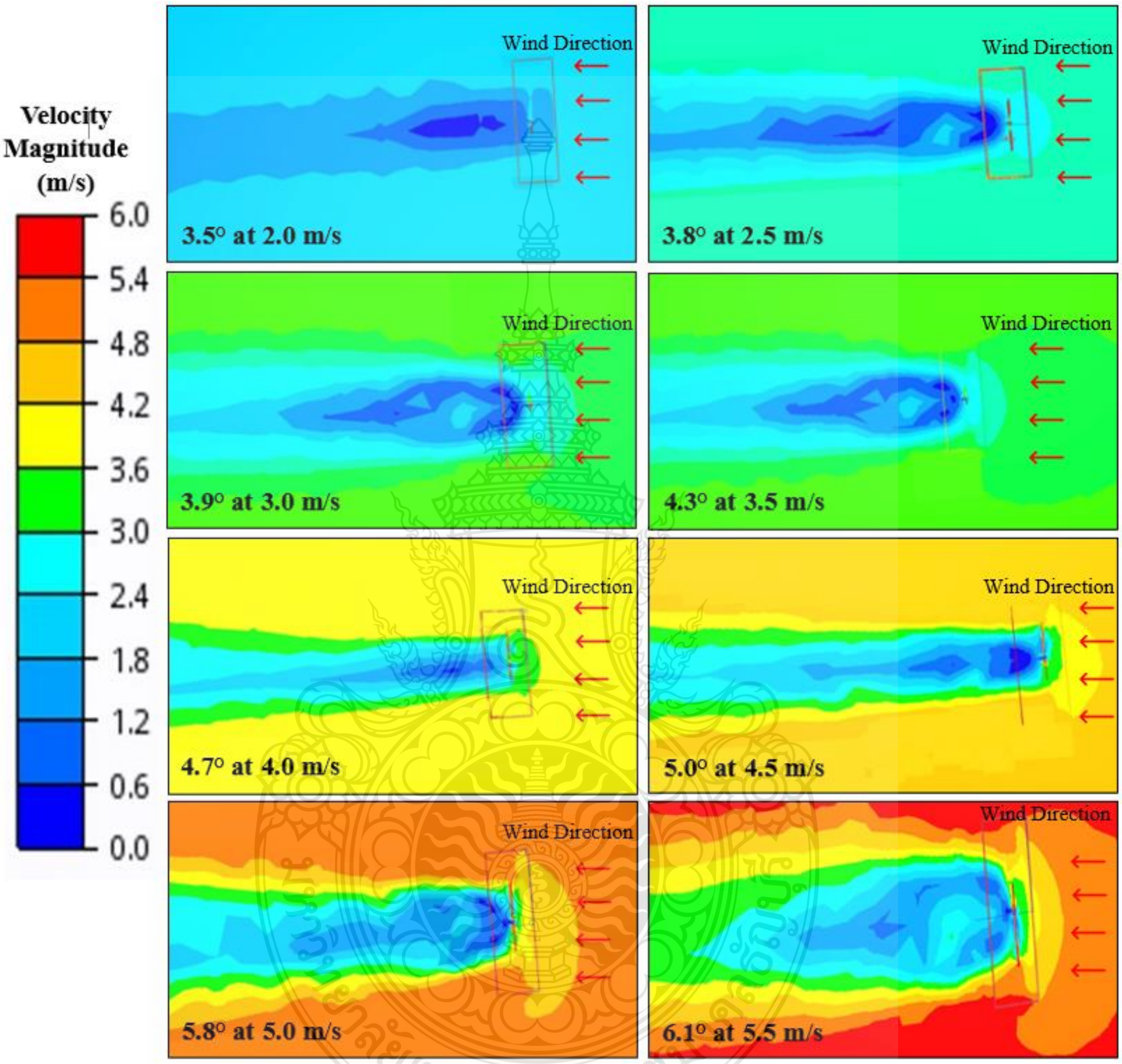

Figure 5.12 Velocity magnitude.

5.5.2 Static Pressure

In Figure 5.13 a static pressure contour diagram is shown, revealing the effect upon the wind turbines when the wind speed is in the range of 2-5.5 m/s while the tilt angle varies in the range of 3.5-6.1°. There is a clear area in front of the wind turbine where the pressure is notably higher than behind the turbine, where the pressure drops sharply to become negative, causing the turbines to rotate. In the area of higher pressure in front of the wind turbine, it was clear that the upper central area displayed much higher pressure than the lower central area. This was particularly noticeable at increasing wind speeds, where there was direct correspondence with the flow currents.

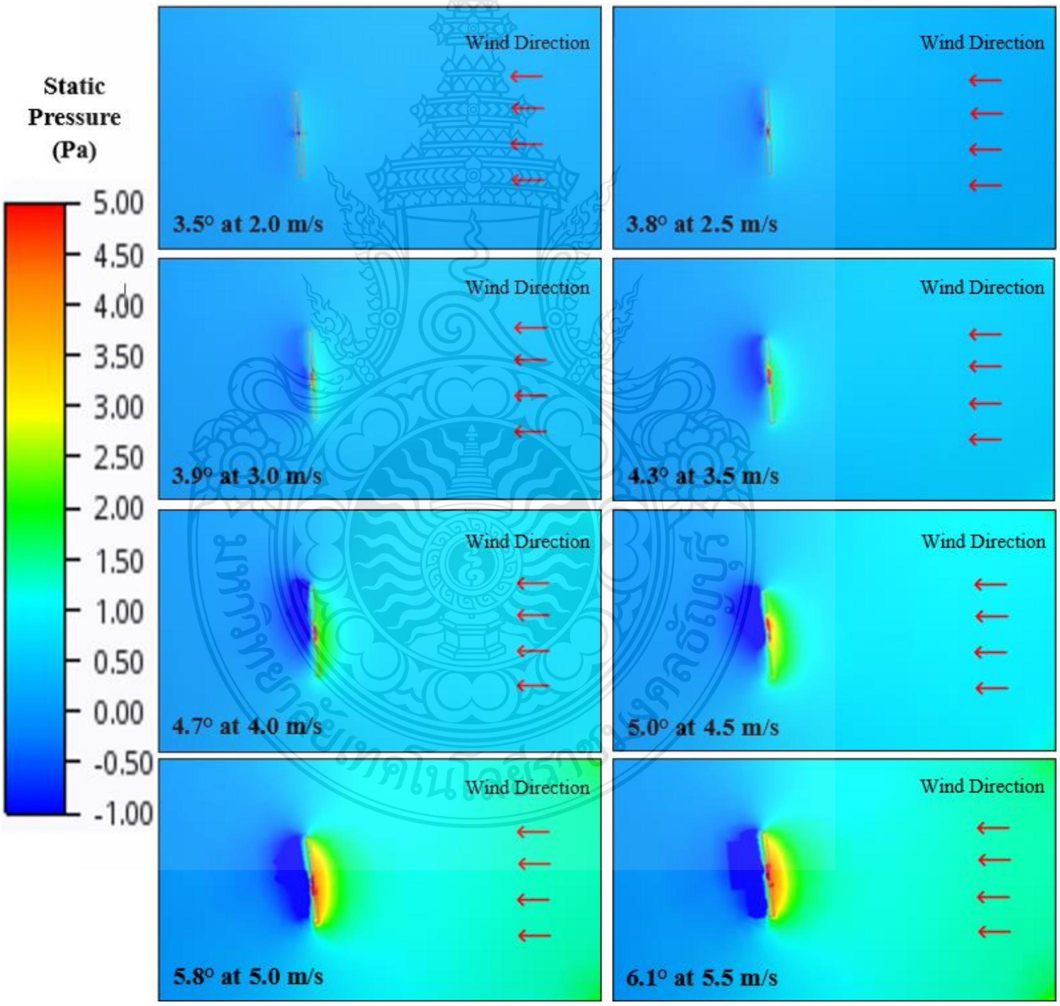

Figure 5.13 Static pressure.

CHAPTER 6
CONCLUSION

This study aimed to analyze the influence of the rotor tilt angle upon monopole tower Floating Offshore Wind Turbines (FOWTs). Experiments were carried out in order to draw comparisons between fixed tower wind turbines and FOWTs via the use of both CFD simulation models and studies conducted using models in a wind tunnel. In these tests the R1235 airfoil blade profile was used along with wind speeds in the range of 2-5.5 m/s and tilt angles in the range of 3.5°- 6.1°. The first experiments were performed using two different floating platform positions: a one-legged columnar tube at the front, and a two-legged columnar tube at the front. The two-legged columnar tubes were then used once again in subsequent experiments due to the significant influence of the tilt angle when analyzing the worst-case situations in the case of FOWTs. Testing was then performed in the wind tunnel using both FOWTs and fixed tower wind turbines, revealing that the rotational speed in the FOWTs was lower than observed in the fixed tower wind turbines by around 36.8% on average because of the effects of the tilt angle in the FOWTs. These results were similar to those obtained when comparing FOWTs in CFD and fixed tower wind turbines in the wind tunnel, for which the mean percentage difference was 17.7%. The rotational speeds of FOWTs in the wind tunnel were then compared to CFD simulation FOWTs, revealing that in CFD the rotational speeds were higher by 16.4% on average. In the case of the power coefficient, the FOWTs performed to a higher level in both the CFD simulation and the wind tunnel experiments, proving able to extend the power coefficient for longer durations. A majority of the power coefficient values were found to exceed 0.30 while the wind speeds were in the range of 2-5.5 m/s, whereas in contrast, the power coefficients of the fixed tower wind turbines began to decline. The study also drew comparisons between the findings for the FOWTs in the CFD simulation and the FOWTs in the wind tunnel experiments. The optimal power coefficients were shown to fall between 0.35-0.36. It was possible to retain these values for tip speed ratios of 7.7-9.6 with a wind speed of 3-5 m/s when the tilt angles were in the range of 3.9-5.8°. In addition, the findings offered further understanding of the new theory of maintaining the power coefficient by utilizing an adjustable tilt angle for small to medium fixed pitch

FOWTs. Thus, the utilization of these floating offshore wind turbines could decrease the expense of the pitch control system.

Future studies may elect to enhance the CFD simulation approach to achieve a reduction in the percentage differences. This may involve setting the boundary conditions to match the conditions in the wind tunnel experiments more closely, thereby more precisely mirroring the wind tunnel dimensions and rotor blade positions. The use of mesh refinements in the model may be more appropriate and elaborate in term of mesh structure, mesh number and mesh type for the flow conditions and allow better solutions to be obtained. In addition, it may be feasible to expand the wind tunnel experiment by using a large water tank which would allow the behavior of the floating platform to be assessed in the context of the relationship with tilt angle effects. The optimum power coefficient method could then be used with R1235 wind turbine commercial products by varying the generator torque loads to assess the influence of the tilt angle on the FOWTs performance in terms of the rotational speed, tip speed ratio, power coefficient and power output. It would then be possible to conduct more accurate comparisons with the performance and economic value of onshore wind turbines.

BIBLIOGRAPHY

[1] Thorium Energy World. (2017). **World Energy Situation**. Retrieved from http://www.thoriumenergyworld.com/energy.html

[2] Jha, A. R. (2011). **Wind Turbine Technology.** London: CRC Press

[3] North Caroline Wind Energy. (2018). **Introduction to Wind Power.** Retrieved from https://wind.appstate.edu/wind-power

[4] BP. (2018). **BP Statistical Review of World Energy**. Retrieved from https://www.bp.com/content/dam/bp/business-sites/en/global/corporate/pdfs/energy-economics/statistical-review/bp-stats-review-2018-full-report.pdf

[5] International Renewable Energy Agency (IRENA). (2019). **Renewable Capacity Statistics 2020**. Retrieved from https://www.buildup.eu/sites/default/files/content/irena_re_capacity_statistics_2020.pdf

[6] Karimirad, M. & Michailides, C. (2015). Dynamic Analysis of a Braceless Semisubmersible Offshore Wind Turbine in Operational Conditions. **Energy Procedia, 80**, 21-29. doi: https://doi.org/10.1016/j.egypro.2015.11.402

[7] Cordle, A. & Jonkman, J. (2011). **State of the Art in Floating Wind Turbine Design Tools.** Paper Presented at the 21st International Offshore and Polar Engineering Conference, Maui, Hawaii, US. Retrieved from National Renewable Energy Laboratory (NREL) Website: https://www.nrel.gov/docs/fy12osti/50543.pdf[8] Snyder, B. & Kaiser, M. J. (2009). Ecological and Economic Cost-Benefit Analysis of Offshore Wind Energy. **Renewable Energy, 34**, 1567-1578. doi: https://doi.org/10.1016/j.renene.2008.11.015

[8] Snyder, B. & Kaiser, M. J. (2009). Ecological and Economic Cost-Benefit Analysis of Offshore Wind Energy. **Renewable Energy, 34**, 1567-1578. doi: https://doi.org/10.1016/j.renene.2008.11.015

[9] Madariaga, A., Alegria, I. M., Martín, J. L., Eguia, P. & Ceballos, S. (2012). Current Facts About Offshore Wind Farms. **Renewable and Sustainable Energy Reviews, 16**(5), 3105–3116. doi: https://doi.org/10.1016/j.rser.2012.02.022

[10] Ponta, F, L., Otero, A, D., Lago, L. I. & Rajan, A. (2016). Effects of Rotor Deformation in Wind-Turbine Performance: The Dynamic Rotor Deformation Blade Element Momentum model (DRD–BEM). **Renewable Energy, 92**, 157-170. doi: https://doi.org/10.1016/j.renene.2016.01.098

[11] Pasqualettia, M. J., Righterb, R. & Gipec, P. (2004). History of Wind Energy. **Encyclopedia of Energy,** 419-433. doi: https://doi.org/10.1016/B0-12-176480-X/00045-0

[12] Fleischer, C. **The History of Wind Energy**. Retrieved from Autodesk Website: https://www.autodesk.com/products/eagle/blog/wind-energy/

[13] Nelson, V. (2009). **Wind Energy: Renewable Energy and the Environment** (2nd ed) London, UK: CRC Press.

[14] Ragheb M. (2017). History of Harnessing Wind Power. In Letcher, T. M. (Ed). **Wind Energy Engineering A Handbook for Onshore and Offshore Wind Turbines** (pp. 127-143), Cambridge, UK: Academic Press.

[15] Price, T. (2005). James Blyth – Britain's First Modern Wind Power Pioneer. **Wind Engineering, 29**(3), 191–200. doi: https://doi.org/10.1260/030952405774354921

BIBLIOGRAPHY (Continued)

[16] Ragheb, M. (2019). **Historical Wind Generators Machines**. Retrieved from https://www.mragheb.com/NPRE%20475%20Wind%20Power%20Systems/Historical%20Wind%20Generators%20Machines.pdf

[17] Hau, E. (2006). Electrical Power from the Wind — The First Attempts. In **Wind Turbines Fundamentals, Technologies, Application, Economics 2nd ed**. (pp. 23-25) New York, US: Springer Berlin Heidelberg.

[18] Johnson, G. L. (2006). **Wind Energy Systems**. Manhattan, US: Kansas State University.

[19] Todkar, V., Shinde, G., Kamble, S. & Gunavant, P. (2017). An Overall of Windmills. **International Advanced Research Journal in Science, Engineering, and Technology, 4**(1), 51-54. doi: https://doi.org/10.17148/IARJSET.

[20] MHI Vestas Offshore Wind. **V164-9.5 MW**. Retrieved from https://mhivestasoffshore.com/category/v164-9-5-mw/

[21] Tarino, G. (2020). **The World's Largest Wind Turbines to Be Used for North Sea Project.** Retrieved from Yale Environment 360 Website: https://e360.yale.edu/digest/the-worlds-largest-wind-turbines-to-be-used-for-north-sea-project

[22] Besta, S. (2019). **Profiling Ten of the Biggest Onshore Wind Farms in the World.** Retrieved from NS Energy Website: https://www.nsenergybusiness.com/features/worlds-biggest-onshore-wind-farms/

[23] Nikolaou, N. (2004). **Deep Water Offshore Wind Technologies at University of Strathclyde**. (Master's thesis, The University of Strathclyde, Glasgow, Scotland).

BIBLIOGRAPHY (Continued)

[24] Verma, A. (2020). **Five of the World's Largest Offshore Wind Energy Farms**. Retrieved from Saur Energy International Website: https://www.saurenergy.com/solar-energy-blog/worlds-largest-offshore-wind-energy-farms

[25] Bolleman, N. (2017). **The Design Engineer, System Integrator and Technology Provider for Floating Foundation Systems and Multi-Purpose Platforms at Sea**. Retrieved from Blue H Engineering Website: https://www.energyportzeeland.nl/data/formulieren/uploads/171128%20introduction%20blue%20h%20engineering.pdf

[26] Nysæther, J. B. (2019). **Experiences from Hywind Scotland and the Way Forward for Floating Offshore Wind**. Retrieved from Equinor Website: https://www.sintef.no/globalassets/project/eera-deepwind-2019/presentations/opening_nysather_equinor.pdf

[27] Department of Alternative Energy Development and Efficiency (DEDE). (2011). **A Guide to Wind Energy Development and Investment**. Retrieved from https://www.dede.go.th/article_attach/h_wind.pdf

[28] Khamprasit, C. (2020). **Wind Energy Development for Power Generation**. Retrieved from https://housingkc.nha.co.th/files/article/attachments/00ed9d23d7dd0e7e33d5f31521037f69.docx

[29] Electricity Generating Authority of Thailand (EGAT). **Lam Takhong Wind Turbine Project**. Retrieved from https://www.egat.co.th/index.php?option=com_content&view=article&id=2229&Itemid=244

[30] Department of Alternative Energy Development and Efficiency (DEDE). (2009). **Demonstration Project of Wind Power Generation, Hua Sai District, Nakhon Si Thammarat Province**. Retrieved from http://www2.dede.go.th/km_ber/inneract/s2-1.pdf

[31] Department of Alternative Energy Development and Efficiency (DEDE). (2020). **Project of Establishing and Installing Wind Turbines to Generate Electricity**. Retrieved from http://e-lib.dede.go.th

[32] Department of Alternative Energy Development and Efficiency (DEDE). **Study, Research, Development and Demonstration of Low Speed Wind Turbine Technology**. Retrieved from http://e-lib.dede.go.th

[33] Modern Manufacturing. (2017). **Thai Wind Turbines Generate Electricity with Local Development**. Retrieved from https://www.mmthailand.com

[34] Waarden, R. V. (2012). **Thai Turbines Power a Country That Isn't Windy**. Retrieved from Climate Central Website: https://www.climatecentral.org/news/wind-turbines-made-in-thailand-for-thailand/

[35] Academic Resource and Information Technology (ARIT). **Science of the King**. Retrieved from https://arit.chandra.ac.th/index.php?option=com_content&view=categories&id=71&Itemid=155

[36] Apai, B. (2014). **Safety, Health, and Environment Programs in a Rapidly Growing Port: Laem Chabang**. Retrieved from International Water Learning Exchange and Resource Network Website: https://iwlearn.net/resolveuid/cabbce0376bd4fce9acf4333d3e8962d

[37] Energy Regulatory Commission (ERC). (2019). **Special Discussion on Roles of Energy Regulatory Commission (ERC) and Challenges in the Energy Business in the Future**. Retrieved from http://www.erc.or.th

[38] Prachachat Online. (2017). **Department of Industrial Works Encourages to Use Renewable Energy, Holds MRP Engineering Matching for Wind Turbine Production for Sale**. Retrieved from https://www.prachachat.net/economy/news-57469

[39] Department of Industrial Works. (2018). **Air Compressor Wind Turbine for Factory**. Retrieved from http://reg3.diw.go.th/

[40] Peiser, B. (2019). **The Impact of Wind Energy on Wildlife and the Environment**. Retrieved from The Global Warming Policy Foundation Website: https://www.thegwpf.org/content/uploads/2019/07/wind-impact-1.pdf

[41] Kondili, E. & Kaldellis, J. K. (2012). Environmental-Social Benefits/Impacts of Wind Power. **Comprehensive Renewable Energy, 2**, 503-539. doi: https://doi.org/10.1016/B978-0-08-087872-0.00219-5

[42] Saidur, R., Rahim, N. A., Islam, M. R. and Solangi, K. H. (2011). Environmental Impact of Wind Energy. **Renewable and Sustainable Energy Reviews. 15**(5), 2423-2430. doi: https://doi.org/10.1016/j.rser.2011.02.024

[43] Wang, S. & Wang, S. (2015). Impacts of Wind Energy on Environment: A Review. **Renewable and Sustainable Energy Reviews, 49**, 437-443. doi: https://doi.org/10.1016/j.rser.2015.04.137

[44] Nazir, M. S., Ali, N., Bilal, M. & Iqbal, H. M. N. (2020) Potential Environmental Impacts of Wind Energy Development - A Global Perspective. **Current Opinion in Environmental Science & Health**. doi: https://doi.org/10.1016/j.coesh.2020.01.002

[45] Leung, D. & Yang, Y. (2012). Wind Energy Development and its Environmental Impact: A Review. **Renewable and Sustainable Energy Reviews, 16**(1), 1031-1039. doi: https://doi.org/10.1016/j.rser.2011.09.024

[46] Dinh, V. N. & Mckeogh, E. (2019). **Offshore Wind Energy: Technology Opportunities and Challenges: Energy and Geotechnics**. Paper Presented at Proceedings of the 1st Vietnam Symposium on Advances in Offshore Engineering, Retrieved from https://www.researchgate.net/profile/Van-Nguyen_Dinh/publication/327869393_Offshore_Wind_Energy_Technology_Opportunities_and_Challenges_Energy_and_Geotechnics/links/5bfa8bfc92851ced67d6e148/Offshore-Wind-Energy-Technology-Opportunities-and-Challenges-Energy-and-Geotechnics.pdf

[47] Ramos, E. S., Assis, L. O., Mena, R. S. and Ramirez, L. F. (2019). Current Status and Future Trends of Offshore Wind Power in Europe. **Energy, 202.** doi: https://doi.org/10.1016/j.energy.2020.117787

[48] Bilgili, M., Yasar, A. & Simsek, E. (2010). Offshore Wind Power Development in Europe and Its Comparison with Onshore Counterpart. **Renewable and Sustainable Energy Reviews, 15**(2), 905-915. doi: https://doi.org/10.1016/j.rser.2010.11.006

[49] Haraldsson, M., Raoux, A., Riera, F., Hay, J., Dambacher, J. M. and Niquil, N. (2020). How to Model Social-Ecological Systems? – A Case Study on the Effects of a Future Offshore Wind Farm on the Local Society and Ecosystem, and Whether Social Compensation Matters. **Marine Policy, 119**, doi: https://doi.org/10.1016/j.marpol.2020.104031

[50] Smythe, T., Bidwell, D., Moore, A., Smith, H. & McCann, J. (2020). Beyond the Beach: Tradeoffs in Tourism and Recreation at the First Offshore Wind Farm

in the United States. **Energy Research & Social Science, 70**, doi: https://doi.org/10.1016/j.erss.2020.101726

[51] Righter, R. W. (1996). **Wind Energy in America. A History**. Oklahoma, US: University of Oklahoma Press.

BIBLIOGRAPHY (Continued)

[52] Stoddard, W. (2002). The Life and Work of Bill Heronemus Wind Engineering Pioneer. **Wind Engineering, 26**(5), pp. 335-341.

[53] Robertson, A. N. & Jonkman, J. M. (2011). **Loads Analysis of Several Offshore Floating Wind Turbine Concepts**. Paper Presented at the International Society of Offshore and Polar Engineers 2011 Conference, Maui, Hawaii, US. Retrieved from National Renewable Energy Laboratory (NREL) Website: https://www.nrel.gov/docs/fy12osti/50539.pdf

[54] Bagbanci, H. (2011). **Dynamic Analysis of Offshore Floating Wind Turbines at Technical University of Lisbon**. (Master's thesis, The Technical University of Lisbon, Lisbon, Portugal).

[55] Roddier, D., Cermelli, C., Aubault, A. & Weinstein, A. (2010). WindFloat: A Floating Foundation for Offshore Wind Turbines. **Journal of Renewable and Sustainable Energy, 2**(3). doi: https://doi.org/10.1063/1.3435339

[56] Roddier, D., Peiffer, A., Aubault, A., & Weinstein, J., (2011). **A Generic 5 MW Windfloat for Numerical Tool Validation and Comparison Against a Generic Spar**. Paper Presented at the Proceedings of the 30th International Conference on Ocean Offshore Arctic Engineering, Rotterdam, Netherlands.

[57] Chen, J., Hu, Z., Wan, D. & Xiao, Q. (2018). Comparisons of the Dynamical Characteristics of a Semi-Submersible Floating Offshore Wind Turbine Based

on Two Different Blade Concepts. **Ocean Engineering, 153**, 305-318. doi: https://doi.org/10.1016/j.oceaneng.2018.01.104

[58] Tran, T. T. & Kim, D. H. (2015). The Platform Pitching Motion of Floating Offshore Wind Turbine: A Preliminary Unsteady Aerodynamic Analysis. **Journal of Wind Engineering and Industrial Aerodynamics, 142**, 65-81. doi: https://doi.org/10.1016/j.jweia.2015.03.009

[59] Wen, B., Dong, X., Tian, X., Peng, Z., Zhang, W. & Wei, K. (2018). The Power Performance of an Offshore Floating Wind Turbine in Platform Pitching Motion. **Energy, 154**, 508-521. doi: https://doi.org/10.1016/j.energy.2018.04.140

[60] Wen, B., Tian, X., Dong, X., Peng, Z. & Zhang, W. (2018). On the Power Coefficient Overshoot of an Offshore Floating Wind Turbine in Surge Oscillations. **Wind Energy, 1**(16). doi: https://doi.org/10.1002/we.2215

[61] Wang, Q., Liao, K. & Ma, Q. (2020). The Influence of Tilt Angle on the Aerodynamic Performance of a Wind Turbine. **Applied Sciences, 10**(15), doi: https://doi.org/10.3390/app10155380

[62] Gumuła, S., Silarska, M. P., Pytel, K., Noga, H. & Kulinowski, W. (2017). Evaluation of the Impact of Adjusting the Angle of the Axis of a Wind Turbine Rotor Relative to the Flow of Air Stream on Operating Parameters of a Wind Turbine Model. **E3S Web of Conferences, 14**. doi: https://doi.org/10.1051/e3sconf/20171401016

[63] Abdelsalama, A. M. & Ramalingamb, V. (2013). **Effect of the Tilt Angle on the Wind Turbine Performance and Wakes**. Paper Presented at the Eighth Asia-Pacific Conference on Wind Engineering, Chennai, India. Retrieved from

https://www.researchgate.net/publication/269252848_Effect_of_the_Tilt_Angle_on_the_Wind_Turbine_Performance_and_Wakes

[64] Kirsch, J. (2009). **Design of a Small Wind Turbine for Electric Power Generation (1-5kW) at University of Southern Queensland**. (Bachelor's dissertation, The University of Southern Queensland).

[65] Sanduk, M., (2013). Wind Energy Technology, ENGM246 Wind Energy Technology, University of Surrey, unpublished.

[66] Tempel, J. V. D., Diepeveen, N. F. B., De Vries, W. E. & Salzmann, C. D. (2011). Offshore environmental Loads and Wind Turbine Design: Impact of Wind, Wave, Currents and Ice. In Sørensen, J. D. & Sørensen, J. N. (Eds.). **Wind Energy Systems Optimising Design and Construction for Safe and Reliable Operation** (pp. 463-478) Cambridge, UK: Woodhead Publishing.

[67] MacEachern, C. & Yildiz, I. (2018). Wind Energy. In Dincer, I. (Eds.) **Comprehensive Energy Systems Volume 1** (pp. 665-701) Cambridge, UK: Elsevier.

[68] Koutroulis, E. (2018). Energy Management in Wind Energy Systems. In Dincer, I. (Eds.) **Comprehensive Energy Systems Volume 5** (pp. 707-741) Cambridge, UK: Elsevier.

[69] RETScreen International, (2004). **Wind Energy Project Analysis**. Retrieved from https://www.slideshare.net/sustenergy/wind-energy-project-analysis-486826

[70] International Renewable Energy Agency (IRENA). (2016). **Wind Power Technology Brief**. Retrieved from https://www.irena.org/-/media/Files/IRENA/Agency/Publication/2016/IRENA-ETSAP_Tech_Brief_Wind_Power_E07.pdf

[71] Vouloudis, A. (2010). **Technical Review of Design Requirements of Wind Energy Conversion Systems and Analysis of Target Set and Progress Achieved in Greece and UK at University of Surrey**. (Thesis's master, The University of Surrey).

[72] Neill, P. S. & Hashemi, M. R. (2018) Offshore Wind. In **Fundamentals of Ocean Renewable Energy Generating Electricity from the Sea**. (pp. 83-106). Cambridge, UK: Elsevier.

[73] Monnerie, N., Houaijia, A., Roeb, M. & Sattler, C. (2015) Methane Production via High Temperature Steam Electrolyser from Renewable Wind Energy: A German Study. **Green and Sustainable Chemistry, 5**, 70-80. doi: http://dx.doi.org/10.4236/gsc.2015.52010

[74] Akpinar, E. K. & Akpinar, S. (2005). A Statistical Analysis of Wind Speed Data Used in Installation of Wind Energy Conversion Systems. **Energy Conversion and Management, 46**(4), 515-532. doi: https://doi.org/10.1016/j.enconman.2004.05.002

[75] Chauhan, A. & Saini, R. P. (2014). **Statistical Analysis of Wind Speed Data Using Weibull Distribution Parameters**. Paper Presented at the 1st International Conference on Non Conventional Energy, Kalyani, India. Retrieved from IEEE Xplore Website: https://ieeexplore.ieee.org/document/6808712

[76] Arikan, Y., Akkas, O. P. & Cam, E. (2015). The Analysis of Wind Data with Rayleigh Distribution and Optimum Turbine and Cost Analysis in Elmadag, Turkey. **IU-JEEE, 15**(1), pp. 1907-1912. Retrieved from Research Gate Website:

https://www.researchgate.net/publication/316520976_The_analysis_of_wind_data_with_rayleigh_distribution_and_optimum_turbine_and_cost_analysis_in_Elmadag_Turkey

[77] Hughes, K. (2019). **Solar Power vs. Wind Power Cost, Types, Pros & Cons of Home Wind & Solar**. Retrieved from https://www.letsgosolar.com/consumer-education/solar-power-wind-power/

[78] Rashid, M. H. (2015). **Alternative Energy in Power Electronics**. Massachusetts, US: Butterworth-Heinemann.

[79] Boyle, G. (1996). **Renewable Energy Power for a Sustainable Future**. Oxford, UK: Oxford University Press.

[80] Clarke, S. (2018). **Electricity Generation Using Small Wind Turbines at Your Home or Farm**. Retrieved from Ontario Website: http://www.omafra.gov.on.ca/english/engineer/facts/03047.pdf

[81] Carrasco, J. M., Galván, E. & Portillo, R. (2011) Wind Turbine Applications. In **Power Electronics Handbook**. (pp.791-822). Cambridge, UK: Elsevier.

[82] Năstase, E. V. (2017). **Influence of the Material Used to Build the Blades of a Wind Turbine on Their Starting Conditions**. Paper Presented at the 21st Innovative Manufacturing Engineering & Energy International Conference, Iasi, Romania. Retrieved from Research Gate Website: https://www.researchgate.net/publication/318112329_Influence_of_the_material_used_to_build_the_blades_of_a_wind_turbine_on_their_starting_conditions

[83] Prabha, M., Dash, N. & Baars, S. (2013). **Site Specific Wind Turbine Foundation Certification**. Retrieved from https://silo.tips/download/site-specific-wind-turbine-foundation-certification

BIBLIOGRAPHY (Continued)

[84] Ayers, D. E. & Dickinson, M. (2011). **Wind Farm Transformer Design Considerations**. Retrieved from Power Engineering Website: https://www.power-eng.com/2011/11/01/wind-farm-transformer-design-considerations/#gref

[85] Brakefield, K., (2017). **Different Types of Wind Turbine Towers Made with Steel**. Retrieved from https://blog.swantonweld.com/steel-wind-turbine-towers

[86] New Green Business Ideas, (2012). **Towers**. Retrieved from http://newgreenbusinessideas.blogspot.co.uk/2012/05/towers.html

[87] Avanti, (2019). **Avanti Wind Turbine Ladder**. Retrieved from https://de.avanti-online.com/admin/public/download.aspx?file=/Files/Files/FPS/Ladders-datasheet.pdf

[88] Abad, G., Lopez, J., Rodriguez, M., Marroyo, L. & Iwanski, G. (2011). **Doubly Fed Induction Machine: Modeling and Control for Wind Energy Generation**. New Jersey, US: John Wiley and Sons.

[89] Sharpley, N. (2015). **Nacelles**. Retrieved from Wind Power Engineering Development Website.

[90] Zipp, K. (2012). **Generators 101**. Retrieved from Wind Power Engineering Development Website: https://www.windpowerengineering.com/generators-101/

[91] Chudnovsky, B. H. (2017). **Transmission, Distribution, and Renewable Energy Generation Power Equipment Aging and Life Extension Technique**. Florida, US: CRC Press.

[92] U.S. Department of Energy. (2018). **The Inside of a Wind Turbine**. Retrieved from https://www.energy.gov/eere/wind/inside-wind-turbine

BIBLIOGRAPHY (Continued)

[93] Ukonsaari, J. (2016). **Wind Turbine Gearboxes**. Retrieved from Energiforsk Website: https://energiforskmedia.blob.core.windows.net/media/21270/wind-turbine-gearboxes-energiforskrapport-2016-279.pdf

[94] Engineering 360. (2017). **Blades (Wind Turbine) Information**. Retrieved from https://www.globalspec.com/learnmore/electrical_electronic_components/power_generation_storage/alternative_power_generators/blades_wind_turbine

[95] Opie, R. (2018). **Pitch Control Critical for Wind Power**. Retrieved from Machine Design Website: https://www.machinedesign.com/mechanical/pitch-control-critical-wind-power

[96] DunoAir. (2018). **DunoAir Components of a Wind Turbine**. Retrieved from https://www.dunoair.com/en/about-windenergy/components-of-a-wind-turbine.html

[97] Roynarin, W. (2004). **Optimization of Vertical Axis Wind Turbines in Northumbria University**. (Thesis's Doctoral, Northumbria University).

[98] Ragheb, M. (2014). **Optimal Rotor Tip Speed Ratio**. Retrieved from http://mragheb.com/NPRE%20475%20Wind%20Power%20Systems/Optimal%20Rotor%20Tip%20Speed%20Ratio.pdf

[99] Cao, H. (2011). **Aerodynamics Analysis of Small Horizontal Axis Wind Turbine Blades by Using 2D and 3D CFD Modelling at University of Central Lancashire**. (Thesis's master, University of Central Lancashire).

[100] Twidell, J. & Weir, T. (2006). **Renewable Energy Resources** (2nd ed.) London, UK: Taylor & Francis Group.

[101] Manwell, J. F., McGowan, J. G. & Rogers, A. L. (2009). **Wind Energy Explained**. (2nd ed.) West Sussex, UK: John Wiley & Sons Ltd.

[102] University of Notre Dame. (2016). **Introduction to Aerodynamics**. Retrieved from https://www3.nd.edu/~tcorke/w.WindTurbineCourse/Intro_Aero_Presentation.pdf

[103] Tong, W. (2010). Fundamentals of Wind Energy. In **WIT Transactions on State of the Art in Science and Engineering. Vol 44**. (pp. 3-48). Southampton, UK: WIT Press.

[104] Rivkin, D. A., Anderson, L. D. & Silk, L. (2013). **Wind Turbine Control Systems**. Massachusetts, US: Jones and Bartlett Learning.

[105] Jabir, M., Illias, H.A., Raza, S. & Mokhlis, H. (2017). Intermittent Smoothing Approaches for Wind Power Output: A Review. **Energies, 10**(10). doi: https://doi.org/10.3390/en10101572

[106] Rao, K. R. (2019). **Wind Energy for Power Generation: Meeting the Challenge of Practical Implementation**. Cham, Switzerland: Springer Nature.

[107] Engineering Ambitiously. (2019). **Wind Turbine Control Methods**. Retrieved from https://www.ni.com/en-th/innovations/white-papers/08/wind-turbine-control-methods.html

[108] Jiawei, C., Changyun, W. & Yongduan, S. (2014). **Power Control Strategy for Variable-Speed Fixed-Pitch Wind Turbines**. Paper Presented at the Proceedings of 13th International Conference on Control, Automation, Robotics & Vision, Singapore. Retrieved from IEEE Xplore Website: https://ieeexplore.ieee.org/abstract/document/7064365

[109] Wang, S., Huang, Y., Li, L., Liu, C. & Zhang, D. (2017). Dynamic Analysis of Wind Turbines Including Nacelle-Tower-Foundation Interaction for Condition

of Incomplete Structure Parameters. **Advances in Mechanical Engineering,9**(3), 1-17. doi: https://doi.org/10.1177/1687814017692940

[110] Osgood, R. M. (2001). **Dynamic Characterization Testing of Wind Turbines**. Retrieved from National Renewable Energy Laboratory (NREL) Website: https://www.nrel.gov/docs/fy01osti/30070.pdf

[111] Yang, W., Tavner, P. J., Crabtree, C. J., Feng, Y. & Qiu, Y. (2014). Wind Turbine Condition Monitoring: Technical and Commercial Challenges. **Wind Energy**. doi: https://doi.org/10.1002/we.1508

[112] Dvorak, P. (2011). **Vibration Control for Turbines**. Retrieved from Wind Power Engineering and Development Website: https://www.windpowerengineering.com/vibration-control-for-turbines/

[113] Lehr, J. H. & Keeley, J. (2016). **Alternative Energy and Shale Gas Encyclopedia**. New Jersey, US: John Wiley & Son, Inc.

[114] Bailey, B. H. (2016). Offshore Wind Farms. In Ng, C. & Ran, L. (Ed.). **Offshore Wind Farms** (pp. 29-58), Cambridge, UK: Woodhead Publishing.

[115] Godø, S. N. (2013). **Dynamic Response of Floating Wind Turbines at Norwegian University of Science and Technology**. (Master's thesis, Norwegian University of Science and Technology, Trondheim, Norway).

[116] Miceli, F. (2012). **Offshore Wind Turbines Foundation Types**. Retrieved from http://www.windfarmbop.com/offshore-wind-turbines-foundation-types/

[117] Malhotra, S. (2011). **Selection, Design and Construction of Offshore Wind Turbine Foundations**. Retrieved from IntechOpen Website: https://cdn.intechopen.com/pdfs/14804/InTech-Selection_design_and_construction_of_offshore_wind_turbine_foundations.pdf

[118] International Renewable Energy Agency, IRENA. (2016). **Floating Foundations: A Game Changer for Offshore Wind Power**. Retrieved from https://www.irena.org/-/media/Files/IRENA/Agency/Publication/2016/IRENA_Offshore_Wind_Floating_Foundations_2016.pdf

[119] Carbon Trust. (2015). **Floating Offshore Wind: Market and Technology Review**. Retrieved from https://www.carbontrust.com/media/670664/floating-offshore-wind-market-technology-review.pdf

[120] Bagbanci, H. (2011). **Dynamic Analysis of Offshore Floating Wind Turbines in University of Lisbon**. (Thesis's Master, University of Lisbon).

[121] Roynarin, W. (2016). **Development of 100 kW Small Wind Machine for the Floating Applications to Support the Island Energy Demand**. Paper Presented at the Proceedings of the 4th International Conference on Wind Turbine and Renewable Energy, Seoul, Korea.

[122] Matha, D. (2019). **Model Development and Loads Analysis of an Offshore Wind Turbine on a Tension Leg Platform, with a Comparison to Other Floating Turbine Concepts**. Retrieved from National Renewable Energy Laboratory (NREL) Website: https://www.nrel.gov/docs/fy10osti/45891.pdf

[123] Head, M., Seo. J., Shokouhian. M. & Schaffer. W. (2016). **Foundation Anchorages for Offshore Wind Turbines in Deep Water Using Composite Materials**. Retrieved from Research Gate Website: https://www.researchgate.net/publication/311442219_Foundation_Anchorages_for_Offshore_Wind_Turbines_in_Deep_Water_Using_Composite_Materials

[124] Karimirad, M. (2012). Mechanical-Dynamic Loads. **Comprehensive Renewable Energy, 2,** 243-268. doi: https://doi.org/10.1016/B978-0-08-087872-0.00210-9

[125] Damiani, R.R. (2016). Design of Offshore Wind Turbine Towers. In Ng, C. & Ran, L. (Ed.). **Offshore Wind Farms** (pp. 263-357), Cambridge, UK: Woodhead Publishing.

[126] Malhotra, S. (2011). **Selection, Design and Construction of Offshore Wind Turbine Foundations, Wind Turbines**. Retrieved from IntechOpen Website: https://www.intechopen.com/books/wind-turbines/selection-design-and-construction-of-offshore-wind-turbine-foundations

[127] Biran, A. & Pulido, R. L. (2014). **Ship Hydrostatics and Stability**. Cambridge, UK: Butterworth-Heinemann.

[128] King Abdulaziz University. (2019). Archimedes Principle. Retrieved from http://www.kau.edu.sa/GetFile.aspx?id=176952&fn=Archimedfinal[1].pdf

[129] Veerendra., (2017) **Understanding Buoyancy Using Archimedes' Principle**. Retrieved from Aplustopper Website: https://www.aplustopper.com/understanding-buoyancy-using-archimedess-principle/

[130] Borg, M. & Collu, M. (2015). A Comparison Between the Dynamics of Horizontal and Vertical Axis Offshore Floating Wind Turbines. **Philosophical Transactions A, 373**(2035). doi: https://doi.org/10.1098/rsta.2014.0076

[131] Collu, M. & Borg, M. (2016). Design of Floating Offshore Wind Turbines. In Ng, C. & Ran, L. (Ed.). **Offshore Wind Farms** (pp. 359-385), Cambridge, UK: Woodhead Publishing.

[132] Zuo, W. (2005). **Introduction of Computational Fluid Dynamics**. Retrieved from http://wwwmayr.informatik.tu-muenchen.de/konferenzen/Jass05/courses/2/Zuo/Zuo_paper.pdf

[133] Singh, K. M. (2012). **Boundary Conditions**. Retrieved from https://nptel.ac.in/courses/112107080/module2/lecture7/lecture7.pdf

[134] Ashgriz, N. & Mostaghimi, J. (2002). An Introduction to Computational Fluid Dynamics. In Saleh, J. M. (Ed.) **Fluid Flow Handbook**. New York, US: McGraw-Hill.

[135] Kanti, P. K. & Chandran, S. (2016). **A Review Paper on Basics of CFD and Its Applications**. Paper Presented at National Conference on Advances in Mechanical Engineering Science (NCAMES-2016), Chennai, India.

[136] Autodesk. (2015). **Chapter 12: Can I Trust my Results?**. Retrieved from https://knowledge.autodesk.com/support/cfd/learn-explore/caas/CloudHelp/cloudhelp/2014/ENU/SimCFD/files/GUID-9D30EB08-3C45-419B-BEC6-976606AC46F5-htm.html

[137] Sodja, J. (2007). **Turbulence Models in CFD at University of Ljubljana**. (Seminar, The University of Ljubljana, Ljubljana, Slovenia).

[138] McDonough, J. M. (2007). **Lectures in Computational Fluid Dynamics of Incompressible Flow: Mathematics, Algorithms and Implementations**. Retrieved from University of Kentucky College of Engineering Website: http://web.engr.uky.edu/~acfd/me691-lctr-nts.pdf

[139] Simscale, (2019). **K-omega SST**. Retrieved form https://www.simscale.com/docs/content/simulation/model/turbulenceModel/kOmegaSST.html

[140] Argyropoulos, C. D. & Markatos, N. C. (2015). Recent Advances on the Numerical Modelling of Turbulent Flows. **Applied Mathematical Modelling, 39**(2), 693-732. doi: https://doi.org/10.1016/j.apm.2014.07.001

[141] Tey, W. Y., Asako, Y., Sidik, N. A. C. & Rui-Zher, G. (2017). Governing Equations in Computational Fluid Dynamics: Derivations and a Recent Review. **Progress in Energy and Environment, 1**, 1-19.

[142] Munson, B. R., Young, D. F., Okiishi, T. H. & Huebsch, W. W. (2009). **Fundamental of Fluid Mechanics** (6^{th} ed). New Jersey, US: John Wiley & Sons.

[143] Department of Energy Affairs. (2001). **Wind Resource Assessment of Thailand**. Retrieved from http://www2.dede.go.th/dede/renew/Twm/ MAIN.htm

[144] Waewsak, J., Landry, M. & Gagnon, Y. (2015). Offshore Wind Power Potential of the Gulf of Thailand. **Renewable Energy, 81**, 609-626. doi: https://doi.org/10.1016/j.renene.2015.03.069

[145] Roynarin, W., Wisatesajja, W. & Aguila, G. (2020). **The Effect of the Number of Blades on the Characteristics of Compressed Air Wind Turbines Using R1235 Airfoil Blade Profile**. Paper Presented at the Proceeding of the 11^{th} International Conference on Mechanical Engineering, Ubon Ratchathani, Thailand.

[146] Kongkapisuth, K., Roynarin, W., & Intholo, D. (2017). Study of Building Effects on Small HAWTs Performance in Building-Obstructed Wind Flow Area by Using a CFD $k\text{–}\epsilon$ Turbulence Model Validated with Site Measurement. **International Energy Journal, 17**(4), 193-210.

APPENDICES

APPENDIX A

CFDesign Usability

CFDesign Usability

Step 1 In the menu bar select the "New" for use the new model as shown in **Figure 1.**

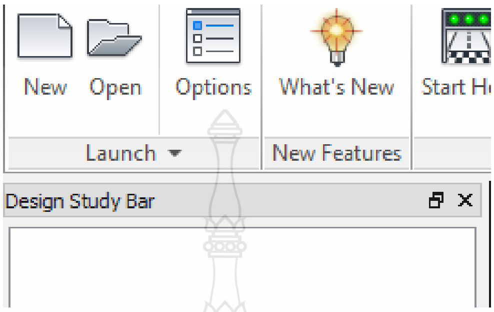

Figure 1. CFDesign menu bar.

Step 2 In the "New Design Study" select "Browse" import the model file as shown in **Figure 2**.

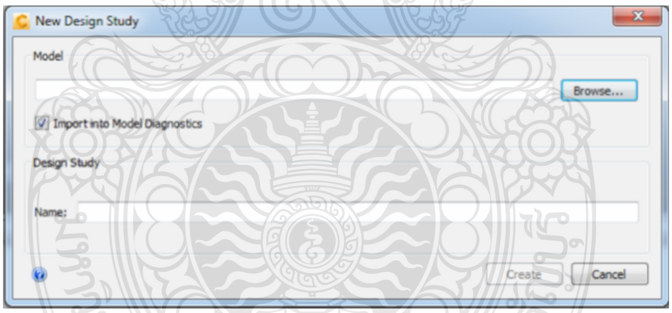

Figure 2. CFDesign import file.

Step 3 The model assessment will check the model compatible "Edge lengths, Surface sliver, Model silvers, Part gaps, Model gaps, and interference" for preparing CFD solving, as shown in **Figure 3.**

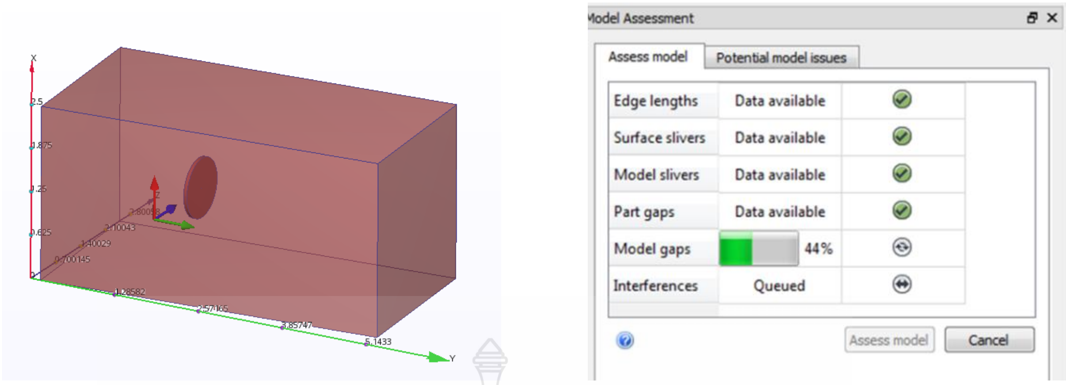

Figure 3. CFDesign model assessment.

Step 4 Overall, the model part must be selected by the material, the wind turbine be selected by the solid part, and the air be selected by air fluid material, and rotating region as turbine as shown in **Figure 4.**

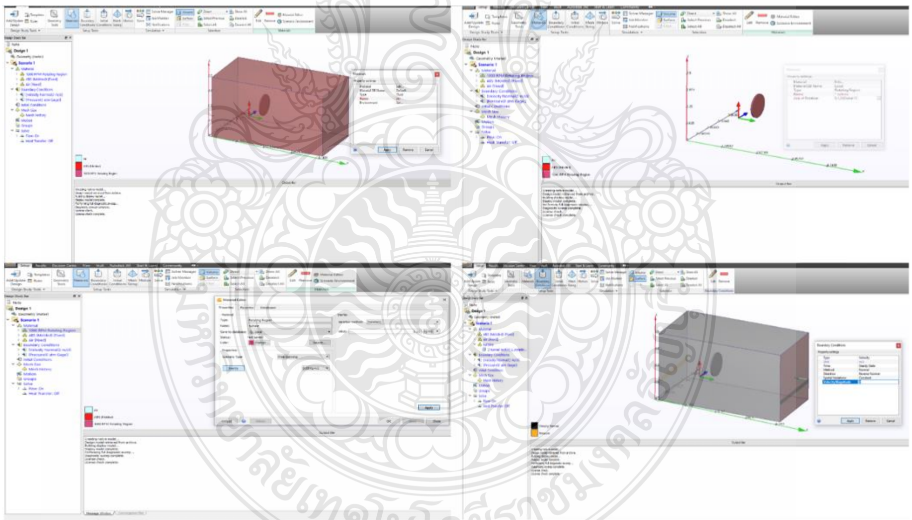

Figure 4. CFDesign material selected.

Step 5 Select the boundary condition of the model; the inlet side of model selected by 2.0-5.5 m/s of air flow and the outlet side by 0 Pa of pressure, as shown in **Figure 5**.

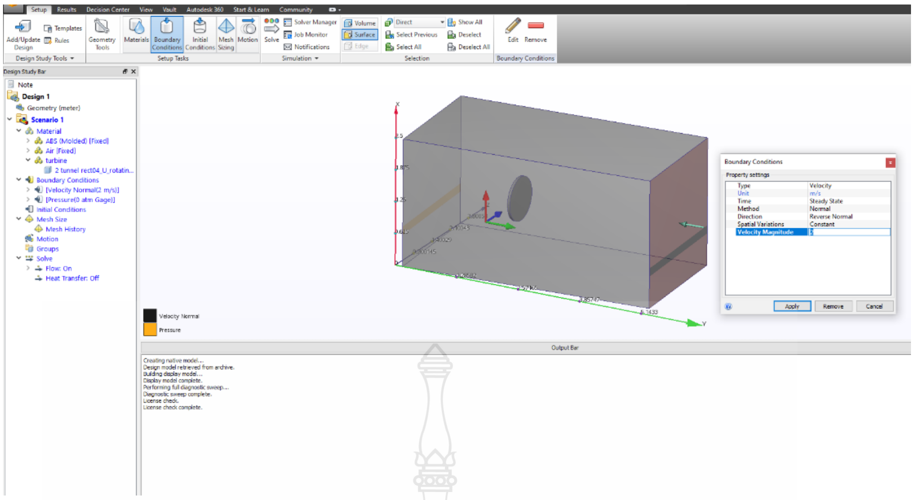

Figure 5. CFDesign boundary condition of the model.

Step 6 After selecting the boundary condition, the “Mashing” will be created as shown in **Figure 6**

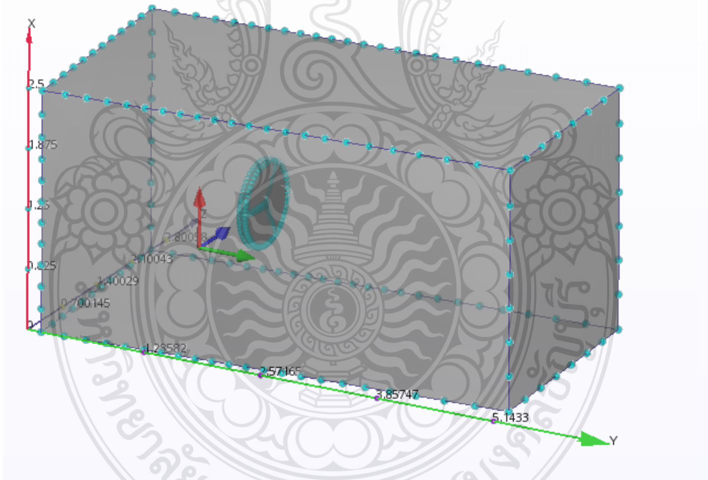

Figure 6. CFDesign mashing.

Step 7 After the model part is mashed, the model will be solved as the "turbulence model", in this model is selected k- ε turbulence model, and the result quantities is selected as shown in **Figure 7**

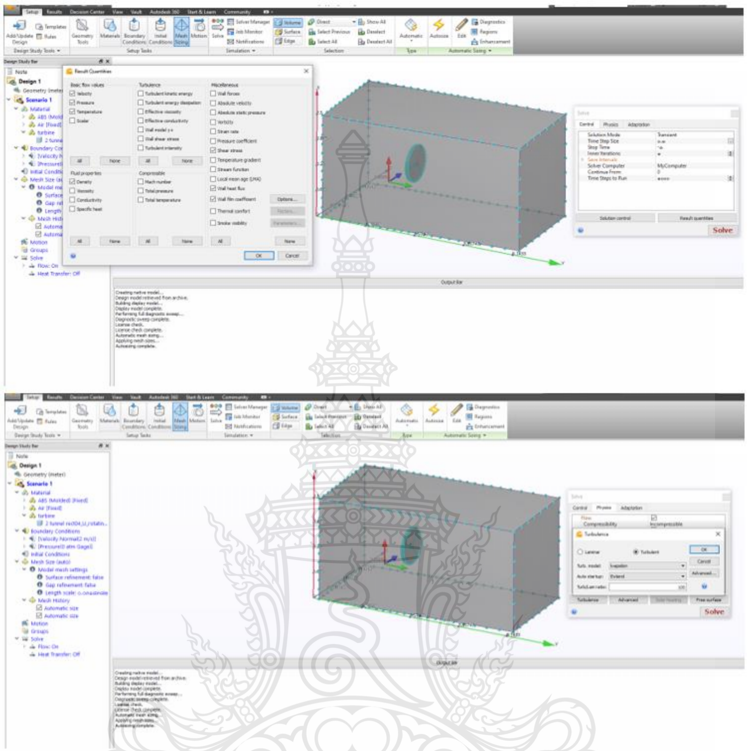

Figure 7. CFDesign turbulent model selection.

Step 8 After all steps are finished, the model will be solved, as shown in **Figure 8**

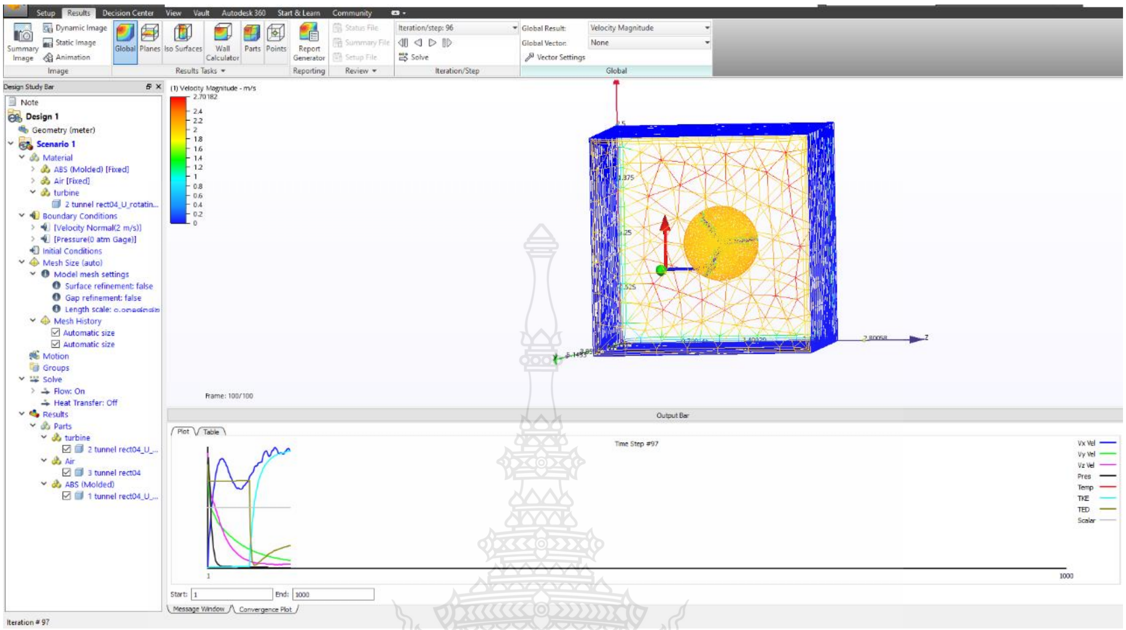

Figure 8. CFDesign solver.

Step 9 After completely solving, torque and angular velocity can be found in summary result file in the CFD solver, as shown in **Figure 9**

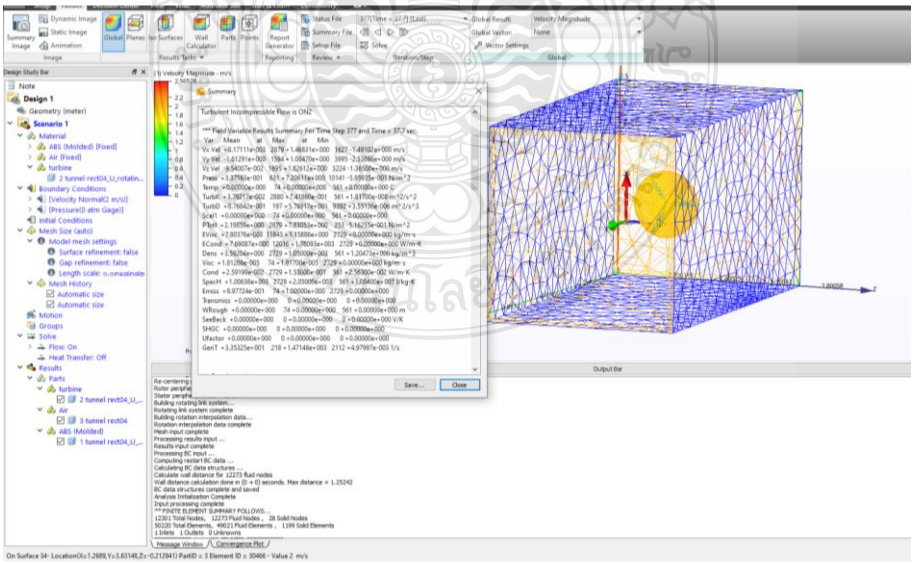

Figure 9. CFDesign solver.

APPENDIX B
CFD k-ε Turbulence Model Results

Table 1. CFD k-ε Turbulence Model Result at 2.0 m/s, 3.5 degree

Time (sec)	Hydraulic Torque (N-m)	Rotating Speed (RPM)	Hydraulic Force X (N)	Hydraulic Force_Y (N)	Hydraulic Force_Z (N)
0.1	0.000196	0	5.27E-05	-0.00851	-5.11E-05
0.2	0.000291	0.003743	7.47E-05	-0.0118	-4.21E-05
0.3	0.000371	0.009297	0.000114	-0.01475	-3.80E-05
0.4	0.000429	0.016378	0.000157	-0.01708	-3.92E-05
0.5	0.00047	0.024564	0.000198	-0.0189	-4.24E-05
0.6	0.000502	0.033549	0.000231	-0.02039	-4.55E-05
0.7	0.000528	0.043133	0.000258	-0.02169	-5.39E-05
0.8	0.000551	0.053212	0.000282	-0.0229	-6.55E-05
0.9	0.000574	0.063738	0.000303	-0.02407	-8.16E-05
1	0.000597	0.074697	0.00032	-0.02525	-0.0001
1.1	0.00062	0.086093	0.000335	-0.02643	-0.00012
1.2	0.000772	0.097934	0.000418	-0.03594	-0.00017
1.3	0.000853	0.112676	0.000449	-0.0407	-0.0002
1.4	0.000898	0.12896	0.000459	-0.04321	-0.00022
1.5	0.000925	0.146103	0.000459	-0.04466	-0.00023
1.6	0.000944	0.163769	0.000458	-0.04562	-0.00026
1.7	0.000959	0.181794	0.000457	-0.04636	-0.00028
1.8	0.000972	0.200102	0.000458	-0.04698	-0.0003
97.7	0.000784	349.4357	0.00085	-0.03684	-0.00045
97.8	0.000787	349.4507	0.000517	-0.03887	0.000318
97.9	0.000791	349.4657	-0.00084	-0.04048	0.001164
98	0.000795	349.4808	-0.00024	-0.0449	-0.0015
98.1	0.000789	349.496	0.000324	-0.04964	-0.00029
98.2	0.000795	349.5111	0.001407	-0.04955	0.001078
98.3	0.000802	349.5262	-0.00176	-0.05076	5.14E-05
98.4	0.000793	349.5416	-4.39E-05	-0.05238	-0.00032
98.5	0.00078	349.5567	0.001162	-0.05616	-0.00187
98.6	0.000787	349.5716	-3.95E-05	-0.05593	0.00262
98.7	0.000775	349.5866	0.000101	-0.05604	-0.00038
98.8	0.000771	349.6014	-0.00203	-0.05775	-0.00163
98.9	0.000765	349.6161	0.003085	-0.06306	0.000143
99	0.000775	349.6307	-0.00084	-0.06193	0.000246
99.1	0.000776	349.6455	-0.00116	-0.06213	0.002213
99.2	0.000775	349.6604	9.17E-05	-0.06397	-0.00385
99.3	0.000791	349.6752	0.000572	-0.06519	0.00114

Table 2. CFD k-ε Turbulence Model Result at 2.5 m/s, 3.8 degree

Time (sec)	Hydraulic Torque (N-m)	Rotating Speed (RPM)	Hydraulic Force_X (N)	Hydraulic Force_Y (N)	Hydraulic Force_Z (N)
0.1	0.000266	0	-8.59E-05	-0.01125	-0.00019
0.2	0.000401	0.005081	-5.73E-05	-0.01594	-0.0002
0.3	0.000522	0.012732	-4.53E-05	-0.02026	-0.00023
0.4	0.000616	0.022701	-3.66E-05	-0.02374	-0.00027
0.5	0.000688	0.034463	-3.22E-05	-0.02647	-0.0003
0.6	0.000744	0.047603	-3.12E-05	-0.0287	-0.00032
0.7	0.000792	0.061817	-3.20E-05	-0.03064	-0.00035
0.8	0.000834	0.076935	-3.46E-05	-0.03241	-0.00038
0.9	0.000874	0.092861	-3.82E-05	-0.03413	-0.00041
1	0.001125	0.109562	-2.42E-05	-0.04782	-0.00049
1.1	0.001258	0.131048	-1.43E-05	-0.0549	-0.00053
1.2	0.001331	0.155067	-7.23E-06	-0.0587	-0.00055
1.3	0.001373	0.180481	-1.94E-06	-0.06088	-0.00058
1.4	0.001402	0.206712	2.08E-06	-0.06229	-0.00061
1.5	0.001423	0.233484	6.76E-06	-0.06332	-0.00066
1.6	0.001441	0.260661	1.20E-05	-0.06416	-0.00071
1.7	0.001457	0.288179	1.46E-05	-0.06492	-0.00077
1.8	0.001474	0.316007	1.80E-05	-0.06566	-0.00083
1.9	0.001492	0.344152	2.19E-05	-0.06641	-0.00089
2	0.00151	0.372639	2.35E-05	-0.06716	-0.00095
2.1	0.001528	0.401471	2.19E-05	-0.06794	-0.00101
2.2	0.001547	0.430658	1.78E-05	-0.06876	-0.00107
48.6	0.0136	548.086093	0.00397	-0.1128	0.001486
48.65	0.01366	548.097934	-0.00545	-0.11207	-0.00408
48.7	0.01355	548.112676	0.004318	-0.11149	0.00626
48.75	0.01333	548.124896	-0.00137	-0.11179	-0.00612
48.8	0.01318	548.146103	-0.00036	-0.11425	0.002619
48.85	0.01301	548.163769	0.00041	-0.11847	0.001324
48.9	0.01315	548.181794	0.002593	-0.12055	-0.00497
48.95	0.01332	548.200102	-0.00509	-0.11968	0.00549
49	0.01333	548.434457	0.007535	-0.13455	-0.0037
49.05	0.0135	548.487507	-0.00607	-0.12813	0.000319
49.1	0.01359	548.467857	0.002378	-0.12397	0.001569
49.15	0.01362	548.480888	0.002734	-0.12429	-0.00106
49.2	0.01354	548.494776	-0.00575	-0.12434	-0.00235
49.25	0.01335	548.511771	0.005277	-0.12458	0.00582

Table 3. CFD k-ε Turbulence Model Result at 3.0 m/s, 3.9 degree

Time (sec)	Hydraulic Torque (N-m)	Rotating Speed (RPM)	Hydraulic Force_X (N)	Hydraulic Force_Y (N)	Hydraulic Force_Z (N)
0.1	0.000302	0	-3.63E-05	-0.01322	-0.00021
0.2	0.000506	0.005776	-3.92E-05	-0.02053	-0.00024
0.3	0.000693	0.015433	-3.57E-05	-0.02707	-0.00026
0.4	0.000837	0.028659	-8.53E-06	-0.03216	-0.00026
0.5	0.000943	0.044653	2.66E-05	-0.03604	-0.00024
0.6	0.001025	0.062671	6.50E-05	-0.03911	-0.00023
0.7	0.001093	0.082248	0.000103	-0.0417	-0.00022
0.8	0.001154	0.103119	0.000137	-0.04404	-0.00022
0.9	0.001502	0.125163	0.000179	-0.06274	-0.00037
1	0.00169	0.153851	0.000177	-0.07221	-0.00041
1.1	0.001797	0.18612	0.000161	-0.07719	-0.00044
1.2	0.001863	0.220439	0.000143	-0.07998	-0.00049
1.3	0.001906	0.256014	0.000115	-0.08165	-0.00054
1.4	0.00194	0.292415	0.000103	-0.08281	-0.00059
1.5	0.00197	0.329462	9.83E-05	-0.08373	-0.00064
1.6	0.001999	0.367079	9.75E-05	-0.08458	-0.00071
1.7	0.002029	0.405257	9.79E-05	-0.08542	-0.00078
1.8	0.002061	0.444013	0.000103	-0.08629	-0.00085
1.9	0.002093	0.483369	0.000102	-0.08721	-0.00093
2	0.002124	0.523335	0.000101	-0.08819	-0.001
2.1	0.002156	0.563902	1.00E-04	-0.08922	-0.00108
2.2	0.002191	0.605076	9.77E-05	-0.09033	-0.00116
2.3	0.002225	0.646926	9.89E-05	-0.09149	-0.00124
2.4	0.002263	0.689428	8.46E-05	-0.0928	-0.00132
0.1	0.000302	702.736138	-3.63E-05	-0.01322	-0.00021
0.2	0.000506	702.03351	-3.92E-05	-0.02053	-0.00024
24.2	0.02547	702.736138	0.007697	-0.08883	-0.00038
24.3	0.02599	702.03351	0.005693	-0.0877	0.005818
24.4	0.02574	702.02235	-0.00291	-0.08761	0.007314
24.5	0.02534	702.1103	-0.00699	-0.08617	0.000749
24.6	0.02592	702.934404	-0.00365	-0.08811	-0.00555
24.7	0.02558	702.24961	0.004643	-0.08856	-0.00752
24.8	0.02551	702.2311	0.007313	-0.0902	0.000421
24.9	0.02609	702.35327	0.004777	-0.08975	0.005783
25	0.02565	70213536	-0.00372	-0.08909	0.007077
25.1	0.02535	702.61417	-0.00763	-0.08836	-0.00099

Table 4. CFD k-ε Turbulence Model Result at 3.5 m/s, 4.3 degree

Time (sec)	Hydraulic Torque (N-m)	Rotating Speed (RPM)	Hydraulic Force_X (N)	Hydraulic Force_Y (N)	Hydraulic Force_Z (N
0.1	0.00041	0	6.66E-05	-0.0171	-0.00033
0.2	0.000641	0.007838	0.00011	-0.02593	-0.00028
0.3	0.000862	0.020079	0.000149	-0.0343	-0.00023
0.4	0.001045	0.036551	0.000208	-0.04111	-0.00019
0.5	0.001191	0.05651	0.000277	-0.04648	-0.00017
0.6	0.001309	0.079249	0.000349	-0.05084	-0.00015
0.7	0.001411	0.10425	0.000417	-0.05452	-0.00015
0.8	0.001895	0.131195	0.000598	-0.08135	-0.00027
0.9	0.002154	0.167377	0.000735	-0.09444	-0.0002
1	0.002292	0.208509	0.000849	-0.10082	-0.00011
1.1	0.002371	0.252282	0.000944	-0.104	-3.80E-05
1.2	0.002419	0.297558	0.001016	-0.10568	-4.78E-06
1.3	0.002454	0.343749	0.001069	-0.1067	7.49E-06
1.4	0.002486	0.390624	0.001118	-0.10748	-3.22E-06
1.5	0.00252	0.438099	0.001163	-0.10827	-3.76E-05
1.6	0.002555	0.486233	0.001191	-0.10907	-8.55E-05
1.7	0.002592	0.535036	0.001205	-0.10997	-0.00015
1.8	0.002634	0.584534	0.001206	-0.11105	-0.00023
1.9	0.002684	0.63483	0.001186	-0.11244	-0.00033
2	0.002739	0.68609	0.001159	-0.11402	-0.00042
2.1	0.002798	0.738397	0.001134	-0.1158	-0.00052
2.2	0.002859	0.791825	0.001107	-0.11783	-0.00065
2.3	0.002921	0.846422	0.001076	-0.1201	-0.00076
2.4	0.002998	0.902205	0.001044	-0.12287	-0.00087
42.6	0.02246	720.2646	-0.00686	-0.1475	0.007141
42.7	0.02247	720.2446	-0.00792	-0.14602	-0.0054
42.8	0.02278	720.7575	0.003063	-0.14657	-0.00874
42.9	0.02182	720.5725	0.009026	-0.14953	-0.00051
43	0.02266	720.8878	0.004543	-0.14734	0.008274
43.1	0.02254	720.5788	-0.00698	-0.14671	0.007159
43.2	0.02247	720.5588	-0.00799	-0.146	-0.00534
43.3	0.02281	720.4578	0.00306	-0.14636	-0.00872
43.4	0.0218	720.7878	0.008997	-0.14975	-0.0006
43.5	0.02268	720.7854	0.004577	-0.14685	0.008274
43.6	0.02251	720.4875	-0.00686	-0.14725	0.007165

Table 5. CFD k-ε Turbulence Model Result at 4.0 m/s, 4.7 degree

Time (sec)	Hydraulic Torque (N-m)	Rotating Speed (RPM)	Hydraulic Force_X (N)	Hydraulic Force_Y (N)	Hydraulic Force_Z (N
0.1	0.000465	0	4.60E-06	-0.0203	-0.00021
0.2	0.000747	0.008888	6.35E-05	-0.0309	-0.00029
0.3	0.001039	0.02315	9.24E-05	-0.04132	-0.00033
0.4	0.00128	0.042997	0.000122	-0.04983	-0.00032
0.5	0.001471	0.067451	0.000154	-0.0565	-0.00029
0.6	0.001625	0.09555	0.000182	-0.06189	-0.00026
0.7	0.001755	0.126592	0.000206	-0.06648	-0.00022
0.8	0.002359	0.160105	0.000337	-0.09921	-0.00046
0.9	0.0027	0.205162	0.000353	-0.11561	-0.00042
1	0.002891	0.256728	0.000347	-0.12376	-0.00034
1.1	0.003005	0.311942	0.000324	-0.12791	-0.0003
1.2	0.003079	0.369335	0.000291	-0.13014	-0.0003
1.3	0.003136	0.428137	0.000259	-0.13159	-0.00035
1.4	0.00319	0.488023	0.000237	-0.13277	-0.00044
1.5	0.003247	0.548952	0.000226	-0.13395	-0.00055
1.6	0.003308	0.610971	0.000217	-0.13525	-0.00068
1.7	0.003377	0.674143	0.000213	-0.13687	-0.00083
1.8	0.003453	0.738634	0.000208	-0.13881	-0.001
1.9	0.003537	0.804577	0.000206	-0.14116	-0.00117
2	0.00363	0.87212	0.0002	-0.14391	-0.00134
2.1	0.003726	0.941439	0.000207	-0.14687	-0.00153
2.2	0.003827	1.01261	0.000212	-0.15029	-0.00173
2.3	0.003914	1.0857	0.000196	-0.15335	-0.00191
86	0.02838	852.2592	-0.00163	-0.17158	0.003825
86.1	0.02763	852.4852	0.000274	-0.17815	-0.00377
86.2	0.02769	852.7842	0.000932	-0.17941	0.002158
86.3	0.02837	852.8545	-0.0025	-0.17299	-0.00123
86.4	0.02889	852.4825	0.003614	-0.1708	0.001178
86.5	0.0287	852.7482	-0.00181	-0.17565	0.000538
86.6	0.02867	852.7555	0.001507	-0.17855	-0.00161
86.7	0.02801	852.2457	-0.0006	-0.17372	0.003621
86.8	0.02756	852.4585	-0.00068	-0.17474	-0.0025
86.9	0.02822	852.4555	0.00269	-0.1756	0.002547
87	0.02891	852.4457	-0.00302	-0.17584	-0.00087
87.1	0.02903	852.4885	0.00278	-0.17152	0.00075

Table 6. CFD k-ε Turbulence Model Result at 4.5 m/s, 5.0 degree

Time (sec)	Hydraulic Torque (N-m)	Rotating Speed (RPM)	Hydraulic Force_X (N)	Hydraulic Force_Y (N)	Hydraulic Force_Z (N
0.1	0.000465	0	4.60E-06	-0.0203	-0.00021
0.2	0.000747	0.008888	6.35E-05	-0.0309	-0.00029
0.3	0.001039	0.02315	9.24E-05	-0.04132	-0.00033
0.4	0.00128	0.042997	0.000122	-0.04983	-0.00032
0.5	0.001471	0.067451	0.000154	-0.0565	-0.00029
0.6	0.001625	0.09555	0.000182	-0.06189	-0.00026
0.7	0.001755	0.126592	0.000206	-0.06648	-0.00022
0.8	0.002359	0.160105	0.000337	-0.09921	-0.00046
0.9	0.0027	0.205162	0.000353	-0.11561	-0.00042
1	0.002891	0.256728	0.000347	-0.12376	-0.00034
1.1	0.003005	0.311942	0.000324	-0.12791	-0.0003
1.2	0.003079	0.369335	0.000291	-0.13014	-0.0003
1.3	0.003136	0.428137	0.000259	-0.13159	-0.00035
1.4	0.00319	0.488023	0.000237	-0.13277	-0.00044
1.5	0.003247	0.548952	0.000226	-0.13395	-0.00055
1.6	0.003308	0.610971	0.000217	-0.13525	-0.00068
1.7	0.003377	0.674143	0.000213	-0.13687	-0.00083
1.8	0.003453	0.738634	0.000208	-0.13881	-0.001
1.9	0.003537	0.804577	0.000206	-0.14116	-0.00117
2	0.00363	0.87212	0.0002	-0.14391	-0.00134
2.1	0.003726	0.941439	0.000207	-0.14687	-0.00153
2.2	0.003827	1.01261	0.000212	-0.15029	-0.00173
2.3	0.003914	1.0857	0.000196	-0.15335	-0.00191
86	0.02838	852.2592	-0.00163	-0.17158	0.003825
86.1	0.02763	852.4852	0.000274	-0.17815	-0.00377
86.2	0.02769	852.7842	0.000932	-0.17941	0.002158
86.3	0.02837	852.8545	-0.0025	-0.17299	-0.00123
86.4	0.02889	852.4825	0.003614	-0.1708	0.001178
86.5	0.0287	852.7482	-0.00181	-0.17565	0.000538
86.6	0.02867	852.7555	0.001507	-0.17855	-0.00161
86.7	0.02801	852.2457	-0.0006	-0.17372	0.003621
86.8	0.02756	852.4585	-0.00068	-0.17474	-0.0025
86.9	0.02822	852.4555	0.00269	-0.1756	0.002547
87	0.02891	852.4457	-0.00302	-0.17584	-0.00087
87.1	0.02903	852.4885	0.00278	-0.17152	0.00075

Table 7. CFD k-ε Turbulence Model Result at 5.0 m/s, 5.8 degree

Time (sec)	Hydraulic Torque (N-m)	Rotating Speed (RPM)	Hydraulic Force_X (N)	Hydraulic Force_Y (N)	Hydraulic Force_Z (N
0.05	0.001044	0	-0.0005	-0.04857	-0.00151
0.1	0.001653	0.009968	-0.00038	-0.07087	-0.00173
0.15	0.002163	0.025748	-0.00035	-0.09012	-0.00186
0.2	0.002519	0.046404	-0.00031	-0.1047	-0.00191
0.25	0.002771	0.07046	-0.00028	-0.11562	-0.0019
0.3	0.002956	0.096924	-0.00023	-0.12407	-0.00188
0.35	0.003107	0.125156	-0.00016	-0.13121	-0.00188
0.4	0.003245	0.154822	-0.00012	-0.13773	-0.00191
0.45	0.003383	0.185813	-8.37E-05	-0.144	-0.00198
0.5	0.004377	0.218122	0.000239	-0.20776	-0.00286
0.55	0.004893	0.259919	0.000176	-0.23811	-0.00316
0.6	0.005173	0.306645	5.77E-06	-0.25287	-0.00326
0.65	0.005341	0.356046	-0.0002	-0.26029	-0.00333
0.7	0.005453	0.407046	-0.00038	-0.26433	-0.00344
0.75	0.005541	0.459115	-0.00051	-0.26687	-0.0036
0.8	0.005622	0.512032	-0.0006	-0.26885	-0.00384
0.85	0.005702	0.565721	-0.00067	-0.27066	-0.00413
0.9	0.005784	0.620168	-0.00074	-0.27259	-0.00448
0.95	0.005868	0.675402	-0.00078	-0.27467	-0.00485
1	0.005955	0.731434	-0.0008	-0.27695	-0.00526
1.05	0.006042	0.788296	-0.00081	-0.27944	-0.00569
1.1	0.006134	0.845994	-0.00082	-0.28216	-0.00615
25.5	0.06493	1202.242	-0.01045	-0.43631	-0.0349
25.55	0.06502	1202.578	-0.01056	-0.43241	-0.03517
25.6	0.0654	1202.445	-0.01074	-0.4268	-0.03591
25.65	0.06558	1202.044	-0.01089	-0.42751	-0.03541
25.7	0.06598	1202.457	-0.01061	-0.42646	-0.03388
25.75	0.06587	1202.544	-0.00982	-0.43036	-0.033
25.8	0.0657	1202.124	-0.00896	-0.42822	-0.03359
25.85	0.06548	1202.584	-0.00832	-0.42399	-0.03411
25.9	0.06542	1202.578	-0.00811	-0.42123	-0.03406
25.95	0.0653	1202.474	-0.00798	-0.42263	-0.03423
26	0.06536	1202.555	-0.0082	-0.4256	-0.03406
26.05	0.06561	1202.642	-0.00912	-0.41261	-0.03195
26.1	0.06576	1202.113	-0.0096	-0.40704	-0.0315

Table 8. CFD k-ε Turbulence Model Result at 5.5 m/s, 6.1 degree

Time (sec)	Hydraulic Torque (N-m)	Rotating Speed (RPM)	Hydraulic Force_X (N)	Hydraulic Force_Y (N)	Hydraulic Force_Z (N
0.05	0.00103	0	-0.0003	-0.04594	-0.00114
0.1	0.00159	0.00982	-0.00022	-0.06716	-0.00153
0.15	0.0021	0.025	-0.00017	-0.08572	-0.00173
0.2	0.0025	0.04509	-0.00014	-0.10018	-0.0018
0.25	0.00278	0.06893	-0.0001	-0.11122	-0.00187
0.3	0.00299	0.09547	-6.92E-05	-0.12001	-0.00191
0.35	0.00316	0.124	-5.53E-05	-0.12746	-0.00197
0.4	0.00331	0.15415	-3.59E-05	-0.13422	-0.00207
0.45	0.00345	0.18572	-1.26E-05	-0.14066	-0.00221
0.5	0.00445	0.21865	-6.39E-05	-0.20277	-0.00294
0.55	0.00499	0.26116	-0.00016	-0.23317	-0.00316
0.6	0.00528	0.30881	-0.00027	-0.24818	-0.00324
0.65	0.00544	0.35923	-0.00033	-0.25576	-0.00334
0.7	0.00553	0.41114	-0.00033	-0.25978	-0.00351
0.75	0.0056	0.46398	-0.00028	-0.26218	-0.00377
0.8	0.00566	0.51747	-0.00021	-0.26389	-0.00407
0.85	0.00572	0.57153	-0.00015	-0.26542	-0.00441
0.9	0.00578	0.62614	-9.50E-05	-0.26702	-0.00479
0.95	0.00584	0.6813	-5.39E-05	-0.26881	-0.0052
1	0.00591	0.73706	-1.29E-05	-0.27083	-0.00563
1.05	0.00598	0.79348	2.57E-05	-0.27307	-0.00609
1.1	0.00606	0.8506	6.31E-05	-0.27554	-0.00655
1.15	0.00614	0.90846	9.71E-05	-0.27831	-0.00703
1.2	0.00624	0.96712	0.000134	-0.28142	-0.0075
1.25	0.00634	1.02667	0.000171	-0.285	-0.00799
86	0.02838	1378.2592	-0.00163	-0.17158	0.003825
86.1	0.02763	1378.4852	0.000274	-0.17815	-0.00377
86.2	0.02769	1378.7842	0.000932	-0.17941	0.002158
86.3	0.02837	1378.8545	-0.0025	-0.17299	-0.00123
86.4	0.02889	1378.4825	0.003614	-0.1708	0.001178
86.5	0.0287	1378.7482	-0.00181	-0.17565	0.000538
86.6	0.02867	1378.7555	0.001507	-0.17855	-0.00161
86.7	0.02801	1378.2457	-0.0006	-0.17372	0.003621
86.8	0.02756	1378.4585	-0.00068	-0.17474	-0.0025
86	0.02838	1378.2592	-0.00163	-0.17158	0.003825

APPENDIX C
List of Publications

List of Publications

International Journal

1. **Wisatesajja, W**., Roynarin, W. and Intholo, D. (2019). Comparing the Effect of Rotor Tilt Angle on Performance of Floating Offshore and Fixed Tower Wind Turbines.

   Journal of Sustainable Development, (12)5 pp. 84-95.

   Quartile 2018 = Q4

   DOI: https://doi.org/10.5539/jsd.v12n5p84
2. **Wisatesajja, W**., Roynarin, W. and Intholo, D. (2020). Analysis of Influence of Tilt Angle on Variable-Speed FixedPitch Floating Offshore Wind Turbines for Optimizing Power Coefficient Using Experimental and CFD Models.

   International Journal of Renewable Energy Development, (10)2 pp. 201-212

   Quartile 2019 = Q3

   DOI: https://doi.org/10.14710/ijred.2021.33195

International Conferences

1. **Wisatesajja, W**., Roynarin, W. and Intholo, D. (2017). Feasibility Study of On-Grid Solar-Wind Hybrid System at Wongsakorn Plaza Market. Proceedings of 121st The IIER International Conference, Bangkok, Thailand, 11 – 12 September 2017.
2. **Wisatesajja, W**., Roynarin, W. and Intholo, D. (2018). Studying of Tower Effects for Floating Wind Turbines. The 6th International Conference on Wind Turbine and Renewable Energy, Kwangwoon University, Seoul, Korea, 25 – 26 May 2018.
3. **Wisatesajja, W**., Roynarin, W. and Intholo, D. (2019). Analyzing of Rotor Tilt Angle Effect on Performance of Floating Wind Turbines Compared to the Fixed Tower wind Turbines. The 2nd International Conference on Applied Science, Engineering and Interdisciplinary Studies, Rajamangala University of Technology Thanyaburi (RMUTT), Pathum Thani, Thailand, 4 – 5 July 2019. (Best Paper).

4. Roynarin, W., **Wisatesajja, W**. and Aguila, G. (2020). The Effect of The Number of Blades on the Characteristics of Compressed Air Wind Turbines Using R1235 Airfoil Blade Profile. The 11th TSME International Conference on Mechanical Engineering, Ubon Ratchathani, Thailand, 1 – 4 December 2020. (Best Paper).

National Conferences

1. **Wisatesajja, W**., Roynarin, W. and Intholo, D. (2017). Feasibility Study of On-Grid Solar-Wind Hybrid System at Wongsakorn Plaza Market. The 10th Thailand Renewable Energy for Community Conference Thaksin University Phatthalung, Thailand, 29 – 30 November 2017.
2. **Wisatesajja, W**., Roynarin, W. and Intholo, D. (2018). Study of a 20 kW Solar-Wind Hybrid System for Wongsakorn Plaza Market Community. The 14th Conference on Energy Network of Thailand. Rayong, Thailand, 13 -15 June 2018.
3. **Wisatesajja, W**., Roynarin, W. and Intholo, D. (2018). Study on the Effect of Angle of Tower Inclination on the Performance of a Small Floating Wind Turbines. The 11th Thailand Renewable Energy for Community Conference, Chaiyaphum Rajabhat University, Chaiyaphum, Thailand, 28 – 30 November 2018.
4. **Wisatesajja, W**., Roynarin, W. and Intholo, D. (2019). Comparing the Effect of Rotor Tilt Angle on Performance of Floating Offshore and Fixed Tower Wind Turbines. The 12th Thailand Renewable Energy for Community Conference, Naresuan University, Phitsanulok, Thailand, 6 – 8 November 2019.

Biography

Name – Surname	Mr. Wongsakorn Wisatesajja
Date of Birth	22 May 1989
Address	95 Saimai Soi 73 Saimai Road, Saimai District, Bangkok, Thailand 10220
Education	Bachelor Degree in Civil Engineering, University of Surrey, United Kingdom Master of Science in Renewable Energy Systems Engineering, University of Surrey, United Kingdom
Work Experiences	Manager at Wongsakorn Plaza Market Manager at English Training Centre Development Engineer Internship at Montana Ambiente Group Property and Project Consultant at Wongsakorn Villa Group and Thongsuk Villa Pranburi
Telephone Number	+668-0933-5151
Email Address	wongsakorn_w@mail.rmutt.ac.th